Design for Additive Manufacturing Considerations for Self-Actuating Compliant Mechanisms Created via Multi-Material PolyJet 3D Printing

Nicholas Alexander Meisel

Dissertation submitted to the faculty of the Virginia Polytechnic Institute and State University in partial fulfillment of the requirements for the degree of

Doctor of Philosophy
In
Mechanical Engineering

Christopher Williams (Chair)
Jan Helge Bøhn
Robert Canfield
Kevin Kochersberger
Robert West

May 5, 2015
Blacksburg, VA

Keywords: Additive Manufacturing, 3D Printing, PolyJet, Topology Optimization, Multiple Materials, In-Situ Embedding, Shape Memory Alloy, Design for Additive Manufacturing

Design for Additive Manufacturing Considerations for Self-Actuating Compliant Mechanisms Created via Multi-Material PolyJet 3D Printing

Nicholas Alexander Meisel

ABSTRACT

The work herein is, in part, motivated by the idea of creating optimized, actuating structures using additive manufacturing processes (AM). By developing a consistent, repeatable method for designing and manufacturing multi-material compliant mechanisms, significant performance improvements can be seen in application, such as increased mechanism deflection. There are three distinct categories of research that contribute to this overall motivating idea: 1) investigation of an appropriate multi-material topology optimization process for multi-material jetting, 2) understanding the role that manufacturing constraints play in the fabrication of complex, optimized structures, and 3) investigation of an appropriate process for embedding actuating elements within material jetted parts. PolyJet material jetting is the focus of this dissertation research as it is one of the only AM processes capable of utilizing multiple material phases (e.g., stiff and flexible) within a single build, making it uniquely qualified for manufacturing complex, multi-material compliant mechanisms. However, there are two limitations with the PolyJet process within this context: 1) there is currently a dearth of understanding regarding both single and multi-material manufacturing constraints in the PolyJet process and 2) there is no robust embedding methodology for the in-situ embedding of foreign actuating elements within the PolyJet process. These two gaps (and how they relate to the field of compliant mechanism design) will be discussed in detail in this dissertation. Specific manufacturing constraints investigated include 1) "design for embedding" considerations, 2) removal of support material from printed parts, 3) self-supporting angle of surfaces, 4) post-process survivability of fine features, 5) minimum manufacturable feature size, and 6) material properties of digital materials with relation to feature size. The key manufacturing process and geometric design factors that influence each of these constraints are experimentally determined, as well as the quantitative limitations that each constraint imposes on design.

DEDICATION

For my wonderful wife, Kacey. You are the best thing that ever happened to me. And without you, none of this would have been possible.

ACKNOWLEDGEMENTS

I'd like to thank all of the people who have helped and guided me over the past five years as I've worked towards the completion of this dissertation:

The Air Force Research Lab, Logistics Management Institute, and Virginia Tech Institute for Creativity, Arts, and Technology, for your financial support during my research endeavors.

Dr. Bruce Orler, for your help and guidance during my dynamic mechanical analysis experimentation.

Dr. James Guest and Dr. Andrew Gaynor for your expert insight and partnership during our study into topology optimization for Additive Manufacturing.

Dr. Jan Helge Bøhn, Dr. Robert Canfield, Dr. Kevin Kochersberger, and Dr. Robert West, for offering your time and expertise as members of my committee.

To all members of the DREAMS Lab, both past and present. Thank you all for making the DREAMS Lab the unique, exciting, and engaging place that it is. You've made me look forward to coming to work each day, and I will miss you all.

Dr. Chris Williams, for all of your patience, excitement, and wisdom. I have learned so much more from you than just what it takes to be a researcher. You have set an example that is truly worth aspiring to as I continue my academic career. You have afforded me countless opportunities to grow and experience the impact that my work can have on the world. I can't thank you enough.

And Mom, Dad, Erin, and Cody. For your constant encouragement and love.

CONTENTS

LIST OF FIGURES

LIST OF TABLES

1. INTRODUCTION AND MOTIVATION

1.1. Motivation for Complex, Multi-Material, Actuated Structures in AM

When engineers design moveable mechanisms, they will often utilize stiff, rigid-link structures with rotational joints. However, when nature designs moveable mechanisms, it may take a starkly different approach, one that favors multi-material structures with both stiff as well as flexible elements. A characteristic example of this can be seen in the natural design of bat wings (as studied in [1]). Bats' wings utilize a series of rigid bones covered in a flexible membrane which allows for smooth, compliant motion. In addition to the rigid bones and flexible membrane, there are numerous muscles beneath the membrane that serve to actuate the wing during flight. This type of complex, compliant, multi-material, self-actuated structure serves as the conceptual motivation for the work contained within this dissertation.

One of the main limiting factors to creating these types of multi-material actuated structures in an engineering setting is the relative complexity of manufacturing them. However, with the maturation of additive manufacturing processes, these types of mechanisms are now within reach. Additive manufacturing (AM, colloquially 3D printing) is a class of manufacturing processes where artifacts are built up one layer at a time. This is in direct contrast to traditional subtractive manufacturing where material is removed from a block of raw material until the desired final shape is formed. The result is that AM processes can create complex parts that are impossible to create in any other way. While there are a wide variety of AM processes (differentiated by how they create each layer), the PolyJet material jetting process is uniquely qualified to manufacture the type of multi-material specimens of interest to this study. The PolyJet process is the only commercially available AM process capable of creating parts with on-demand material composition. The process achieves this through the inkjet deposition of polypropylene-like and rubber-like photopolymer material droplets. As each droplet is deposited, it is cured with a UV light. This allows for the creation of parts with properties that can range from stiff to flexible, with numerous allowable gradients in-between. A diagram of the process is shown in Figure 1.1.

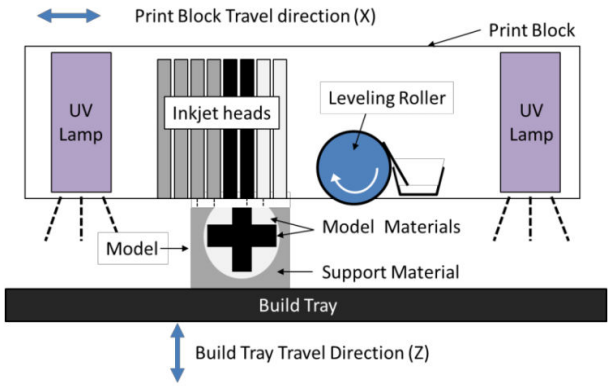

Figure 1.1. Diagram of the PolyJet Material Jetting Process

1.1.1. Motivating Example

The potential offered by the concept of biomimetic, multi-material, actuated mechanisms in engineering design can be best demonstrated through a simple motivating example. In [2], the authors presented the simple case study of an actuated finger model which was created with the PolyJet additive manufacturing process. A monofilament fiber was embedded into the finger during printing. After the part was finished, the entire finger could curl by pulling on a simple sliding joint. This example can be seen in Figure 1.2.

(a) (b) (c)

Figure 1.2. (a) CAD Model of Finger, (b) Manufactured Part, (c) Actuated

While this example serves to spark the imagination, it also raises several questions about the design and fabrication of similar parts. First, the joint-like sections were given a traditional crescent living-hinge shape; however, there is no guarantee that this is the optimal shape or location for these hinges. Automated design methodologies, such as topology optimization (TO), can help to address the deficiencies in this type of instinctual design, which might be based, in part, on an unspoken adherence to traditional manufacturing. Understanding and

incorporating manufacturing limitations will also help designers to ensure that the joint-like sections are printable and able to withstand any necessary post-processing. Finally, while the above example is able to utilize embedded filament, the embedding methodology is not easy to apply to other more complex, and potentially more robust, foreign actuating elements. Even with this simple example, it is possible to observe the gaps in knowledge which drive the research questions to be discussed in Sections 1.2-1.5.

1.2. Overall Research Goal

The content in Section 1.1 provides motivation for a need to address gaps within the realms of (i) compliant mechanism design, (ii) PolyJet AM, and (iii) component embedding that will be filled by the research presented in this dissertation. With these gaps filled, one could realize optimized, self-actuating, multi-material compliant mechanisms.

The area of optimized part design is currently of significant interest throughout the AM research community. However, while there are AM researchers who have attempted to pursue the idea of optimized AM parts independently (see for example [3,4]), the author asserts that, in order to completely achieve the idea of manufactured, multi-material compliant mechanisms, an interdisciplinary partnership must be formed between the AM research community and the topology optimization community. Through such a partnership, it becomes possible to leverage the optimization design knowledge of the TO community with the manufacturing and embedding knowledge of the AM community. This relationship, and its service to the idea of optimized, self-actuating, multi-material compliant mechanisms, is shown in Figure 1.3.

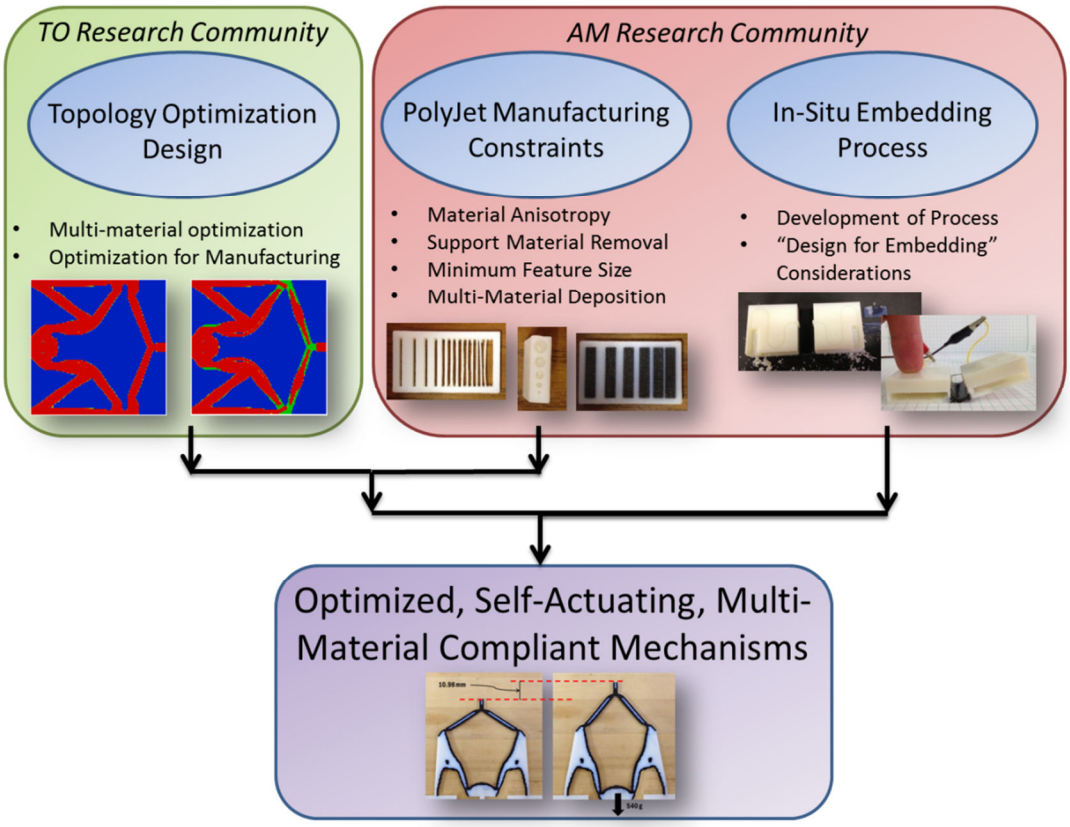

Figure 1.3. Motivating Idea and Contributing Realms of Research

The goal of the research presented herein is to understand the manufacturing limitations and advantages of the PolyJet process in the context of fabricating optimized, multi-material, self-actuating compliant mechanisms. This is accomplished by addressing the gaps present in the realms of PolyJet manufacturing constraints and in-situ embedding, with an eye towards how filling in these gaps may prove beneficial to work being performed by the design and TO communities.

Based on the framework presented in Figure 1.3, the overall motivating goal of the work can be stated as follows:

The **Overall Motivating Goal** is to gain an understanding of how the manufacturing constraints of the PolyJet material jetting process affect the creation and mechanical properties of multi-material structures. Understanding these constraints is essential to furthering the use of innovative design tools, such as Topology Optimization (TO) methods, for the realization of optimized, multi-material, self-actuating compliant mechanisms.

1.3. Research Question 1: Single-Material DfAM Constraints

As already stated, the research herein is meant to provide a thorough understanding of the single-material manufacturing restrictions which might prove essential in the design of complex, multi-material mechanisms with AM. These restrictions are specifically concerning material-jetting AM in the form of the PolyJet 3D printing process. Primary Research Question 1, presented below, addresses the desire to better understand these manufacturing considerations.

Primary Research Question 1 (PRQ 1): How do the single-material manufacturing constraints of PolyJet AM, such as machine resolution and support material usage, affect the as-manufactured geometric features of final parts?

Answering PRQ 1 establishes links in the process-structure-behavior chain inherent in using PolyJet AM to create single-material parts. PRQ 1 seeks to investigate some of the more typical AM manufacturing considerations included in the PolyJet process. Within PRQ 1, there is a series of Secondary Research Questions which address each of the key single-material constraints of the PolyJet process. These questions are as follows:

Secondary Research Question 1.1 (SRQ 1.1): What geometric or process parameters influence the minimum manufacturable feature size in PolyJet AM? What is the quantifiable value of this geometric limitation on part design?

Secondary Research Question 1.2 (SRQ 1.2): What geometric or process parameters influence the geometric limitations imposed by i) the need to clean a part without damaging it, ii) the need to clean channels of support material, and iii) the need for faces to be self-supporting in the absence of support material? What are the quantifiable values of these geometric limitations on part design?

1.4. Research Question 2: As-Manufactured Multi-Material Properties

The manufacturing considerations in SRQ 1.1-1.2 (minimum feature size, support material usage) are not necessarily unique to the PolyJet process; all additive manufacturing processes are impacted in some way by these types of considerations. However, the unique multi-material capabilities of the PolyJet process introduce a host of other manufacturing considerations that are exclusive concerns to PolyJet printing. PRQ 2 addresses the need to better understand these multi-material considerations in general.

Primary Research Question 2 (PRQ 2): How do the PolyJet process's multi-material deposition methods affect the as-manufactured properties of final parts?

As with PRQ 1, answering this question allows for a link between the manufacturing potential of AM and design innovation. There are several Secondary Research Questions within PRQ 2 which address specific multi-material concerns in PolyJet printing.

Secondary Research Question 2.1 (SRQ 2.1): How do the material properties of the PolyJet's digital materials change with respect to the percent composition of base materials? How do these properties affect the potential digital material design space?

Secondary Research Question 2.2 (SRQ 2.2): How does feature size affect the manufactured properties of printed digital materials? Why do the material properties of digital materials shift as feature size decreases?

1.5. Supplemental Question 1 (Development): Embedding Process and Design

In order to create self-actuating compliant mechanisms, a process must also be developed to allow for the in-situ embedding of complex foreign actuating components in printed parts. Developing this embedding process, and establishing the related "design for embedding" considerations, forms the basis for Supplemental Question 1, seen below.

Supplemental Question 1 (Development): How can foreign actuating components be embedded into parts manufactured with the PolyJet process? What design considerations drive the ability to successfully embed these components?

1.6. Dissertation Roadmap

Each chapter that follows in this dissertation represents an individual paper submitted for journal publication in the field of AM. Each of these journal publications is summarized in Table 1.1, along with the current status of each publication (i.e., to be submitted, in review, or published).

Chapter 2 provides motivating research in the area of multi-material AM of optimized compliant mechanisms. This work was performed in conjunction with the Topology Optimization Group led by Dr. Jamie Guest at Johns Hopkins University. The resultant optimized structures from this study act as a catalyst for the manufacturing considerations to be investigated in Chapters 3 and 4. Chapter 3 focuses on the role of single-material manufacturing constraints in DfAM. The specific constraints under investigation include minimum manufacturable feature size, support material removal from channels, minimum self-supporting angle, and minimum survivable feature size. In contrast, Chapter 4 emphasizes the importance

of multi-material manufacturing constraints and material properties in PolyJet AM. To begin, this chapter contains an investigation of the material properties of the PolyJet process's digital composites with respect to composition. From there, the chapter presents research comparing the as-manufactured properties of multi-material regions to the as-designed properties. This comparison is based on the possibility of inaccurate recreation of digital material properties in small features. Chapter 5 presents the process for embedding actuating components within multi-material PolyJet compliant structures. Along with establishing the process, Chapter 5 also proposes several "design for embedding" considerations to guide designers in their embedding endeavors. Finally, Chapter 6 offers conclusions and discusses limitations and directions for future work.

Table 1.1. List of Journal Publications that Comprise this Dissertation

Publication Title/Chapter	Journal	Status
Multiple-Material Topology Optimization of Compliant Mechanisms Created via PolyJet Three-Dimensional Printing (Chapter 2)	ASME Journal of Manufacturing Science and Engineering	Published, 2014
An Investigation of Key Design for Additive Manufacturing Constraints in Multi-Material 3D Printing (Chapter 3)	ASME Journal of Mechanical Design	In Revision, 2015
Process/Structure Relationships in Composite Parts Manufactured via Multi-Material Jetting (Chapter 4)	Rapid Prototyping Journal	To Be Submitted, 2015
A Procedure for Creating Actuated Joints via Embedding Shape Memory Alloys in PolyJet 3D Printing (Chapter 5)	Journal of Intelligent Material Systems and Structures	Published, 2014

1.7. Summary of Design for Manufacturing Goals and Scientific Contributions

With research questions established, it is possible to provide a summary that guides the entirety of this research study. This summary collects the overall gap filled by the primary research questions in addition to providing the hypothesis, methods, and impact related to successfully answering each research question.

Gap
There exists a lack of understanding regarding how the manufacturing constraints of the PolyJet 3D printing process

affect the creation and mechanical properties of multi-material structures. Understanding these constraints is essential to furthering the use of innovative design methods, such as Topology Optimization (TO), for the realization of optimized, multi-material, self-actuating compliant mechanisms.

Primary Research Gap 1	
The single-material manufacturing constraints inherent in the PolyJet AM process are currently underresearched. It is necessary to fill in the unknown limitations caused by the manufacturing process in order to best determine how to link PolyJet AM with design innovation.	
Primary Research Question 1	
Question	*Hypothesis*
How do the single-material manufacturing constraints of PolyJet AM, such as machine resolution and support material usage, affect the as-manufactured geometric features of final parts?	The machine resolution, support material attributes, and post-processing requirements will each impose a lower bound on the smallest geometry that can be manufactured by the PolyJet process. Each of these lower bounds will be driven by key process and geometric parameters that have a statistically significant impact on the constraint.
Methods	*Impact*
Experimental methods will vary depending on the individual manufacturing consideration under investigation (discussed with the Secondary Research Questions). In general, individual manufacturing considerations will be examined with a series of Design of Experiments test specimens and characterized to determine appropriate numerical limitations.	Answering this question will clarify the effects of PolyJet single-material manufacturing constraints on printed part geometry. This will in turn help those in the TO community better incorporate AM limitations and advantages into their algorithms as well as helping other designers gain an intuitive understanding of how to design for PolyJet.

Secondary Research Gap 1.1	
While some preliminary investigation has been performed into the minimum manufacturable feature size with the PolyJet process [5], this information has not been studied to a degree that would allow for robust incorporation into the topology optimization design of optimized structures.	
Secondary Research Question 1.1	
Question	*Hypothesis*
What geometric or process parameters influence the minimum manufacturable feature size in PolyJet AM? What is the quantifiable value of this geometric limitation on part design?	The PolyJet printing process will limit the smallest feature that can be manufactured in an optimum topology, based on the orientation of the part, the chosen part surface finish, the printed material type, the direction of the part's features, and

	the general shape of the part's features.
Methods	*Impact*
Minimum feature elements from the standardized test part developed by the National Institute of Standards and Technology (NIST) in [11] will be used to determine the minimum resolvable feature size. Changes in relation to PolyJet printing parameters (e.g. material choice, surface finish, orientation) will be determined.	Answering this question will mark the first attempt to robustly quantify the minimum feature size of PolyJet parts. While investigation of minimum feature size may have been performed for other AM processes, it has not been done in such a way that directly considers its effect on the creation of multi-material PolyJet parts.

Secondary Research Gap 1.2	
The PolyJet process uses a unique, hydrophobic support material which has a direct effect on feasible, printable designs. No research has yet been performed to determine the channel size necessary to successfully remove support material from printed PolyJet parts. Likewise, no work had been performed to determine the potential damage to fine printed features when removing support material with a water jet.	
Secondary Research Question 1.2	
Question	*Hypothesis*
What geometric or process parameters influence the geometric limitations imposed by i) the need to clean a part without damaging it, ii) the need to clean channels of support material, and iii) the need for faces to be self-supporting in the absence of support material? What are the quantifiable values of these geometric limitations on part design?	The PolyJet process's support material will limit the diameter, shape, and connectivity of cavities allowed within an optimized part, to ensure that they are possible to clean. It will simultaneously affect the minimum feature size that can be manufactured, driven by the feature's material type, length, diameter, and connectivity. In the absence of support material, the quality of self-supporting faces will be dictated by material type and face orientation.
Methods	*Impact*
A test part will be designed which evaluates the ability to remove support material based on the cross-sectional area of the cavity, the length of the cavity, and the connectivity of the cavity with the surfaces of the part (similar to that in [6]). Minimum feature specimens similar to those in SRQ 1.1 will be used to determine the size at which parts will fracture due to cleaning.	Answering this question will clarify the use of support material within PolyJet parts. Because of the unique nature and potential difficulty of removing support material from PolyJet parts, this information is essential to understand as we seek to integrate manufacturing considerations into design for PolyJet parts.

Primary Research Gap 2

The PolyJet process has the distinction of being one of the only commercial AM process types capable of manufacturing parts with multiple-materials in a single monolithic structure. However, despite this unique advantage, the nature of how these multiple materials are created and how their material properties are manifested has not been researched to date. This in turn limits the ability to properly represent these materials and their limitations in design methods.

Primary Research Question 2	
Question	*Hypothesis*
How do the PolyJet process's multi-material deposition methods affect the as-manufactured properties of final parts?	The composite deposition method and bitmap representation of digital materials are key features of the PolyJet process which affect the as-manufactured properties of multi-material PolyJet parts. These aspects will inform the baseline material properties of the digital materials as well as cause material property shifts within small features.
Methods	*Impact*
Experimental methods will vary depending on the individual aspect under investigation (discussed with the Secondary Research Questions). In general, individual multi-material manufacturing considerations will be examined with a series of test specimens of different feature sizes and characterized to determine limitations and causes.	Answering this question will help to provide a more complete picture of the multi-material properties of PolyJet composites, as well as the effect that design and manufacturing constraints can have on those properties. This will in turn help those in the TO community better incorporate multi-material AM properties, limitations and advantages into their algorithms as well as helping other designers gain an intuitive understanding of how to design multi-material structures for PolyJet.

Secondary Research Gap 2.1	
The drop-by-drop inkjet deposition methods of the PolyJet process allow for the creation of so-called "digital" composite materials made from two base materials. By default the PolyJet process has a set of composites that it is designed to manufacture. However, no researchers have yet identified the potential composite design space that these materials occupy, nor have they studied the relationship between percent composition and the properties of these digital materials.	
Secondary Research Question 2.1	
Question	*Hypothesis*
How do the material properties of the PolyJet's digital materials change with respect to the percent composition of base materials? How do these properties affect the potential digital material design	As the proportion of VW+ increases in the PolyJet's digital materials, the storage modulus of the structures will increase following a consistent relationship. Because of the great difference in material properties between the base materials

space?	(VW+ and TB+) the resultant composite design space will be significantly larger than what the commercial PolyJet system currently allows for.
Methods	*Impact*
Dynamic Mechanical Analysis will used be to identify the elastic properties of the PolyJet's digital materials at various compositions. From this measurement, a relationship will be drawn between material composition and material properties, which includes identification of a theoretical composite design space.	Answering this question not only assist designers in understanding the existing property trends followed by the commercial PolyJet systems, but it will also provide them with a theoretical composite design realm that they might fill with their own composite dithering patterns.

Secondary Research Gap 2.2	
Because of the way in which the PolyJet process deposits multiple materials on a drop-by-drop basis (similar to multi-colored ink in a normal inkjet printer), there is the potential for the properties of the printed digital materials to change based on feature scale. This effect has not yet been investigated in literature, but has the potential to have a profound effect on how the multi-material properties are used in PolyJet part design.	
Secondary Research Question 2.2	
Question	*Hypothesis*
How does feature size affect the manufactured properties of printed digital materials? Why do the material properties of digital materials shift as feature size decreases?	As the size of printed features decreases, the as-manufactured storage modulus will change for parts which utilize the PolyJet's digital materials. This is because the necessary deposition pattern of multi-material droplets cannot be fully replicated in a small feature space.
Methods	*Impact*
Dynamic Mechanical Analysis will be used at varying feature scales and candidate digital materials to determine how the as-manufactured material properties of digital material parts differ from the as-designed properties as scale size decreases.	Answering this question will mark the first time the multiple-material capabilities of the PolyJet process have been investigated to understand the as-manufactured properties due to digital materials not being fully represented in small features. This will help designers to better account for the variations in the PolyJet's multiple material properties when designing parts for manufacturing.

Supplemental Gap 1 (Development)
Embedding is of growing interest in the AM research community. However, there is no existing process or "Design for Embedding" considerations for the embedding of complex actuating elements in PolyJet AM.

Supplemental Question 1 (Development)	
Question	*Approach*
How can complex foreign actuating components be embedded into parts manufactured with the PolyJet process? What design considerations drive the ability to successfully embed these components?	Key design features such as actuator fixation points, shape converters, and channel design will be considered in the detailed design stage of the design process to successfully adapt parts for manufacturing with the PolyJet in-situ embedding method.
Impact	
By establishing a clear process and set of design considerations for embedding complex foreign actuating elements in PolyJet parts, it is possible to move towards the design and manufacture of true, self-actuating, multi-material compliant mechanisms, rather than relying on hypothetical "input elements" to apply forces to the mechanism.	

2. MULTIPLE-MATERIAL TOPOLOGY OPTIMIZATION OF COMPLIANT MECHANISMS CREATED VIA POLYJET 3D PRINTING

Coauthors: Dr. Andrew Gaynor, Dr. James Guest, Dr. Christopher Williams

2.1. Abstract

Compliant mechanisms are able to transfer motion, force, and energy using a monolithic structure without discrete hinge elements. The geometric design freedoms and multi-material capability offered by the PolyJet 3D printing process enables the fabrication of compliant mechanisms with optimized topology. The inclusion of multiple materials in the topology optimization process has the potential to eliminate the narrow, weak, hinge-like sections that are often present in single-material compliant mechanisms and also allow for greater magnitude deflections. In this paper, the authors propose a design and fabrication process for the realization of 3-phase, multiple-material compliant mechanisms. The process is tested on a 2D compliant force inverter. Experimental and numerical performance of the resulting 3-phase inverter is compared against a standard 2-phase design.

2.2. Additive Manufacture of Multi-Material Compliant Mechanisms

Howell defines compliant mechanisms as those that utilize the deformation of flexible members to successfully transfer motion, force, and energy [7]. This is in direct contrast to traditional mechanisms that rely on movable joints in order to perform their function. Compliant mechanisms are encountered on a daily basis in the forms of binder clips, paper clips, and various compliant latches. In addition to the various man-made examples, nature also makes use of compliant mechanisms, with many living organisms displaying parts that are both strong and flexible [8]. Advantages of compliant mechanisms include part consolidation and improved mechanism robustness. However, as the design of compliant mechanisms increases in complexity, traditional manufacturing methods become infeasible. This drives the authors' overall goal of integrating design optimization with additive manufacturing (AM) methods, with a particular focus herein on the design and fabrication of compliant mechanisms.

While there are many examples of single-material compliant mechanisms present in everyday life, man-made, multi-material compliant mechanisms are rare. This is because manufacturing complexity increases significantly with the introduction of additional material

phases. The potential benefit, however, may likewise increase significantly. For example, Aguirre and Frecker make a strong case for the need of multi-material compliant mechanisms in the medical field [9]. By including both a stiff and flexible material phase in the design of contact-aided compliant mechanism forceps for natural orifice translumenal endoscopic surgery, the authors were able to achieve larger total jaw openings and blocked forces. This improved mechanism performance has the potential to directly impact the success rate of the surgery. However, Aguirre and Frecker's design was limited by their intuitive understanding of how forceps should look. This paper takes a more systematic design approach based on topology optimization to leverage multi-material AM processes.

PolyJet 3D printing is one of the only AM processes capable of utilizing stiff and flexible material phases within a single build, making it uniquely qualified for manufacturing complex, multi-material compliant mechanisms. PolyJet 3D printing is an AM material jetting process, wherein droplets of liquid photopolymer are deposited directly onto an elevator substrate via a series of inkjet print heads [10]. As the material is deposited, two ultraviolet (UV) lamps cure the photopolymer in multiple passes. Each subsequent layer is jetted on top of the previous one. A representation of this process can be seen in Figure 2.1.

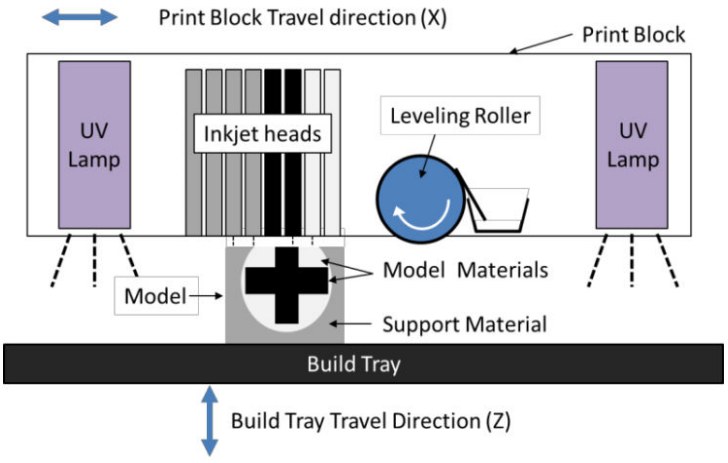

Figure 2.1. Representation of Direct 3D PolyJet Printing Process

The PolyJet process offers a high resolution print, with a layer thickness of 16-30 microns and an in-plane resolution of 42 microns. In addition, the PolyJet process offers one significant and unique advantage among modern additive manufacturing process: the PolyJet process is

capable of depositing two different materials on a pixel-by-pixel basis. One material is a rigid, white plastic-like material (VeroWhite+), while the other is an elastomeric, flexible black material (TangoBlack+). The two materials can be combined in various ratios to create nine gradient material blends with properties ranging along the continuum of the two extremes. By including multiple material phases such as these in the design of compliant mechanisms, the maximum deflection of the mechanism can potentially be improved, while potentially decreasing the likelihood of fatigue failure at the structure's joint-like sections.

2.2.1. Introduction to Compliant Mechanism Design and Topology Optimization

In general, the compliant mechanism design process can be separated into a series of key decisions that the designer must make. Each one of these decisions serves to lead the designer towards a final design methodology. The decisions include the general approach to be used (kinematics-based or optimization-based), the finite element representation of the design space (continuum, discrete, or hybrid), and the appropriate optimization algorithm (gradient-based or stochastic). A decision tree that represents these key decisions in the design process is shown in Figure 2.2.

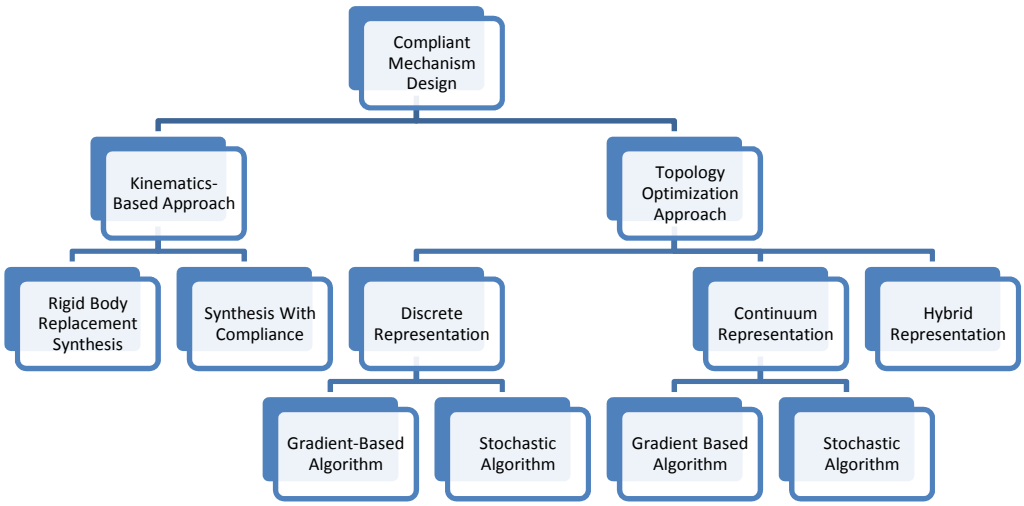

Figure 2.2. General Compliant Mechanism Design Decision Tree

The first decision is whether or not to pursue a kinematics based approach or a topology optimization approach. For the kinematics approach, the designer equates the desired compliant mechanism design to more traditional rigid-link kinematics design. This approach relies heavily

on the designer's intuition and preconceptions regarding the final compliant system. In this way, it does not fully leverage the design freedom allowed by AM and will not be pursued herein.

For the topology optimization approach, the general compliant mechanism design domain is defined (with applied forces, supports, and desired responses) and material is systematically distributed (added or removed) throughout the domain in a manner that minimizes (or maximizes) the defined objective function within a prescribed set of design constraints. This results in the effective and efficient use of material within the part. The use of the topology optimization approach as applied to the design of compliant mechanisms can be traced back to work by Sigmund, as well as by Frecker and coauthors [11,12].

As the next section will show, the field of topology optimization in AM is incredibly varied, with different researchers using different finite element (FE) representations and optimization algorithms according to the context of the particular problem, as well as personal preference.

2.2.2. Topology Optimization in Additive Manufacturing

While little to no work has yet been done regarding the manufacturing of optimized, multi-material compliant mechanisms via AM, several researchers have investigated the use of AM as a means of realizing topology-optimized parts, including small scale material microstructures (e.g., [7-9]). The "free complexity" inherent in the AM process makes it ideal for the realization of final optimized parts. While there are several topology optimization groups looking at manufacturing processes, the following section seeks to elucidate the larger hubs specializing in manufacturing research that have also pursued design optimization.

At Loughborough University, work has been performed to assist in the design of optimized artifacts while specifically considering the necessary manufacturing constraints provided by AM. Brackett and coauthors recently offered an overview of some of the largest perceived opportunities in this sector, including the importance of mesh resolution, support material constraints, and adaptations of the Solid Isotropic Material with Penalization (SIMP) material interpolation for lattice-based and multiple-material structures [13]. On the utilization of multiple-material topology optimization, they specifically mention the abilities of the PolyJet process and offer an example of how a designer could map the various blends onto the densities produced by the SIMP. They also acknowledge challenges, however, such as maintaining a formal sensitivity analysis and the need for experiments to ensure a reasonable mapping scheme,

and that the constitutive relations in SIMP and the blended material may not be consistent. Brackett also proposed a dithering optimization method based on stress analysis for the creation of functionally graded lattice structures within a part [14]. Aremu and coauthors investigated the suitability of Bi-Directional Structural Optimization (BESO) for AM, and extended the BESO strategy to include adaptive meshing around the boundaries [15], similar to topology optimization strategies proposed by [13-15] for enhancing computational efficiency. Watts and Hague utilized the design program "DesignLab" to investigate the performance of multiple materials in optimization [16]. Unfortunately, the genetic algorithm approach used in their preliminary study proved too computationally expensive to efficiently optimize for multiple materials along a fine mesh. Regularization was also not used, leading to the appearance of numerical instabilities in the form of checkerboard patterns and mesh dependence [17].

At the Georgia Institute of Technology, emphasis has been placed on the development of cellular structure design, optimization, and analysis techniques for application to AM. Wang and Rosen developed a methodology for the design of conformal cellular truss structures that could easily be translated to AM parts, and later automated the design and synthesis of these structures through a truss sizing optimization and application to mechanism structures [17–19]. Graf developed a Size Matching and Scaling (SMS) approach, which utilizes a unit cell library consisting of different truss arrangements optimized to support particular loading conditions. He subsequently offers a comparison of the SMS approach against the Particle Swarm Optimization method and least-squares minimization optimization method [20–22] and found that the SMS method could offer performance comparable to the results of these other two algorithms, while significantly decreasing the computation time due to the non-iterative nature of SMS. Finally, Rosen introduced a formal framework for the concept of Design for Additive Manufacturing, based on the process-structure-property-behavior framework from material science [23,24]. He demonstrated the use and applicability of this framework through the design of a size-optimized lattice structure to support a cover plate.

At the University of Southern California, Chen adapted Rosen's framework to assist in the design of cellular structures that offer specific compliant performance. He developed a CAD tool to design a mesostructure allowing for heterogeneous material properties within an AM printed part, in essence creating functionally graded materials from a single material [25,26]. Maheshwaraa, Bourell, and Seepersad, at the University of Texas at Austin, used truss ground

structure optimization for investigating the use of lattice structures in the creation of deployable skins manufactured via AM [27]. At Cornell University, Hiller and Lipson have developed a design methodology which represents the design space as a matrix of frequency amplitude components [3,28]. These frequency components can be rendered as specific object geometry via an inverse discrete cosine transform and optimized via stochastic evolutionary algorithms, such as genetic algorithms. The paper highlights the inherent advantage evolutionary-based algorithms have with respect to the multi-objective optimization problem, as solutions tend not to become trapped in local minima. The algorithm, however, is not demonstrated on large scale problems, where genetic algorithms tend to struggle and frequently lack convergence. While Hiller and Lipson have not physically created their multi-material structures, they do attempt to consider the general advantages of multi-material AM.

Obviously the body of work discussed above is incredibly varied. There are researchers investigating the manufacture of optimized single-material structures in AM, researchers who are developing manufacturing rules related to single-material optimization in AM, and researchers who are investigating how multi-material optimization could generally be implemented in AM. However, in the above investigation, there were no examples of authors attempting to develop a process for the optimization and subsequent fabrication and testing of multi-material compliant mechanisms, while also incorporating the manufacturing constraints and advantages of the PolyJet printing process. It is this process that we seek to develop in our work, starting with the initial results presented herein.

2.2.3. Theoretical Representation of Multiple Materials in Topology Optimization

In order to apply topology optimization to the PolyJet process, an appropriate scheme for representing the multiple candidate materials must be chosen. While some potential schemes have already been touched upon in the review of AM optimization (such as optimality criteria, BESO, and genetic algorithms) there are yet other multi-material representations that might also prove applicable to the realm of PolyJet printing.

The most well-known continuum-based topology optimization approach is the Solid Isotropic Material with Penalization (SIMP) approach initially proposed by Bendsøe [29]. This method discretizes the design domain into a series of pixels (voxels in 3D) and assigns each one a pseudo-density, or volume fraction. These pseudo-densities are used to interpolate between two

phases of material: solid and void. In essence, if the pseudo-density value of a pixel approaches zero, it is assigned void material and if it tends towards one, it is assigned solid material. Typically the resulting structure is analyzed with finite elements and thus these pixels are the continuum finite elements. By introducing a second pseudo-density term to each pixel, it is possible to further interpolate between three material phases: one stiff, one flexible, and one void [30]. This idea may be further extended by introducing an additional pseudo-density variable to each pixel accounting for each additional material phase that is available. This method has been shown to perform reliably, but relies on a large number of design variables, as each additional material introduces additional design variables on the order of the number of pixels in the design space (e.g. four non-zero material options creates four times as many design variables).

Yin and Ananthasuresh take a different gradient-based approach in their work with multiple-material compliant mechanism analysis [31]. They use a peak function model to interpolate material properties of the continuum. A normal distribution function is used to convert a continuous design problem into one with more discrete material options. As the algorithm progresses, the normal function is contracted and additional peaks begin to appear at the locations of the discrete candidate materials. The goal is to have each design variable settle towards one of these peak values and thereby result in a discrete material distribution. The key advantage of this approach is that only one design variable is needed per pixel, regardless of the number of material choices. However, it is possible that intermediate stiffness values may still appear in the final result since the design variables are not necessarily driven to value at the top of a peak. Instead they are simply driven to non-zero values, and may therefore lie anywhere along the normal distribution function between zero and the peak value. Although using a small standard deviation for the distribution function sharpens the function, it remains non-zero over a finite range that is accessible to the optimizer (i.e., it is not a true step function). A second disadvantage is that the interpolation space contains many peaks and valleys making the final solution highly dependent on the initial pseudo-density guess. To help mitigate the issue, the authors use a continuation method.

Saxena tackled the multi-material compliant mechanism problem by discretizing the domain with frame elements and using a genetic algorithm with rounding to assign available material phase values to the frame members [32,33]. As discussed, however, stochastic search approaches

such as genetic algorithms become intractable for large-scale optimization problems such as continuum-based topology optimization.

2.2.4. Manufacturing of Multi-Material Compliant Mechanisms

While literature has offered some discussion regarding how to optimize the design of multiple material compliant mechanisms, there has been little content detailing their actual fabrication. The few instances of literature pertaining to the fabrication of multiple material compliant mechanisms will be discussed herein, but it is important to note that none of the objects fabricated have been subjected to structural optimization. Following a review of the literature, the authors conclude that there is no prior work where multiple material compliant mechanisms have been designed, optimized, and subsequently fabricated.

One of the more prevalent examples of the manufacturing of multiple-material compliant mechanisms is from Bailey and Rajagopalan. They discuss the design and manufacturing of a biomimetic leg that operates under the principle of heterogeneous material compliance [34,35]. While the final design is not driven by the concept of optimization, the authors specifically address the process of multi-material. They adapt the process of Shape Deposition Manufacturing (SDM) to allow for the creation of flexible joints while maintaining stiff members for the rest of the leg shape. SDM involves the deposition of material in layers, followed by machining in order to form the material layer into the desired shape (in this way it is like a combination of additive manufacturing and traditional CNC machining). Because the process offers continuous access to the part interior, specialized sub-pieces can be embedded during creation. In this case, the authors embedded separate flexible joints in their biomimetic leg.

Several authors have also investigated the use of multi-material molding (MMM) for the creation of multiple material compliant mechanisms [36–38]. MMM is a process whereby the various materials in the final part are created volumetrically, as opposed to the layer-by-layer methods of both AM and SDM. While there are several variations on the process, the general MMM flow involves the creation of a one material phase being molded separately and then being inserted into a mold for the second stage material phase. Filling this second stage mold will embed the first material phase within the part.

For the fabrication of small-scale multiple material compliant mechanisms, there are two examples that are derivations of the MMM process. Rajkowski proposes a prototyping process that uses a curable rigid polymer as well as a curable, flexible silicone as the two material phases [39]. By placing the material phases down in bulk and using a mask to cure only the desired sections of the part, the author offers a quick, inexpensive solution for the fabrication of multiple-material mechanisms on the millimeter scale. Vogtmann proposes a process whereby the negative space for the flexible material phase is cut from a bulk piece of the rigid phase [40]. The flexible material is deposited, cured, and planed, before the desired mechanism profile is cut from the bulk material.

While the above processes have been shown to successfully create multiple material compliant mechanisms, they all also have limitations when considering complexity and distributed compliance of the final pieces. The examples presented are relatively geometrically simple when compared to traditional results of multiple-material optimization, and thus were all manufacturable. However, these processes do not scale well. As the complexity of topology and multi-material distribution increases, the processes will require significantly more user interaction and time investment to create the necessary mechanisms. In addition, the presented examples all rely on the principle of lumped compliance, where the flexible material phase is implemented at the location that would traditionally be represented by a revolute joint. These processes would be ill-prepared to manufacture mechanisms based on distributed compliance, where the flexible material phases would be more interspersed among the rigid material.

2.2.5. Context

The study presented in this paper demonstrates a start-to-finish process for the realization of optimized, multi-material compliant mechanisms. This represents an important first step in unlocking the design potential of the multi-material PolyJet process. The authors determine an appropriate compliant mechanism design process, based on the decision tree presented earlier in Figure 2.2, in Section 2.3.1. A SIMP and projection-based optimization method (Section 2.3.2) is applied to the design of a compliant force inverter, a well-known compliant mechanism case-study. Results from experimentally testing the printed multi-material optimized structures are provided in Section 2.4. Concluding remarks are offered in Section 2.5.

2.3. Process for Design and Manufacturing of 3-Phase Compliant Mechanisms

This section discusses the optimization approach that was implemented to design optimized compliant mechanisms. Section 2.3.2 discusses the multivariate SIMP optimization method, and how it is applied to multiple material optimization. In addition, Section 2.3.1 will discuss the logic behind the selection of this approach.

2.3.1. Determination of Compliant Mechanism Design Process Suitable for PolyJet Printing

As has already been mentioned in Figure 2.2, the design of compliant mechanisms can be divided into a hierarchal decision tree. For the first decision, we have already determined the use of the kinematics approach does not sufficiently leverage the potential of AM, so we instead follow a topology optimization path. The next decision is dependent on how the designer wishes to represent the finite element discretization in the design space. The discrete element representation, such as that used in truss and frame topology optimization with the ground structure approach, has the potential to drastically reduce the computational intensity of the optimization routine, due to the (relatively) low number of degrees of freedom. However, this comes at the cost of resolution and design freedom, as the design domain has already been restricted by in selecting the ground structure. A continuum representation, on the other hand, offers the potential for a more free-form representation of topology (depending on the chosen mesh size). It is worth noting that a hybrid representation might be able to balance the speed of the discrete representation with the resolution of the continuum method. While such hybrid approaches generally exist in literature, such as a truss-continuum models simultaneously optimized to place steel and concrete materials [41], the authors are unaware of any hybrid representations being used in conjunction with multiple material AM at this time.

The authors have instead chosen to pursue a continuum representation, due in part to the quality of its resolution as well as the way in which a continuum representation aligns with the PolyJet process' method of printing. When printing, the PolyJet process utilizes a series of multi-colored bitmaps that are sent to the printer. Each bitmap represents a single slice of the printed part, with multiple colors used in each slice to denote the material to be deposited. While the ability does not currently exist, the authors hope to eventually be able to use the image outputs from 2D topology optimization as a direct bitmap slice input to the printer. In this way, translating the topology optimization output to an STL file will become unnecessary and the

process of manufacturing optimized multi-material compliant mechanisms will become more streamlined.

The final decision to be made when considering the design decision tree in Figure 2.2 is whether to solve the chosen formulation with a gradient-based optimization algorithm or stochastic search optimization algorithm. Stochastic algorithms, such as genetic algorithms and particle-swarm optimization, randomly sample the design space and are thus capable of handling discrete formulations and facilitating escape from low performance local minima. They have been used in a wide range of applications, including manufacturing processes to optimize system design and order policy [46], system identification to obtain model parameters [47,48], identification of manufacturing process parameters [49], assembly system reconfiguration planning [50], sheet roll forming [51] and folding [52], and shape optimization of orienting devices [53]. Stochastic search algorithms, however, can be computationally expensive and may break down in high dimension spaces such as those of continuum topology optimization. Although strategic dimension control algorithms have been proposed for such cases (e.g., [42]), gradient-based optimization methods are much better suited to handle the many design variables inherent in a continuum representation. In this preliminary study, the Method of Moving Asymptotes (MMA) will be utilized as the optimizer [54].

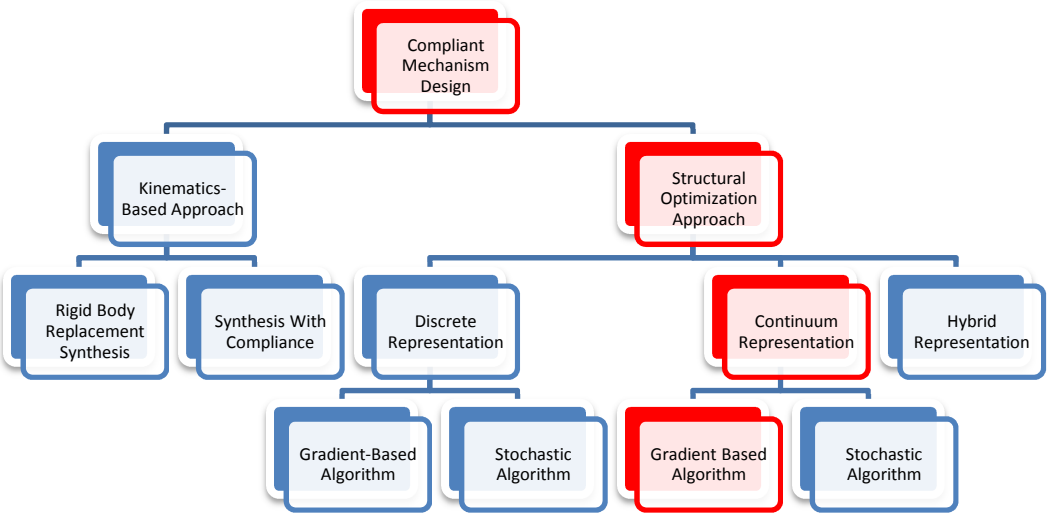

Figure 2.3. Chosen Compliant Mechanism Design Approach (Highlighted in Red)

2.3.2. Optimization Approach 1: Multiphase SIMP Method

Previously, Bendsøe and Sigmund [32] proposed a multiphase topology optimization method in which three phase solutions were possible. This formulation used two sets of design variables. The first set of design variables ρ_1 are used in determining the optimal topology of the compliant mechanism, while the second set of design variables ρ_2 are used for selecting the material at each location within the topology. The resulting material stiffness of an element is then given as

$$E^e = \rho_1^e(\phi_1)^\eta \left[\rho_2^e(\phi_2)^\eta E_1 + \left[1 - \rho_2^e(\phi_2)^\eta\right] E_2 \right] \tag{2.1}$$

where E_1 and E_2 are Young's modulus of the first and second phases, respectively. As can be seen in Eq. 2.1, the modulus E^e of each element is a function of both ρ (and their corresponding independent design variables ϕ_1 and ϕ_2). If $\rho_1 = 0$, then the element takes on a modulus of 0. If $\rho_1 = 1$ and $\rho_2 = 0$, then $E^e = E_1$, and when $\rho_1 = 1$ and $\rho_2 = 1$, $E^e = E_2$.

Embedded in this formulation is the Heaviside Projection Method (HPM) [55]. HPM uses independent design variables ϕ that are projected onto the ρ space using regularized Heaviside functions in a manner that enables direct control over the minimum length scale of designed features. This is meant to mimic the AM manufacturing process as material is computationally 'deposited' into the design domain in a circular shape with radius r_{min}, the resolution length scale of the liquid droplets [43,44]. Note, however, that the length scale r_{min} used in the examples is chosen much larger than the smallest achievable droplet so as to design simple structures that may better elucidate the benefits of using multiple materials.

While most work has focused on controlling length scale on solid-void structures, controlling length scale on each material phase in three-phase (or more) topology optimization remains a challenge. Using Eq. 2.1, the designer has control over features sizes but does not have rigorous control on the length scale of the individual material phases within the feature. While rapid phase variation within the member is not possible, prescribed length scale may become violated when ϕ_2 variables located outside of the member take on non-zero values, allowing thin bands of material to form on the member edges.

As stated previously, the Method of Moving Asymptotes (MMA) is used as the optimizer [45], and full algorithmic details of coupling HPM and MMA are available in [46]. It should

also be noted that controlling minimum length scale circumvents the aforementioned numerical instabilities of solution mesh dependence and checkerboard patterns.

2.3.3. Optimization Approach 2: Combinatorial SIMP Method

A new approach proposed here involves a combination of design variables in a SIMP scheme to produce multi-material topologies. The idea is that each phase contributes to a 'total' Young's modulus for an element. The base modulus is the modulus of the most compliant phase (typically void), and each phase i has the capability of adding a discrete magnitude ΔE_i of stiffness. For the case of equal increments ΔE in Young's modulus between the phases, this may be written as follows:

$$E = \sum_{i=1}^{n} \rho(\phi)_i^{\eta_i} \Delta E \tag{2.2}$$

where n is the number of design variables ρ per element. To achieve a three phase solution containing voids ($E = 0$), stiff material ($E = E_{stiff}$), and complaint phase (e.g., $E = 0.5\ E_{stiff}$), two elemental design variables per element are required and $\Delta E = 0.5\ E_{stiff}$. An element is then assigned the stiff phase when $\rho_1 = \rho_2 = 1$, compliant phase when ρ_1 or ρ_2 are equal to 1, and void when $\rho_1 = \rho_2 = 0$. Parameter η_i is the SIMP exponent on design variable i and is needed to drive the design variables to 0 or 1, and ultimately the modulus of an element, to the allowable magnitudes. It is generally good practice to make the η_i slightly offset to prevent sensitivities from being equal during the first iteration.

Again we embed HPM in this formulation, making ϕ_i the independent optimization variables that are projected onto finite element space. An interesting advantage here is that each design variable simultaneously indicates material existence and phase selection. This ultimately provides slightly different length scale control over the phases in the design. Specifically, if stiff phase appears near a member edge, it can be shown that it will achieve a minimum thickness (diameter) of $2r_{min}$. We have also observed this on the interior of thick members (of width larger than $2r_{min}$), although this cannot be mathematically guaranteed. Disadvantages are that the designer does not have control over the minimum length scale of the compliant phase within a member (as before), and at present the algorithm requires the materials to have equal increments

in stiffness (ΔE). We note the latter may be quite appropriate for the multi-material Polyjet process.

2.4. Case Study: Compliant Force Inverter

In order to demonstrate the utility of the presented optimization and printing method, the authors consider the well-established example of a force inverter compliant mechanism. This case study was initially demonstrated in [11] and has become one of the benchmark problems in topology optimization. As seen in Figure 2.4 the design domain for the mechanism is square, with the displacements at the top and bottom points on the left side of the design domain fixed. An input force is applied to the left hand-side of the space, along with an input spring constant value. A reaction force and spring constant are also applied to the right hand side of the space. The objective of the study is to maximize the work done on the output spring. If the ratio of k_{out} to k_{in} is larger, greater force transfer to the output location is targeted. Conversely, the ratio of k_{out} to k_{in} is smaller, greater displacement of the output location is targeted.

Figure 2.4. Design Domain and Loading for Inverter Case Study

It should be noted that the analysis used in the topology optimization was limited to the assumption of small displacements, and thus linear elastic analysis. This can be achieved by using a small magnitude of the applied load. As load magnitude and resulting motion increases, literature has shown that the assumption of linear analysis at best underestimates motion of the final topology and, at worst, may miss a failure mode [47,48]. However, the creation of these optimized pieces should still offer a useful point of comparison between 2-phase and 3-phase

results, even though the experimental deflection values of each specimen under (relatively) large loads may differ from any predicted theoretical values.

2.4.1. Optimization: General formulation

In the case of the inverter problem, a common benchmark in topology optimization, the goal is to maximize negative displacement (minimize displacement) at an output port under a given load **F** at an input port. This is expressed mathematically in general as follows:

$$\begin{aligned} \min_{\boldsymbol{\phi}} \quad & \mathbf{L}^T\mathbf{d} \\ \text{subject to} \quad & \mathbf{K}(\boldsymbol{\phi})\,\mathbf{d} = \mathbf{F} \\ & \sum_{e\in\Omega} \rho^e(\boldsymbol{\phi}) v^e \le V \\ & 0 \le \phi_i \le 1 \quad \forall\, i \in \Omega \end{aligned} \tag{2.3}$$

where **d** are the nodal displacements, the unit vector **L** extracts the output port degree-of-freedom, **K** is the global stiffness matrix, V is the allowable volume of material, v^e is the elemental volume, and $\boldsymbol{\phi}$ is the independent design variable vector, described below. All examples were solved using a uniform distribution of material as the initial guess.

2.4.2. Robust Topology Optimization Formulation

When using topology optimization to design compliant mechanisms, it is well-known that solutions may contain one-node hinges, a situation where two solid elements are connected only at a corner node. One node hinges allow for lumped compliance and the performance of such elements is overestimated with low-order finite elements. Obviously, if a one-node hinge were printed, it would instantaneously fail due to the stress concentration at a point. While projection methods enable control of a minimum feature size, it was discussed in the original works that design variables could theoretically deposit two tangent circles, which would manifest in a one-node hinge [48]. A number of researchers have specifically tackled the one-node hinge issue in the context of the compliant inverter. Sigmund [60], for example, simultaneously optimized an eroded and dilated version of the topology to mimic over- and under-etching, respectively. This led to a min-max formulation, with the idea that over-etching would lead to a disconnected

structure, and thus zero performance, if one-node hinges were present. While the method successfully eliminates one-node hinges from designs, an actual "blue-print" design, which is passed to the manufacturer, is not clearly identified. A number of other authors have tackled the issue by using Monte Carlo simulation to represent manufacturing uncertainties in the context of projection schemes [61,62] and level set methods [63].

This paper adopts the same basic idea as Sigmund, employing a min-max formulation that simultaneously optimizes a larger projection and smaller projection of the same design variables. For this paper, however, we consider a minimum length scale r_{min} set by the user to represent the expected radius of the droplet, and then vary that droplet size by directly varying the radius r used in projection. This introduces two additional length scales, defined as:

$$\begin{aligned} r_{\text{minlarge}} &= r_{\text{min}} + \Delta r \\ r_{\text{minsmall}} &= r_{\text{min}} - \Delta r \end{aligned} \tag{2.4}$$

where Δr is the variation in length scale. The resulting min-max compliant mechanism optimization formulation then takes on the form:

$$\begin{aligned} \min_{\boldsymbol{\phi}} \quad & \max\{\mathbf{L}^{\mathrm{T}}\mathbf{d}_{(\mathbf{r}_{\mathbf{minsmall}})}, \mathbf{L}^{\mathrm{T}}\mathbf{d}_{(\mathbf{r}_{\mathbf{minlarge}})}\} \\ \text{subject to} \quad & \mathbf{K}(\rho(\boldsymbol{\phi})_{(\mathbf{r}_{\mathbf{minsmall}})})\mathbf{d}_{(\mathbf{r}_{\mathbf{minsmall}})} = \mathbf{F} \\ & \mathbf{K}(\rho(\boldsymbol{\phi})_{(\mathbf{r}_{\mathbf{minlarge}})})\mathbf{d}_{(\mathbf{r}_{\mathbf{minlarge}})} = \mathbf{F} \\ & \sum_{e\in\Omega} \rho^e(\boldsymbol{\phi})_{\mathbf{r}_{\min}} v^e \le V \\ & 0 \le \phi_i \le 1 \quad \forall\ i \in \Omega \end{aligned} \tag{2.5}$$

While the formulation in Eq. 2.5 is nearly identical to Sigmund [60], there is a subtle difference in achieving the geometric perturbation: Sigmund's dilate and erode variations actually simulate over-depositing and over-etching, which may represent different manufacturing processes and lead to different concavities of the material interface, while Eq. (2.5) simulates only the deposition process and the idea of an inkjet droplet being larger and smaller than anticipated. Though subtle, we feel the latter more accurately reflects the AM process. A continuation scheme on the β Heaviside parameter is used to achieve a quality solution. The β

for $r_{minlarge}$ is started at 0 and increased by 1 each continuation step. Alternatively, the β for the $r_{minsmall}$ is started large and reduced by 1 each step till it reaches 0. This essentially increases the strength of the over- and under-depositing as the algorithm progresses. The results found in this paper performed 11 continuation steps with 60 MMA optimization iterations for each continuation step. As our focus is on the multi-material aspect of these designs, the finer details of this robust topology optimization formulation and algorithm tuning are not explored here.

2.4.3. Force Inverter – Topology-Optimized Solutions

The compliant inverter is first solved using only two phases, solid and void, as in traditional topology optimization. The robust formulation is used with a length scale variation of 0.9 units to ensure the existence of reasonable hinges in the final topology. This, and all following examples, use a 30% total allowable volume fraction, a 240 x 120 finite element mesh (utilizing symmetry), and begin with a uniform distribution of material as the initial guess.

The resulting two-phase solution is shown in Figure 2.5 and resembles solutions reported in [53]. The topology is near binary (solid-void), does not exhibit any one-node hinges, and satisfies the length scale prescribed by the designer.

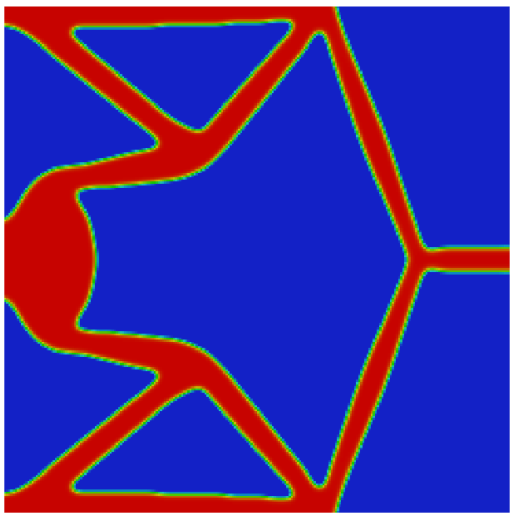

Figure 2.5. 2-phase (Solid-Void) Inverter Result found using the Robust SIMP Approach

We now examine the three-phase solutions, with one material phase being void, the second being compliant, and the third being stiff, where the stiffness ratio of stiff to compliant material is 2:1. Figure 2.6 displays the solution using the combinatorial SIMP scheme. The result aligns

with intuition: the algorithm places the stiff phase in the bar-like members to enable efficient force transfer and places the compliant phase in a hinge-like region. Note that all features have a length scale of least $2*r_{min}$, and that the compliant phase has a length scale of at least r_{min} at all locations, including the hinge-feature, meaning length scale is satisfied and one-node hinges are eliminated by using the robust formulation. Notice that the solution has compliant hinges at both ends of the inclined members (near the bottom and top domain boundaries). It is possible that there should be an additional complaint hinge hear the applied load on the lefthand side, and that the optimizer had a difficult time satisfying length scale of the compliant phase around the hinge region, as it would need to progress into the stiff regions of the inverter.

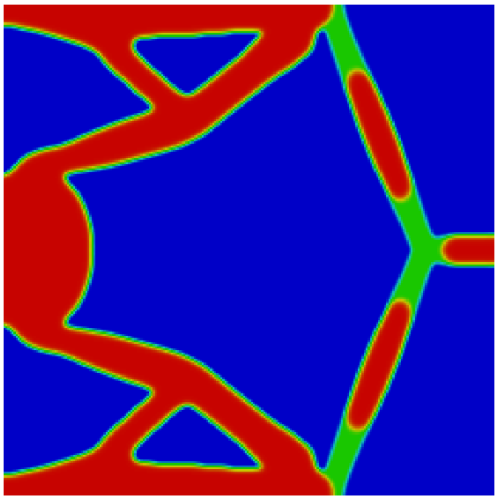

Figure 2.6. 3-phase Inverter Result found using the Robust Combinatorial SIMP Approach (2:1 Stiffness Ratio)

The compliant inverter is also solved using the Bendsøe and Sigmund multiphase approach with the robust formulation (4) to prevent one-node hinges. As can be seen in Figure 2.7, the phase distribution is more complex looking than that of the multivariate SIMP approach seen in Figure 2.6. This is due to the fact that the topology (ρ_1) and material ρ_2) projections, are performed separately in this approach, and are then combined to generate topology. This leads to the tapering of stiff material in the load transfer members near the output port and, although the entire structural member satisfies length scale of $2*r_{min}$, the individual phases do not. This is a subtle, but important difference between the two multi-material approaches. As in the combinatorial SIMP approach, the more compliant green material is concentrated at the hinge

regions, though there is a semi-hinge that appears near the applied load here, while the stiffer material is concentrated in the load transfer members.

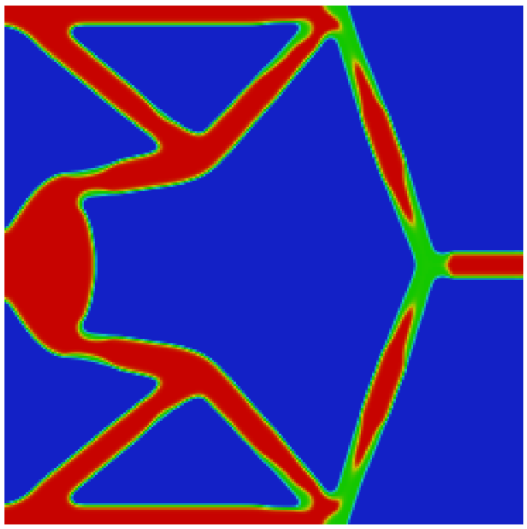

Figure 2.7. 3-Phase Inverter Result found using the Robust, Multiphase SIMP Approach

2.4.4. Mechanical Testing

Both the 2-phase and 3-phase inverters were printed on an Objet Connex 350. The stiff material was VeroWhite+ and the flexible material was RGD8530. Each inverter was printed to fill a 12 x 12 cm bounding box, with a thickness of 3.175 mm. An additional structure was added to each compliant mechanism in order to provide a location for the necessary force to be applied, as well as to ensure a cantilevered fixation at the appropriate point on the structure. The final printed specimens can be seen in Figure 2.8.

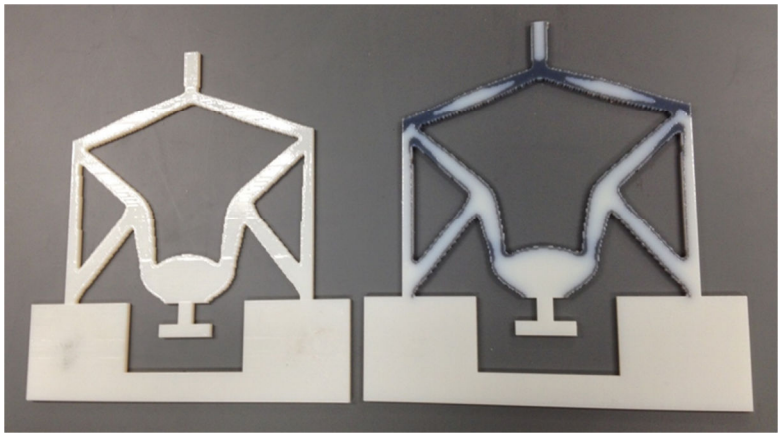

Figure 2.8. Compliant Specimens with Load and Cantilever Attachments

Each inverter was actuated by applying a 9.65 kg load at the "T" shaped attachment at the bottom of mechanism. The output tip location was marked before and after application of the load. The resulting mechanism motion is shown in Figure 2.9. The 2-phase inverter tip deflected 1.33 mm while the 3-phase inverters deflected 1.53mm and 2.45 mm for the combinatorial SIMP and multiphase SIMP approach respectively. Notably, this is a performance improvement of 84% for the multiphase SIMP case and a small improvement for the combinatorial SIMP approach. Although we were expecting a the multiphase SIMP approach to outperform the combinatorial, as it is less restrictive on the length scale of the individual material phases within a member, the actual magnitude of difference is quite surprising, and confirm the 'details' of the design are important. Looking at the multiphase SIMP (Figure 2.7) and combinatorial SIMP (Figure 2.6) solutions, we see a thin compliant, green border around all stiff, red regions. This border is likely not optimal, but instead an artifact of using small values for the β Heaviside parameter associated with the projection scheme. This fading effect can be mitigated by simply using larger values of β (see [57] for full discussion), though this was not done here.

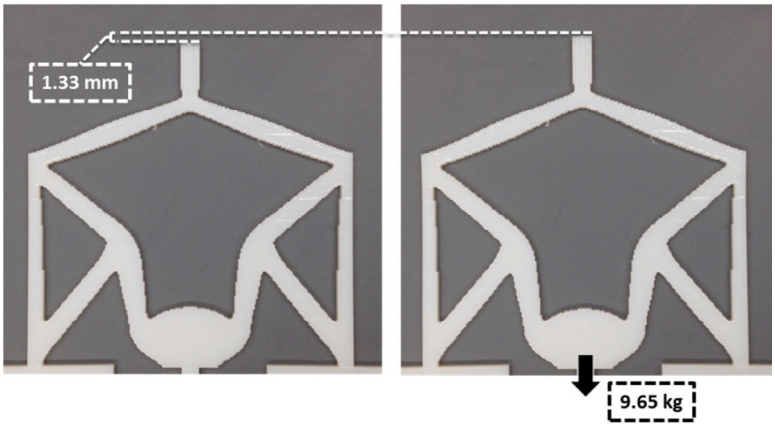

(a)

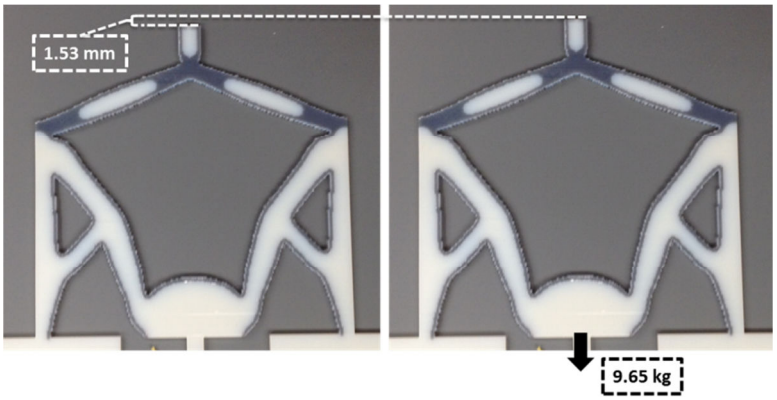

(b)

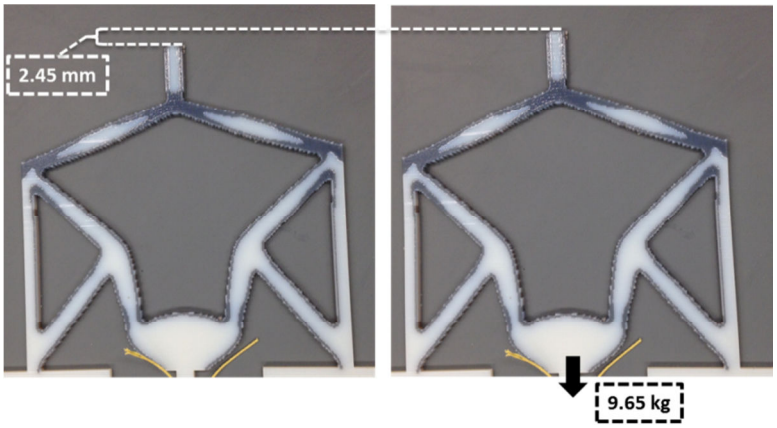

(c)

Figure 2.9. Deflection of a) 2-phase Inverter, b) 3-phase Combinatorial SIMP Inverter, and (c) 3-phase Multiphase SIMP Inverter (All under 9.65 kg Applied Load)

To demonstrate the ultimate potential of the PolyJet process's array of materials, an additional optimization was performed using a stiffness ratio of 20:1 between the two non-void candidate materials. This ratio is intended to more closely resemble the stiffness difference between the stiff VeroWhite+ material and TangoBlack+, the most elastomeric material offered by the Objet process. The optimized topology is shown in Figure 2.10 using the robust, multiphase SIMP approach.

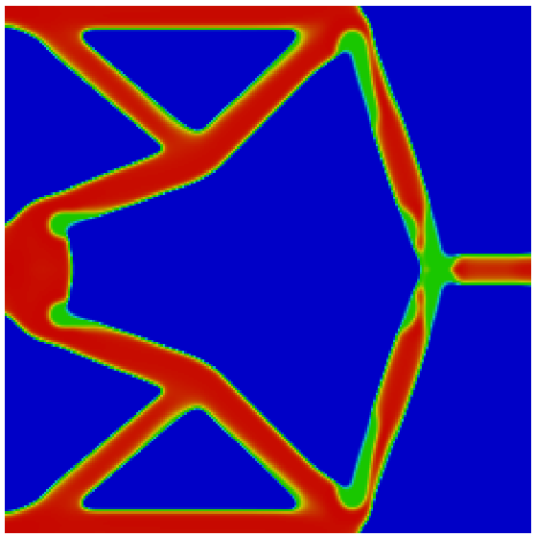

Figure 2.10. 3-Phase Inverter Topology found using the Robust, Multiphase SIMP Approach (20:1 Stiffness Ratio)

The TangoBlack+ and VeroWhite+ inverter achieved a deflection of 11.58 mm with only 2.75 kg of applied load, as shown in Figure 2.11. This is almost 9 times larger in displacement and 3 times less in load, or an improvement in efficiency of approximately 30. It is important to note that modulus of elasticity information for TangoBlack+ has yet to be published by the manufacturer or by independent researchers, and so the performance of the printed specimen has the potential to differ significantly from the performance predicted by the optimization algorithm (since the stiffness ratio is purely an estimation). However, it nevertheless demonstrates the dramatic displacement improvements that might be achieved when using the most elastomeric material for the PolyJet process.

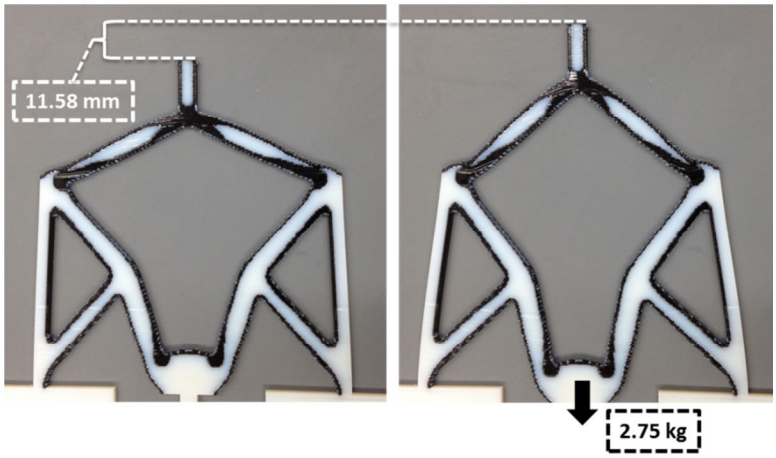

Figure 2.11. Deflection of 3-Phase Inverter with TangoBlack+ Material (under 2.75 kg of Applied Load)

It is also interesting to note the double curvature present in the deformation seen in Figure 2.11. This is forced through the robust topology optimization method. In the process of eliminating the one-node hinge design normally found for compliant inverter domains, the algorithm produces a structure with distributed compliance. While the lumped compliance present in the solution of a non-robust formulation will have better theoretical performance than the distributed compliance of the robust solution, the actual lumped compliance inverter would fail instantly due to the stress concentration at the one node hinge. Furthermore, achieving distributed compliance is fundamental to the original assumption of compliant mechanisms – compliance through material deformation of the structure.

2.5. Conclusions and Recommendations for Future Work

In this paper, the authors have presented a preliminary study into the development of a start-to-finish process for the design and manufacture of optimized, multi-material compliant mechanisms. The previous literature was reviewed in order to determine an appropriate compliant mechanism design and optimization approach, taking care to consider the unique opportunities afforded by multi-material PolyJet printing. A robust topology optimization algorithm, modified from Sigmund [60], was used in combination with a combinatorial SIMP approach and multiphase SIMP approach to design manufacturable, multi-material topologies. Experimental results of the compliant force inverter problem show that the addition of a second non-zero candidate material with stiffness of approximately one-half the base phase increases the

deflection (and efficiency) of the compliant inverter by as much as 84%, and by nearly a factor of 30 when the second non-zero phase is TangoBlack+.

Future work will first focus on independently quantifying the material properties of all the PolyJet materials (with a focus on TangoBlack+) in order to provide a more accurate comparison between the numerical and experimental results. Second, additional candidate materials will be introduced into the optimization routine to create optimized inverters with more material phases. The effect of smoothing the boundaries of each material phase, so as to remove any undesirable stress concentrations that may be present because of the pixelated nature of the final printed specimen, will also be examined. Finally, efforts will be placed on quantifying the printing limitations of the PolyJet process, so that manufacturing limitations might be included in the topology optimization algorithm.

3. AN INVESTIGATION OF KEY DESIGN FOR ADDITIVE MANUFACTURING CONSTRAINTS IN MULTI-MATERIAL 3D PRINTING

Coauthors: Dr. Christopher Williams

3.1. Abstract

The PolyJet material jetting process is uniquely qualified to create complex, multi-material structures. However, key manufacturing constraints need to be explored and understood in order to guide designers in their use of the PolyJet process including 1) minimum manufacturable feature size, 2) removal of support material, 3) survivability of small features, and 4) the self-supporting angle in the absence of support material. The authors use a Design of Experiments approach to identify the statistical significance of geometric and process parameters and to quantify the relationship between these significant parameters and part manufacturability. The results from this study include the identification of key variables, relationships, and quantitative design thresholds necessary to establish a preliminary set of Design for Additive Manufacturing guidelines for material jetting. Experimental design studies such as the one in this paper are crucial to provide designers with the knowledge to ensure that their proposed designs are manufacturable with the PolyJet process, whether designed manually or by an automated method, such as topology optimization.

3.2. Design for Additive Manufacturing (DfAM)

Additive manufacturing (AM) allows for the creation of parts of seemingly infinite complexity. While it is often said that "complexity is free" for AM relative to traditional manufacturing technologies, there are still manufacturing constraints that must be considered when designing parts for AM. These manufacturing constraints vary between the different AM process types, with certain constraints playing a larger role in one process than in another. As an example, material extrusion processes must consider the significant material anisotropy that occurs in the layering direction, while direct metal processes must account for added support scaffolding and anchoring. As these constraints differ from traditional manufacturing processes, dedicated "Design for Additive Manufacturing" (DfAM) guidelines are needed to assist engineers in realizing products that make effective use of AM's capabilities. A crucial

component of these DfAM guidelines is identifying which geometric and process parameters will affect the manufacturing constraints (e.g., does layer thickness affect anisotropy in material extrusion parts?).

Modern automated design methods, such as topology optimization, can help engineers design parts that may have been almost unthinkable prior to the advent of AM. In fact, numerous researchers are investigating the use of topology optimization (TO) in the field of AM (see, for example [13,16,21]). It is important that manufacturing constraints are represented in TO algorithms to ensure that these automated methods produce meaningful designs that can be accurately printed. At a basic level, this could be as simple as knowing the dimensions of the printer's build volume to ensure that the algorithm cannot design a part that is larger than the machine can build. A more complex example is the incorporation of the anisotropic properties of printed materials in the analysis phase of topology optimization.

3.2.1. Establishment of a DfAM Framework

Several researchers are working to establish Design for Additive Manufacturing (DfAM) frameworks to help designers better account for the advantages and limitations of AM processes in their designs. Rosen proposed a modified Process-Structure-Property-Behavior framework with a varying size scale [23]. The framework connects the behavior of parts back to key aspects of the manufacturing process. He utilized this framework to create a DfAM system for the creation of complex cellular structures. This framework is advantageous because the behavior, properties, and structure of a part can all be mapped back to the advantages and constraints of the manufacturing process used to produce it.

Hascoet and co-authors proposed what they termed a "global approach" to the incorporation of DfAM into printed parts [49,50]. Within this framework they suggest combining the functional requirements of the finished part with the manufacturing constraints of an AM process to develop a final geometry; this approach can be likened to the backward mapping that might occur from behavior to process in Rosen's framework. The global approach is in contrast to the "partial approach" where a part's geometry is designed beforehand and then adjusted to ensure manufacturability with AM. Hascoet cites work by Harzheim and Graf as a suitable example of this global approach. Harzheim and Graf combined the concept of topology optimization with

the limitations of traditional metal casting (rather than AM) to create final parts directly from functional specifications and manufacturing constraints [51,52].

Maidin's approach to DfAM relies more on detailed investigation of case studies than the more predictive analytic methods of Rosen and Hascoet. Maidin established a design feature database meant to spark inspiration in designers hoping to use AM for creation of their products [53]. He looked to existing products from AM and attempted to distill their novel aspects into a taxonomy useable by those unfamiliar with AM (example features included "dual material products," "internal structuring," and "weight saving features"). Finally, Seepersad and coauthors used a similar experimental case study approach to establishing DfAM rules, but focused more on establishing clear quantitative inputs for DfAM. They performed a series of experiments to establish a designer's guide for creation of holes, thin walls, text, and mating gears in the selective laser sintering (SLS) process [54]. They created matrices to help provide guidelines for designers in common situations, e.g., a determination of how large embossed lettering should be in order to be legible when made via laser-sintering.

3.2.2. Context

By understanding material jetting process constraints, designers will be able to better prepare printable parts. In addition, automated design tools such as topology optimization (TO) would be well served by quantifiable manufacturing constraints. In essence, TO is an automated design methodology where a general design domain is defined (with associated forces, supports, and responses). Material is then systematically distributed in the space, according to a particular algorithm. The final result is a part that efficiently and effectively uses material to satisfy all constraints and maximize or minimize an objective function. Emerging algorithms are able to incorporate various manufacturing constraints during the optimization process (see, for example, [43,55]). The goal of the research in this paper is to better understand the AM constraints that could be accounted for in a TO algorithm with embedded process constraints.

As previous work has demonstrated, the PolyJet process is uniquely capable of producing multi-material structures that could potentially be optimized through TO [56]. However, there are several key constraints that arise in such complex, multi-material parts. In this paper, the authors address these constraints and how they are influenced by various PolyJet geometric and process parameters. Specifically, the authors first identify four key PolyJet manufacturing

constraints that could affect part design (Section 3.3.3). The four sources of constraints are (i) support material removal (Section 3.4), (ii) minimum resolvable feature size (Section 3.5), (iii) feature survivability during cleaning (Section 3.6), and (iv) minimum self-supporting angle (Section 3.7). The authors utilize a Design of Experiments (DOE) approach to i) identify the geometric and process variables that have a statistically significant effect on each manufacturing consideration and ii) quantify recommended design limits for each consideration. Conclusions and recommendations for future work are offered in Section 3.8.

3.3. DfAM for PolyJet Material Jetting

3.3.1. PolyJet Overview

The multi-material AM jetting process (e.g., PolyJet) is unique because of its fine feature resolution, layer thickness, and its ability to selectively deposit multiple materials simultaneously, which allows for functional grading of material properties. The PolyJet material jetting process selectively deposits droplets of liquid photopolymer onto an elevator via a series of inkjet print heads [10]. As the material is deposited, two ultraviolet (UV) lamps cure the photopolymer in multiple passes. Each subsequent layer is jetted on top of the previous one. A representation of this process can be seen in Figure 3.1.

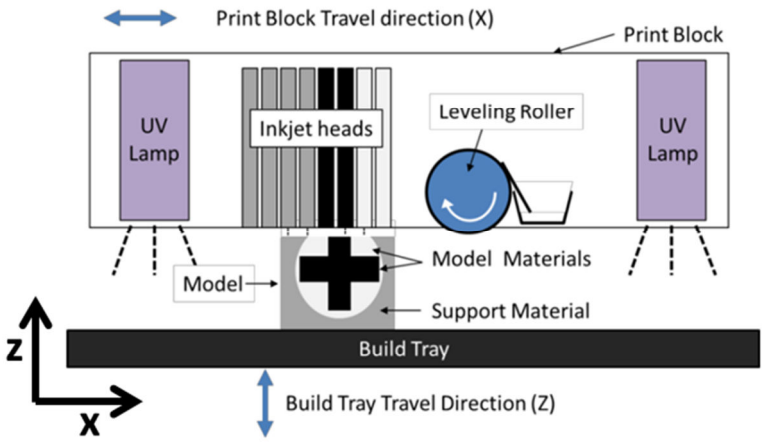

Figure 3.1. Representation of Direct 3D PolyJet Printing Process

The PolyJet process is able to create small features as it has a layer thickness of 16-32 microns and an in-plane resolution of 42 microns. In addition, the PolyJet process offers one significant, unique advantage among modern additive manufacturing process: the PolyJet process is capable of depositing two different materials on a pixel-by-pixel basis. This allows for creation of monolithic structures from multiple materials in a single build. One material combination of engineering relevance is VeroWhite+ (VW+) and TangoBlack+ (TB+), both of which are proprietary, acrylate-based photopolymers from Stratasys, Ltd. [57]. When cured during the printing process, VW+ material adopts the properties of a white, rigid, opaque plastic, while TB+ adopts the properties of a black, flexible elastomer. The two materials can be combined in various ratios to create nine gradient material blends with elastic modulus properties ranging along the continuum between the two extremes. The PolyJet process also uses a sacrificial, hydrophobic support material during part creation. After printing, this gel-like photopolymer must be manually removed using the recommended water jet cleaning station.

3.3.2. Prior Characterization of PolyJet

No researchers have yet created a detailed guide of DfAM constraints for the PolyJet process. Likewise, few have attempted to determine the effects of the PolyJet's various parameters (print head resolution, support material usage, multi-material options, etc.) have on these constraints. A review of existing work shows that i) existing studies tend to focus on material characterization, ii) process/property relationships have not been fully explored, and iii) the key process constraints of PolyJet have yet to be identified.

Regarding material characterization, Moore and Williams investigated the fatigue life of the elastomeric TangoBlack+ material produced by the PolyJet process [58]. They were able to create an experimental curve relating the percent elongation of a TB+ specimen to the expected life of the specimen. They also derived several design rules from their study; one example is to avoid necks in a designed part, since necks were found to reduce the fatigue life of specimens. Pilipovic and co-authors measured the tensile and flexural properties of VeroBlack, VeroBlue, and Fullcure 720 materials; they found that the Fullcure 720 performed the best of the three, with a flexural strength slightly higher than the manufacturer's quoted value [59]. The Fullcure material was also found to have a tensile strength lower than the manufacturer's cited value. Vieira and co-authors found that the flexural modulus of Fullcure 720 can be further improved

through UV or thermal post-processing, though this also has a negative effect on fatigue life [60]. Finally, Gibson and coauthors investigated the elastomeric properties of Fullcure 720 in both compression as well as bending [61]. Their experimentation showed that, while the material can be used for the creation of "living hinge" designs, its elastomeric properties are not strong enough to withstand heavy use.

In addition to material characterization, there has also been some prior work into characterizing the PolyJet process and its effect on final parts. Udroiu investigated the surface finish of parts made of Fullcure 720 and found that the machine's glossy surface finish setting gave parts a much lower surface roughness than the matte setting [62,63]. He also performed a basic investigation into how build time and material consumption changes relative to part orientation. From this investigation, he was able to provide several guidelines for optimal part orientation (e.g., "the smallest dimension along z-axis" and "highest part to the left"). Singh likewise characterized the material consumption and build time of a nominal test part with the PolyJet process and confirmed Udroiu's claim that the largest part dimensions should be aligned in the X-axis [64,65]. In addition, he investigated the dimensional accuracy of the part when built in different orientations and found that the x-axis orientation also offered the best dimensional accuracy for parts.

Kim and Oh also offer an investigation of PolyJet material and system characterization. In their paper, they investigate numerous properties of manufactured PolyJet parts [5]. The authors discovered a 50% decrease in PolyJet tensile strength in the z-direction of parts compared to the x-direction. They also discovered that the tensile strength of PolyJet parts decreases steadily and significantly as temperature is increased. While Kim and Oh did investigate minimum feature size, one of the goals of the research proposed in this paper, they did so only with simple rib and rectangular/circular gap shapes in a glossy finish. These shapes are capable of providing a benchmark minimum feature size, but may not capture the variation in size that may come from alternate orientations, surface finishes, and feature shapes (for example, the droplet-based nature of the PolyJet may allow it to recreate positive circular features more effectively than rectangular ones).

Investigation of the properties at the interface of disparate printed materials is one of the potential key focuses of PolyJet research. In addition to their study of general PolyJet material fatigue life, Moore and Williams also investigated the effect that the presence of a sharp material

interface would have on the fatigue failure location of a test specimen [58]. They found that having a sharp interface between TangoBlack+ and VeroWhite+ loaded in shear would almost always cause the specimen to fail at the interface (92% of their specimens failed at the shear interface while only 8% failed at the weaker TB+ material). However, despite being a central tenet behind the creation of PolyJet parts, the multi-material interface is still generally under-investigated in existing literature.

As this review demonstrates, PolyJet characterization research has included some investigation into manufacturing constraints such as material anisotropy and feature size. However, each of these studies tends to focus on one or two constraints and investigate the effects of only one variable on the constraints. A broader approach is needed in order to i) establish a larger field of PolyJet manufacturing constraints, ii) identify the essential process/geometry variables for each constraint, and iii) determine a quantifiable design recommendation associated with each constraint. The experimental methods (Sections 3.4-3.7) of this work seek to fill this gap in understanding.

3.3.3. Identification of PolyJet Manufacturing Constraints

To illustrate how constraints might influence the design of topology, consider the optimized compliant inverters from [56] (Figure 3.2). Both were designed using TO methods and subsequently printed via PolyJet AM.

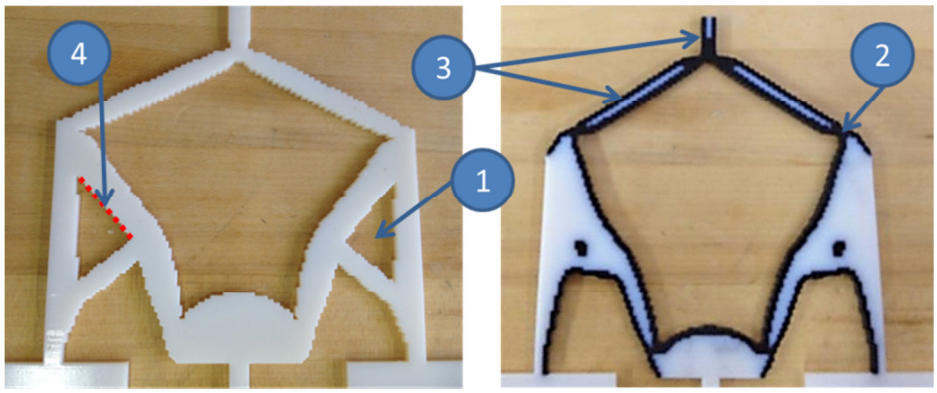

Figure 3.2. Optimized Compliant Inverters Manufactured via PolyJet AM [56]

The geometry of these inverters helps to illustrate certain concerns and possibilities that may arise in the use of automated design tools in AM. These potential manufacturing constraints are identified as follows (note that the callouts in Figure 3.2 match the numbering below):

1. Support Material Removal: Depending on part orientation and surface finish, the triangular holes in the single-material specimen would be filled with the PolyJet process's hydrophobic support material. It is necessary to ensure that these holes are large enough to allow for rapid, manual removal of the support material when cleaned with the provided water jet station.
2. Minimum Feature Size: In the case of the compliant inverter design domain, the TO algorithm tends to create narrow, hinge-like sections in the final design in order to increase deflection at the tip. This type of geometry illustrates the need for knowing the minimum manfacturable feature size in the PolyJet process, as the TO formulation would attempt to design these joints to be as small as possible.
3. Survivable Feature Size: As mentioned, PolyJet support material must be removed manually with a high-pressure water jet. Experience shows that it is possible for smaller features (such as the long, thin arms and tip of the inverter) to break during the cleaning process. Because of this, it is crucial to determine the factors that drive part breakage and establish the minimum feature size that can survive the cleaning process.
4. Self-Supporting Angle: It is possible to completely eliminate support material in the creation of PolyJet parts, thus removing any concerns about support cleaning or feature survivability. However, by doing this, it becomes necessary to ensure that angled faces (such as the one highlighted with the dashed line) will not collapse without support material. This can be predicted by determining the self-supporting angle of angled faces.

The authors employ a DOE framework to identify the geometric and process variables that have a statistically significant effect on these four manufacturing constraints. Without first understanding which parameters have an effect on the constraints, it is difficult (if not impossible) to establish a robust set of quantitative DfAM relationships. Once these key parameters are defined, additional experimentation presented in this paper will identify i) the underlying trends between the significant variables and the manufacturing constraints and ii)

recommended quantitative values to help guide designers in their use of PolyJet manufacturing. In addition, the experimental techniques used in this paper could be used for characterizing and benchmarking future material jetting processes and materials.

3.4. Support Material Removal

3.4.1. Motivation

As mentioned in Section 3.3.1, the PolyJet process uses a hydrophobic, gel-like photopolymer as a secondary sacrificial support material. As in other AM processes, this support material is used to ensure overhanging and angled structures are built properly (as was mentioned in reference to the triangular gaps in Figure 3.2). As the support material also affects a part's surface finish, the PolyJet process offers two surface finish options during pre-processing: selecting the "matte finish" provides a uniform surface finish to the part by coating every surface in support material (even top-facing surfaces); selecting the "glossy finish" only provides support material to overhanging features (typically resulting in the top-facing surfaces having a more glossy finish than the remainder of the part). This support material is then removed manually with a high-pressure water jet. The need to manually remove support material places significant limitations on the final geometry from an automated design process. Any fully enclosed cavities will be filled completely with support material that cannot be removed. In addition, certain long, narrow cavities may be difficult to clean.

The experiments described in this section are designed to answer the question, *What process parameters and geometric features affect the ability to successfully remove support material from printed parts?*

3.4.2. Experimental Methods

While no research has been done in support material removal specifically for the PolyJet, Vayre and coauthors investigated the cross-sectional size necessary to remove powder support material from channels in parts manufactured with electron beam melting [6,66]. They used compressed air to remove loose support powder from cylindrical channels of varying diameters and measured the depth of powder removed after a specified period of time. They found that as the cross-sectional area of a channel was increased, the amount of powder removed from it

(measured by depth of cleaning) also increased. They also noticed a qualitative difference between the channel geometry and how much powder was removed (cylindrical tubes were more easily cleaned than square ones).

A similar experiment is performed here with PolyJet support material removed via water jet. The support-filled channel specimens for this experiment rely on variation of three independent variables: (i) channel geometry, (ii) channel cross-sectional area, and (iii) channel connectivity (open at both ends or closed at one end). The geometry and cross-sectional area variables are included since they were found to have importance by Vayre and coauthors, while connectivity is a new inclusion based on the authors' existing experience with the PolyJet cleaning process. Each variable, its two states, and its associated hypothesis are presented in Table 3.1. For this experiment, the length of the channel is held constant (at an arbitrary length of 44.2 mm) as is the total cleaning time (set at 2 minutes). Representative test specimens are shown in Figure 3.3.

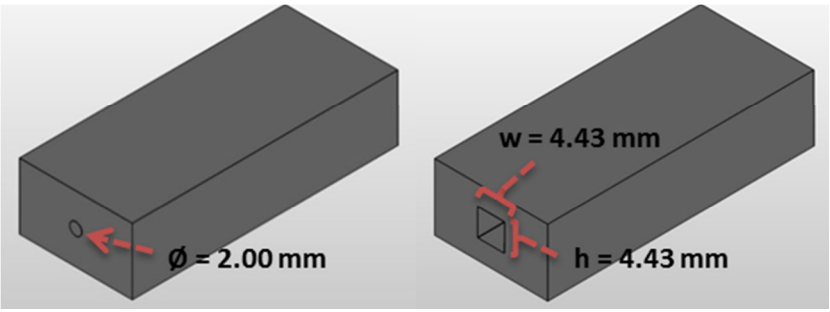

Figure 3.3. Example of Support Cleaning Test Specimens

Table 3.1. Experimental Variables in Support Material Removal

Independent Variables			
Variable Name	*State 1*	*State 2*	*Rationale/Hypothesis*
Cross-Sectional Geometry	Circle	Square	Support material may prove more difficult to remove from the sharp corners of a square cross-section.
Cross-Sectional Area	3.14 mm^2	19.64 mm^2	It may prove more difficult for the water stream to break away the support material in a smaller area.
Connectivity	Closed	Open	If the channel is closed at one end, support material may be removed more slowly since it will only have one exit point.
Dependent Variable			
Variable Name	*Units*		*Rationale*
Support Material Removed	% (by mass)		Measuring the percent mass of support material removed will help to determine the variables that slow the cleaning process (or impede it entirely).

To facilitate careful and consistent cleaning practice, a test rig was designed to maintain a constant distance and angle from the support-filled channels using a constant water pressure of 1750 psi (Figure 3.4). Because the emphasis of this work is on the effect of geometric and PolyJet process variables on manufacturing constraints, all post-process cleaning variables are held constant. This removes any variability due to cleaning approach, water pressure, etc. The specimens were each cleaned for two minutes using this rig; the percentage of support material removed (by mass) was then calculated by comparing the mass of the printed specimens before and after cleaning. This metric represents the ease of support material removal; the higher the percentage of support material removed at the end of the two minutes, then the easier the geometry is to clean.

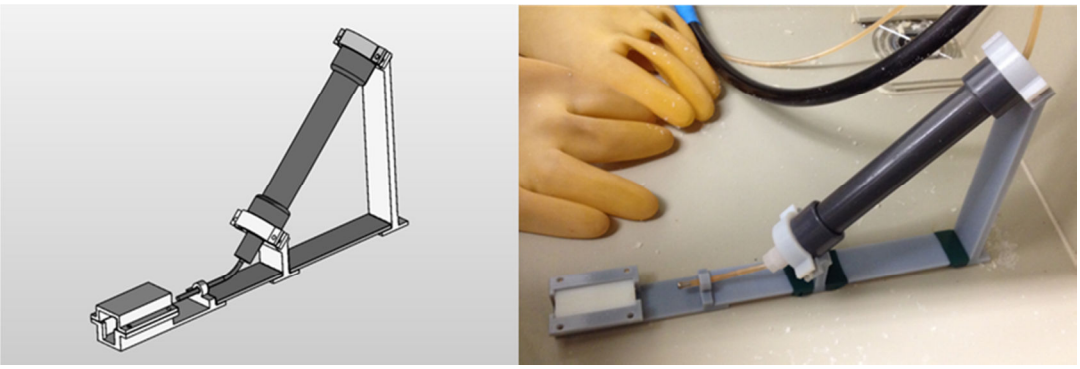

Figure 3.4. Cleaning Test Rig

3.4.3. Identifying Key Design and Process Variables

ANOVA analysis was performed on an L8 Taguchi array with two iterations of specimen cleaning. Observing a normal quantile plot of the residuals confirms that the data conforms to ANOVA's residual normality assumption (represented by the linear pattern seen in Figure 3.5a). In addition, a plot of the residuals against predicted values (Figure 3.5b) shows the residuals centered on zero with a seemingly random distribution, which confirms the constant residual variance assumption also inherent in the use of ANOVA.

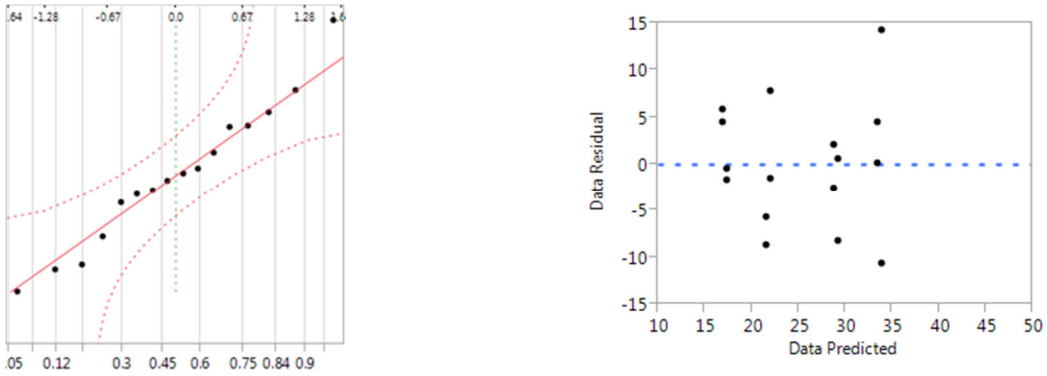

(a) (b)

Figure 3.5. a) Normal quantile plot of residuals and b) plot of residuals versus predicted values to confirm normality and constant variance ANOVA assumptions, respectively.

With the data properly following the key assumptions of ANOVA, the results in Table 3.2 offer details about the role of each variable. The information in the table suggests that only the cross-sectional area of the cleaning specimens significantly affects the amount of support

material removed in a fixed amount of time; it is the only variable with a p-value < 0.05. As hypothesized, the larger cross-sectional area results in a higher percentage of support material removal; this result aligns well with intuition as well as the results found by Vayre and coauthors. Figure 3.6 shows the desirability predictions based on the ANOVA analysis; as hypothesized, the larger cross-sectional area is predicted to offer the highest percentage of support material removed (again, the other two variables are not deemed statistically significant).

Table 3.2. Parameter Estimates – Support Cleaning

Term	Estimate	Std Error	t Ratio	Prob>|t|
Intercept	25.409	1.874	13.56	<.001*
Geometry[Circle]	-2.331	1.874	-1.24	0.282
Cross-Sectional Area[1]	-5.903	1.874	-3.15	0.035*
Connectivity[Closed]	0.233	1.874	0.12	0.907
RSquare	*0.742*			

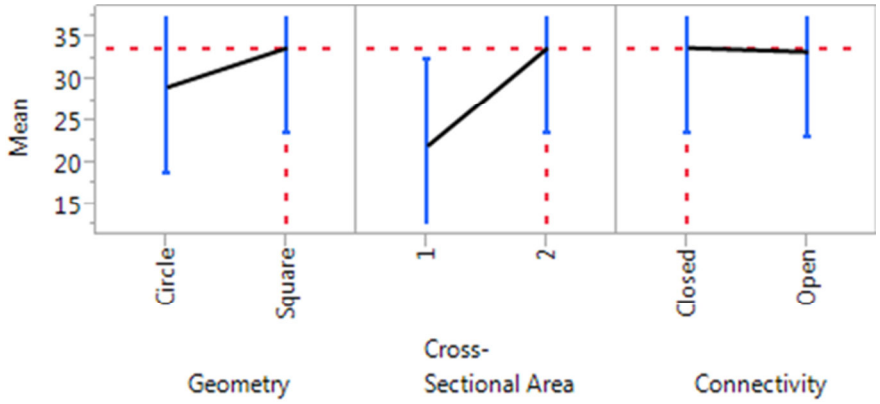

Figure 3.6. Desirability Prediction – Support Cleaning

3.4.4. Establishing Quantitative Design Recommendations

Experimentation is performed using additional values of cross-sectional area to establish a quantitative understanding of how channel area impacts the amount of support material removed. Since channel geometry and connectivity were not determined to have a statistically significant effect, they are held constant with a square geometry and closed connectivity, respectively. Five values of cross-sectional area are tested, with each area tested six times (Figure 3.7)

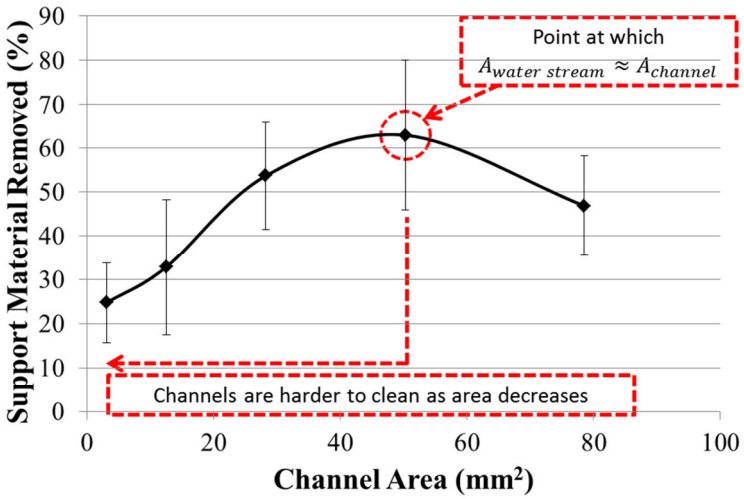

Figure 3.7. Mean Support Material Removed at Each Candidate Channel Area

The results of this experimentation confirm that the cross-sectional area of the channel does have a significant effect on the ability to remove support material from the channel. In general, the channels become easier to clean as the cross-sectional area increases to 50 mm^2. The plot in Figure 3.7 suggests that, at this point, the area of the water jet stream is approximately equal to the area of the channel; this ensures the most thorough cleaning when the water jet is held in a stationary position. As the area increases from 50 mm^2, the percentage of support material removed begins to decrease again. It can be assumed that this is because the area of the channel becomes larger than the area of the water stream; with the water jet held stationary, it is unable to reach the support material along the channel's walls. Based on this experimentation, the final recommendation would be to ensure that no channels/holes are smaller than 50 mm^2, which is approximately equal to the diameter of the water spray. Note that this channel diameter does not denote the smallest channel diameter that can possibly be cleaned; rather it represents the diameter that would allow for the most efficient cleaning. It is possible that the smaller diameter channels could be completely cleaned, but they would need to contain a significantly smaller mass of support material (and thus have a shorter length) in order for this to occur.

3.5. Minimum Resolvable Feature Size

3.5.1. Motivation

Every AM process has a limit on the smallest feature that it can create. This is most closely tied to the size of the deposition nozzle (or beam diameter, or particle size, depending on process type), the layer thickness, and the resolution of the x, y, and z positioning motors in the printer frame. Stratasys specifies that the PolyJet process has a resolution of 42 micron in the x- and y-directions with a layer thickness between 16 and 32 microns. However, it is necessary to validate how these quoted resolution values influence the smallest feature size that can be printed. While there has been some preliminary investigation into this with simple single-material rib shapes, as seen in [5], it is important to understand if the minimum manufacturable feature size differs between VeroWhite+ and TangoBlack+ material, surface finish types (denoted in the printer as "matte" vs. "glossy"), part orientation, feature direction (embossed or debossed), and feature shape.

The experiments described in this section are designed to answer the question, *What process parameters and geometric features affect the smallest part feature size that can be created by PolyJet?*

3.5.2. Experimental Methods

A standardized test specimen has been proposed by authors from NIST for use in characterizing the products of AM processes [67]. This specimen includes both rectangular and circular features to quantify the minimum feature size of the AM machine. As the high resolution of the PolyJet process is one of its primary advantages, there was concern over whether or not the NIST specimen would be small enough to identify the uniquely high resolution of the PolyJet AM process. As such, a specimen was designed which maintains the same minimum feature test geometry as the NIST specimen, but utilizes even smaller lower limits on the feature geometry being printed (Figure 3.8).

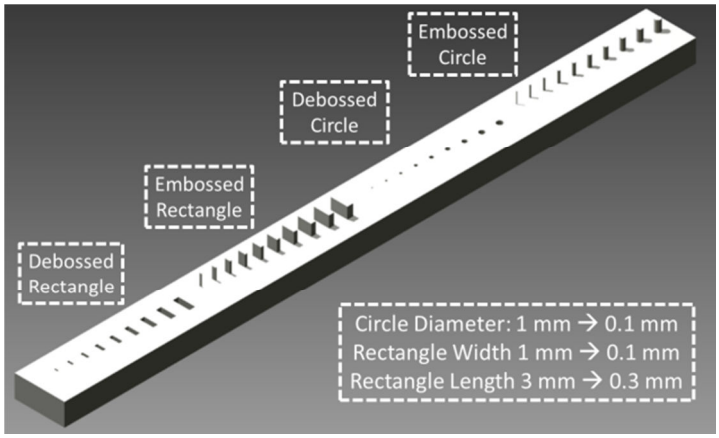

Figure 3.8. Minimum Feature Specimen

The independent variables for this experiment include (i) material type, (ii) surface finish, (iii) orientation, (iv) feature direction, and (v) feature shape. These variables, their two states, and the hypothesis associated with each are shown in Table 3.3. The dependent variable is the minimum feature recreated by the PolyJet process. All specimens were cleaned using an Objet-recommended water-jet station with a pressure of 1750 psi. Two iterations of each tested variable combination were performed.

Table 3.3. Experimental Variables in Minimum Resolvable Feature Size

Independent Variables			
Variable Name	*State 1*	*State 2*	*Rationale/Hypothesis*
Material Type	TB+	VW+	The compressive force of the roller may deform small features in the flexible TB+ during printing, hampering creation of smaller features.
Surface Finish	Glossy	Matte	The extra support material required for the matte surface finish may better support smaller embossed features and maintain the geometry of smaller debossed features.
Orientation	XY	XZ	The PolyJet's Z-resolution of 32 microns is actually finer than the XY resolution of 42 microns, so smaller features may be possible in the XZ orientation.
Feature Direction	Debossed	Embossed	The compressive force of the roller may damage embossed features during printing (but cannot damage debossed features). Cleaning may also damage smaller embossed features.
Shape	Circle	Rectangle	The droplet-based deposition pattern of the PolyJet process may have difficulty recreating the sharp corners of rectangular cross-sections at small feature sizes.
Dependent Variable			
Variable Name	*Units*		*Rationale*
Minimum Feature Size	mm		Measuring the minimum feature size will determine the smallest feature allowed in an automated design algorithm.

3.5.3. Identifying Key Design and Process Variables

Because of the larger number of independent variables under consideration, as well as the potential two-factor interaction effects between them, ANOVA analysis was used on a full-factorial L32 Taguchi array. A feature was considered resolvable if it maintained the true nature of the cross-sectional shape when observed with a digital microscope (e.g., rectangles had 4 distinct linear sides) and was of the same height/depth as the other specimens. As in Section 3.4.3, residual plots were used to successfully confirm adherence to the normality and equal variance assumptions inherent in the use of ANOVA. Note that the patterns for these minimum feature residual plots appear very similar to those already shown for support material removal in Figure 3.5 and, as such, they are omitted for the sake of brevity. Statistically significant values are denoted with an asterisk.

The results of experimentation show two statistically significant factors ($p < 0.05$) that contribute to the minimum PolyJet feature size, as well as three significant two-factor interactions. Shown in Table 3.4, these are the surface finish ($p < 0.001$) as well as the feature shape ($p = 0.004$). The statistically significant interactions are between surface finish and orientation ($p < 0.001$), surface finish and feature direction (p-value = 0.028), and orientation and feature direction ($p = 0.042$). In addition, orientation and the interaction between orientation and feature direction are each statistically significant, but only at a p-value of 0.062.

Table 3.4. Parameter Estimates – Minimum Feature

Term	Estimate	Std Error	t Ratio	Prob>|t|
Intercept	0.565625	0.015566	36.34	<0.001*
Material Type[TB+]	-1.73e-18	0.015566	-0.00	1.000
Surface Finish[Glossy]	-0.071875	0.015566	-4.62	<0.001*
Orientation[XY]	0.03125	0.015566	2.01	0.062
Feature Direction[Debossed]	-1.73e-18	0.015566	-0.00	1.000
Shape[Circle]	0.053125	0.015566	3.41	0.004*
Material Type[TB+]*Surface Finish[Glossy]	0.00625	0.015566	0.40	0.693
Material Type[TB+]*Orientation[XY]	-0.009375	0.015566	-0.60	0.555
Material Type[TB+]*Feature Direction[Debossed]	0.015625	0.015566	1.00	0.330
Material Type[TB+]*Shape[Circle]	-0.00625	0.015566	-0.40	0.693
Surface Finish[Glossy]*Orientation[XY]	-0.06875	0.015566	-4.42	<0.001*
Surface Finish[Glossy]*Feature Direction[Debossed]	0.0375	0.015566	2.41	0.028*
Surface Finish[Glossy]*Shape[Circle]	-0.015625	0.015566	-1.00	0.330
Orientation[XY]*Feature Direction[Debossed]	-0.034375	0.015566	-2.21	0.042*
Orientation[XY]*Shape[Circle]	-0.03125	0.015566	-2.01	0.062
Feature Direction[Debossed]*Shape[Circle]	-0.0125	0.015566	-0.80	0.434
RSquare	*0.823*			

The desirability predictions shown in Figure 3.9 predict that the smallest feature will be created with a combination of a glossy surface finish, an XZ orientation, and a rectangular shape.

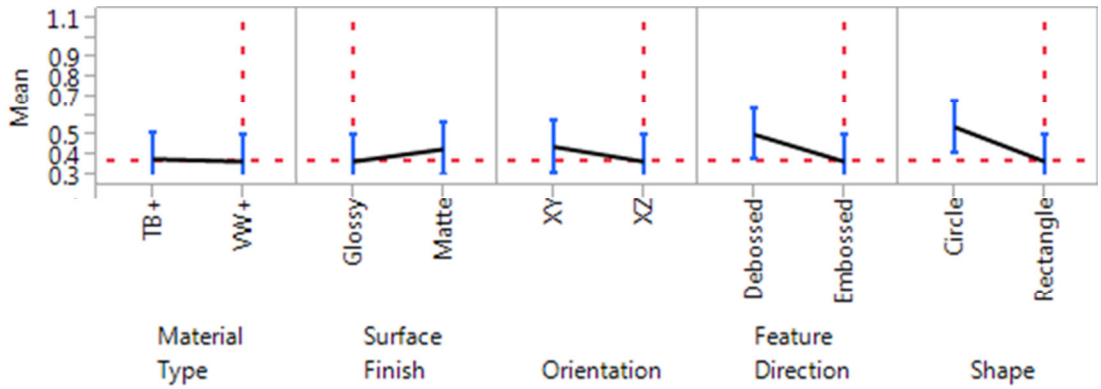

Figure 3.9. Desirability Prediction – Minimum Feature

While feature shape was determined to be significant, the analysis suggests that rectangular features will be better resolved than circular features. This is in direct opposition to the initial hypothesis that predicted that the sharp corners of small rectangular features would be more difficult to create. However, upon careful inspection, it appears that the larger cross-sectional area of the rectangular specimens allowed them to be more easily resolved, when compared to the circular specimens.

Testing and analysis also showed a clear advantage for the glossy finish over matte finish, mainly due to the recommended cleaning process for the PolyJet process. As discussed earlier in Section 3.2.2, the force of the water jet cleaning tends to break smaller parts. This type of breakage can be seen very clearly in these minimum feature size specimens when comparing glossy specimens to matte specimens. Specimens with matte, embossed features are especially susceptible to breakage, since there is more support material that needs to be removed from around the delicate embossed features. However, with the exception of the glossy XY specimens, all specimens require cleaning after printing (for consistency, the glossy XY specimens were cleaned as well, even though they had no support material). This means that it is impossible to tell the "true" minimum manufacturable feature size, since it is always possible that features will break during cleaning. Section 3.6 will present experiments where different features were placed under load by the water jet to determine the variables that affect a feature's ability to survive the cleaning process.

The interaction plots from Figure 3.10 illuminate several interesting two-factor effects on the minimum manufacturable feature size. The leftmost plot shows, as already mentioned, that surface finish has a direct effect on features in the XY plane. However, when the specimens are

oriented in the XZ plane, they require support material regardless of the surface finish condition, thus negating any advantages observed by using a glossy finish in the XY orientation. The second plot denotes an advantage in creating embossed features in the XZ plane; observing the specimens, the lengths of smaller features are more accurate at the XZ orientation rather than in the XY orientation. The final plot in Figure 3.10 reiterates the breakage of delicate embossed features when support material is removed with the water jet.

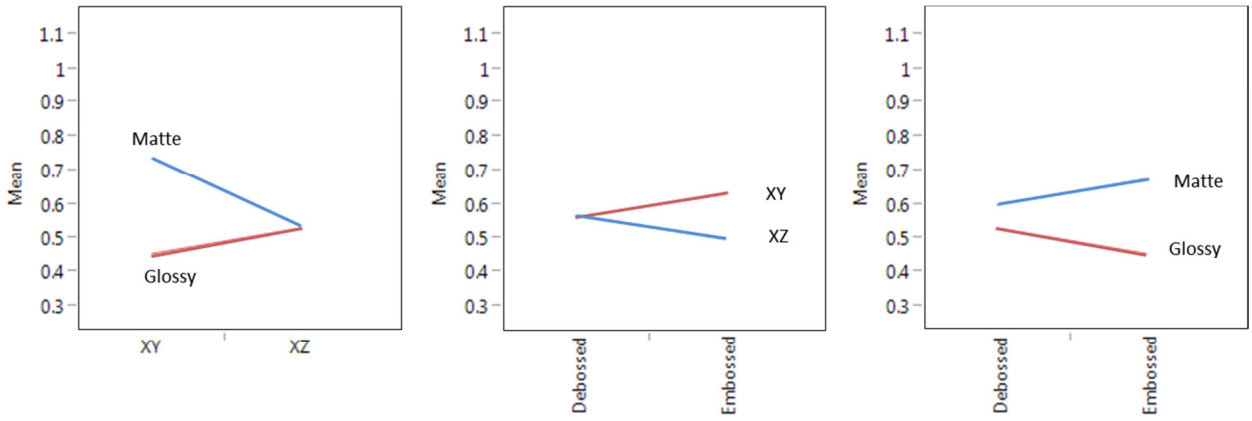

Figure 3.10. Significant Interaction Plots – Minimum Feature

The latter two interaction plots in Figure 3.10 also demonstrate why the embossed feature direction is chosen for the optimal configuration of independent variable states (as seen in Figure 3.9). Because of the significant interaction effects, the embossed feature direction will allow for a smaller manufacturable feature size when combined with an XZ orientation and glossy surface finish, despite the fact that the main effect of feature direction is not statistically significant by itself ($p = 1.000$).

3.5.4. Establishing Quantitative Design Recommendations

Several quantitative design recommendations can be made directly based on this full-factorial experimentation. In general, the "worst-case" scenario from experimentation can be used to recommend a minimum feature size that can be incorporated by a designer or by an automated design algorithm. Accounting for interaction effects, the poorest feature size would occur with a matte surface finish, XY orientation, embossed feature, and circular feature shape. This combination corresponds to a mean resolvable feature size of 0.897 mm in diameter (this

value was observed directly from the tested specimens). However, if the designer is able to account for all of the statistically significant variables investigated here, then it is possible to design minimum features of approximately 0.372 mm (a "best-case" scenario, again observed directly from the experimental specimens).

3.6. Survivable Feature Size

3.6.1. Motivation

An interesting additional consideration for the PolyJet process is that, while the system may be able to produce fine geometric features (as shown in Section 3.5), the feature may be broken while using the water jet to clean the part. To ensure that a part can survive the cleaning process, the minimum survivable feature might be larger than the minimum printed feature. This section will focus on determining the variables that have a dominant effect on the survivability of any printed parts.

The experiments described in this section are designed to answer the question, "*What process parameters and geometric features affect the smallest part feature size that can be cleaned without breaking?"*

3.6.2. Experimental Methods

To ensure consistent forces during cleaning, the same rig from the support cleaning tests (Figure 3.4) is used to determine the factors which affect minimum survivable feature size. However, the geometry of the specimens, and thus the specimen holder, differs slightly. Experience with the PolyJet process and the associated water jet cleaning process has shown that small, beam like features (such as those seen in complex cellular structures or in the previously discussed minimum feature test specimens) tend to be susceptible to breakage during cleaning. As such, this experimentation will focus on investigating variables that may have an impact on this type of beam-like geometry. The independent variables under investigation include (i) feature cross-sectional area, (ii) feature length, (iii) build material, and (iv) connectivity (e.g., cantilevered at one end or fixed at both ends). Investigating these variables will provide a general understanding of those factors that most drive breakage during cleaning.

Representative specimens are shown in Figure 3.11. Survivability is considered binary (either the feature broke after the allotted 1-minute cleaning time or it did not break). A full factorial experiment of these three variables was performed twice: once using VW+ for all of the tests and once using TB+ for all tests. The variables, their possible states, and the hypothesis for each are collected in Table 3.5.

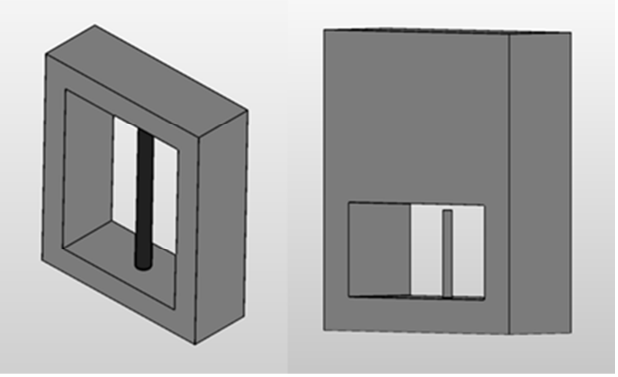

Figure 3.11. Example of Cleaning Survivability Test Specimens

Table 3.5. Experimental Variables for Survivable Feature Size

Independent Variables			
Variable Name	*State 1*	*State 2*	*Rationale/Hypothesis*
Connectivity	Fixed	Cantilevered	Having the feature cantilevered at only one end would result in a higher reaction load at that point, increasing the shear stress and the likelihood of part breakage at the joint.
Cross-Sectional Diameter	0.75 mm	1.50 mm	A smaller cross-sectional area will result in larger stresses in the feature due to the force of cleaning, which would again increase the likelihood of breakage.
Length	17.00 mm	6.86 mm	Having a longer specimen should increase the length of the moment arm at the fixation points due to the force of the water jet. This will increase the normal stresses at the joint and the potential for breakage.
Dependent Variable			
Variable Name		*Units*	*Rationale*
Survivability		Yes or No	Measuring survivability (in simple yes/no terms) will help to determine the variables that determine if a particular element in a final design will be able to survive the cleaning process.

3.6.3. Identifying Key Design and Process Variables

The survivability specimen experimentation was first performed for all 8 possible combinations of the main factors for VW+ material. Because the possible outcomes of testing are binary (i.e., a score of 2 denotes a survivable feature, while a score of 1 denotes a broken feature), the resulting data violates the residual normality assumption inherent in the use of ANOVA. Because of this, logistic regression is instead used with a likelihood-ratio Chi-square test to analyze the statistical significance of the three independent variables. As the p-values in Table 3.6 demonstrate, almost all of the broken VW+ specimens are due to the cross-sectional area (p-value of < 0.001). The resulting probability data is shown in Figure 3.12; note that, in this figure, the y-axis represents the probability of achieving a data value of "1" (i.e., a broken specimen). Because the desired data value is a "2" (i.e., a specimen that survived cleaning) the optimal configuration is one which minimizes the probability on the y-axis. The probability predictions in Figure 3.12 reinforce the importance of cross-sectional area; the predictions recommend a large cross-section to minimize VW+ specimen breakage.

Table 3.6. Likelihood-ratio Chi-square test – survivable feature size

Term	ChiSquare	Prob>|ChiSq|
Connectivity	1.726	0.189
Cross-Sectional Area	18.644	<0.001*
Length	1.726	0.189
RSquare	*0.936*	

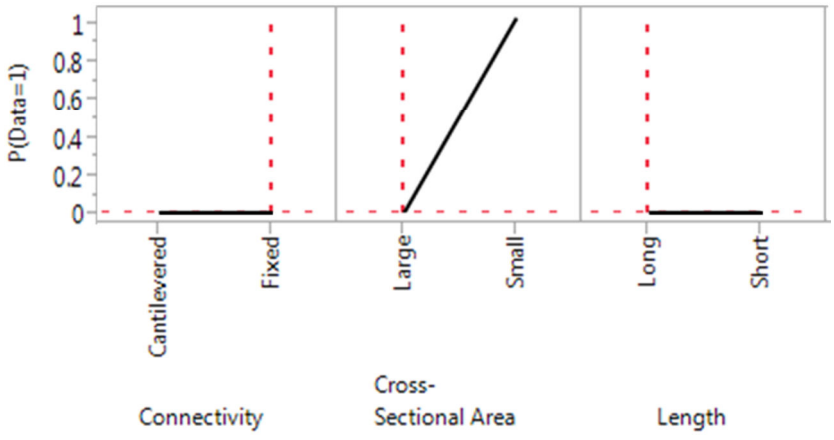

Figure 3.12. Probability of fracture based on factor configuration (data value of 1 denotes "fractured")

After performing the experiment with VW+ material, the same 8 combinations were printed using TB+ material. When tested, every cantilevered TB+ specimen survived cleaning, while every specimen fixed at both ends broke, regardless of length or cross-sectional area. This shows that connectivity should be the only significant independent variable when considering survivability of TB+ material. This differs from the VW+ specimens, which break almost entirely due to the specimen's cross-sectional area.

The differing results between VW+ and TB+ specimens make intuitive sense. For the more rigid VW+ material, thin features will not flex under the load of the water jet. Because of this, the cross-sectional area dominates whether a feature will survive, with larger areas experiencing lower shear stress from the water jet load. This gives them a higher chance for survival. On the other hand, when cantilevered, the elastomeric nature of the TB+ material causes it to flex under the water jet instead of fracturing. When the load is removed, the flexible material returns to its original position. When the TB+ specimen is fixed at both ends, it is unable to freely deflect and instead ruptures at the point of loading.

3.6.4. Establishing Quantitative Design Recommendations

Based on the statistical analysis, there are two directions that merit further exploration. These are i) the minimum cross-sectional area that can survive cleaning when made from VW+ and ii) whether fixed TB+ specimens can survive the cleaning process if their diameter is increased beyond the initial 1.50 mm. For both of these investigations, the test features are placed in the fixed connectivity condition and the long length condition is used. The VW+ features are tested at the same initial cross-sectional diameters (0.75 mm and 1.50 mm) as well as 4 other diameter values evenly spaced between the two extremes. The TB+ features were tested at the initial 1.5 mm diameter as well as 2.0 mm, 2.5 mm, 3.0 mm, and 3.5 mm diameters. Six runs were performed for each diameter value for each material. The resulting mean and standard deviation data is shown in Figure 3.13; note that, once again, a value of 1 designates a broken feature and a value of 2 designates a feature that survived cleaning.

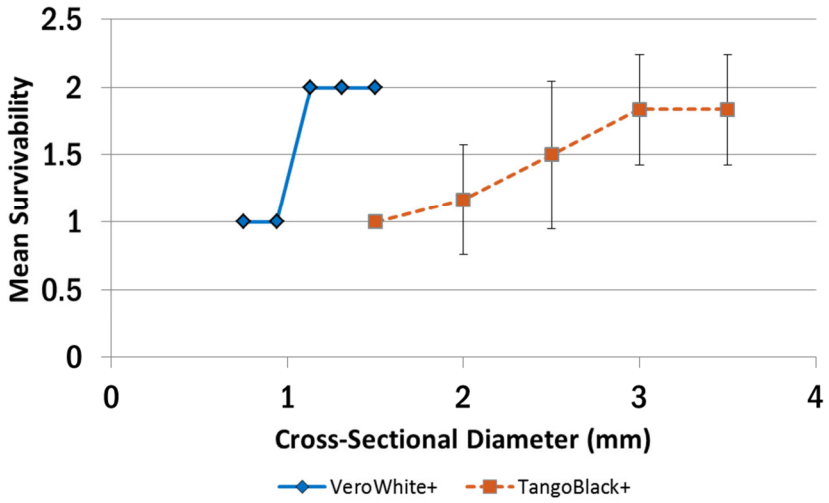

Figure 3.13. Mean Survivability for Each Candidate Diameter (Value of 2 Denotes "Survived")

The VW+ specimens show that small features can survive if the diameter is greater than or equal to 1.13 mm. There was no variation in the VW+ tests; for each diameter tested, either all specimens survived or all specimens failed. Meanwhile, the TB+ specimens show that it is possible for features to survive the cleaning process when fixed at both ends; five of the six 3.00 mm specimens were able to survive cleaning. However, fixed TB+ specimens below 3.00 mm were not able to consistently survive the cleaning process; features with a smaller diameter than this must be cantilevered in order to maximize the possibility of survival. These cross-sectional diameter values (1.13 mm for VW+ and 3.00 mm for TB+) can be incorporated by designers as minimum size constraints to help to ensure that the resulting designs can survive the water jet cleaning process.

3.7. Self-Supporting Angle

3.7.1. Motivation

While the PolyJet process in its default configuration relies on the use of support material for any constructed angle (save for perfectly vertical faces), it is possible to completely disable the use of support material. This would allow a designer to create a specimen without concern for 1) whether or not the small holes could be cleaned easily or 2) whether or not the water jet would damage small features. To take full advantage of this feature, it is important to know how

certain process variables affect the self-supporting angle when support material has been eliminated. By understanding these effects, a designer could be confident that angled surfaces (such as the surface highlighted with a dashed line in Figure 3.2) could be created properly without compromising the geometry of the final part or the safety of the machine.

The experiments described in this section are designed to answer the questions, "*What process parameters affect the most acute angle that can be created in the absence of support material?"*

3.7.2. Experimental Methods

The specimen used to test the self-supporting angle (seen in Figure 3.14) contains 10 faces, starting from a vertical 90 degree face (measured from the horizontal) and moving to a 72 degree face in 2 degree increments. The two independent variables under investigation are (i) material choice and (ii) orientation of the angled face with respect to the print head's roller. These variables are collected in Table 3.7 along with their associated hypotheses. Each possible combination of variables was tested twice.

Orientation is tested to determine if the roller is potentially pushing deposited droplets off of the self-supporting edge. If the roller is pushing droplets, this could result in a poorer self-supporting angle when the motion of the roller is perpendicular to the front edge of the specimen instead of parallel. The candidate orientations are 1) with the specimen's longest dimension aligned in the printer's x-direction and 2) with the specimen's longest dimension aligned in the y-direction.

Table 3.7. Experimental Variables in Self-Supporting Angle

Independent Variables			
Variable Name	*State 1*	*State 2*	*Rationale/Hypothesis*
Material Type	TB+	VW+	The compressive force of the roller may deform the flexible TB+ material during printing, causing fresh droplets to fall off the upper surface. If the material droplets have different viscosity properties, then one may be able to support higher angles than the other.
Orientation	X-Dominated	Y-Dominated	The roller may be pushing droplets off of the edge, which could result in a poorer self-supporting angle for a specimen predominantly oriented in the y-direction.
Dependent Variable			
Variable Name		*Units*	*Rationale*
Self-Supporting Angle		Degrees (from Horizontal)	Measuring the self-supporting angle with the given independent variables will show the recommended angle, orientation, and material type for printing optimized parts without support material.

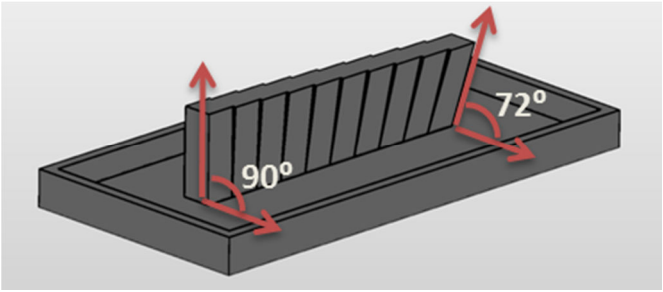

Figure 3.14. Self-Supporting Angle Specimen

3.7.3. Identifying Key Design and Process Variables

Experimentation shows that all specimens failed before the final 72 degree angled face. This failure is observed through stalagmites that appear to grow beneath the angled face (an example is shown in Figure 3.15). These stalagmites are formed by cured resin which has dropped off of the layer currently being manufactured.

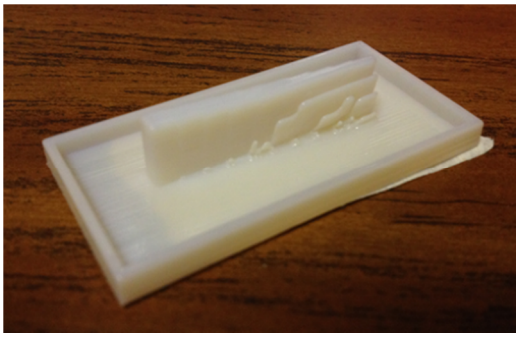

Figure 3.15. Stalagmites Denote a Non-Self-Supporting Angled Face

The maximum self-supporting angle was determined to be at the face before stalagmite growth was shown. The maximum angle was recorded for each of the 8 printed specimens. ANOVA analysis was performed on a full-factorial array to determine which of the factors, if any, had a significant effect on the maximum self-supporting angle. The data from the analysis confirms that the residuals are normally distributed with equal variance, which supports the use of ANOVA to identify significant variables. Once again, these residual plots are omitted from this paper for the sake of brevity.

From this analysis, it appears that material choice ($p = 0.205$) does not have a statistically significant effect ($p < 0.05$) on the maximum self-supporting angle (shown in Table 3.8). However, there does seem to be a potential pattern related to orientation ($p = 0.064$), which is expected due to the influence of the roller in the print head assembly. Based on the desirability predictions from this experiment (seen in Figure 3.16), the best self-supporting angle would be achieved on a specimen oriented in the y-direction (with the length of the specimen perpendicular to the travel of the print head).

Table 3.8. Parameter Estimates – Self-Supporting Angle

Term	Estimate	Std Error	t Ratio	Prob>|t|
Intercept	84.5	0.25	338.00	0.002*
Material[TB+]	-0.75	0.25	-3.00	0.205
Orientation[X-Dominated]	2.5	0.25	10.00	0.064
RSquare	*0.991*			

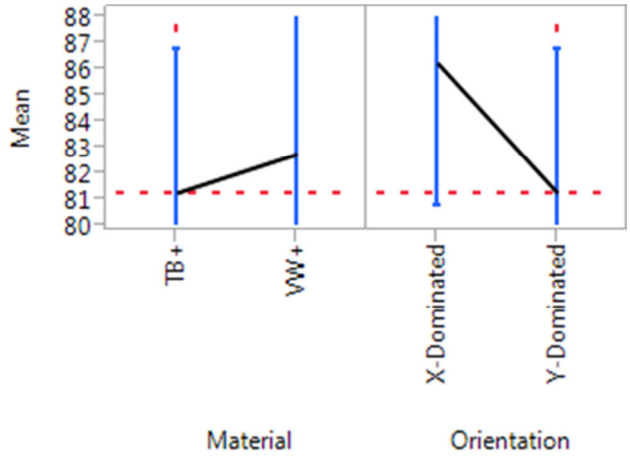

Figure 3.16. Desirability Prediction – Self-Supporting Angle

It is worth noting that the desirability predictions in Figure 3.16 are directly contrary to the initial hypothesis that specimens oriented in the x-dominated direction would see a better self-supporting angle. This data suggests that having the roller passing over the material droplets in the direction of the angled face's leading edge is actually beneficial.

3.7.4. Establishing Quantitative Design Recommendations

As was done with support material removal and survivable feature size, additional expanded testing is performed in order to confirm the quantitative effect that orientation has on the self-supporting angle. Since the material choice is determined not to have a significant effect from initial testing, a constant TB+ material is used in refined testing. The specimen is printed in the same x- and y-dominated orientations as before, as well as additional –x and –y orientations (180 degree rotations about the Z-axis). 6 specimens are printed for each of the four orientations.

Results confirm that orientation is a statistically significant factor in the self-supporting ability of printed PolyJet parts. The +/-y specimens performed significantly better than the +/-x specimens; the mean self-supporting angle was 85.16 degrees for the +/-x specimens while the mean angle for the +/-y specimens was 80 degrees. However, as Figure 3.17 shows, there was no significant difference between the +x and –x orientations, nor between the +y and –y orientations. It is also worth noting that the self-supporting angle was also far more consistent for the y-dominated orientations (denoted by the standard deviation bars in Figure 3.17); both y-dominated orientations had a standard deviation of zero. This testing shows that in order to

obtain the minimum (and most consistent) self-supporting angle, the critical angled faces should be oriented in the y-direction on the build tray.

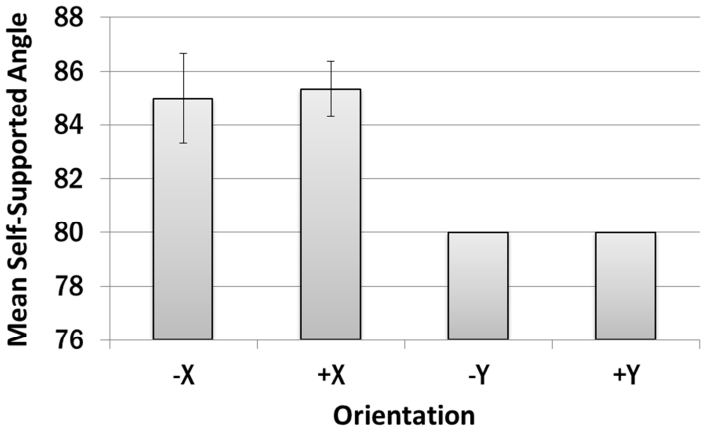

Figure 3.17. Mean Self-Supported Angle for Each Candidate Orientation

3.8. Conclusions and Recommendations for Future Work

DfAM guidelines have the potential to assist designers in better preparing manufacturable products for creation with multi-material jetting. This work presents a series of designed experiments to determine the key parameters that influence four specific manufacturing constraints in the PolyJet process. Once the key parameters were identified, additional experiments were performed to quantify the trends and minimum recommended values for the manufacturing constraints under investigation. The variables that affect minimum feature size, support material removal, feature survivability, and self-supporting angles, as well as the observed trends associated with each, are identified as follows:

- Support material removal is limited by the cross-sectional area of the channel as the dominant independent design variable. A minimum cross-sectional area approximately equal to the diameter of the water jet spray will result in highest percentage of support material removed from small channels.
- The minimum resolvable feature size has been shown to rely on surface finish and feature shape, as well as the interactions between surface finish and orientation, surface finish and feature direction, and orientation and feature direction. If a designer can account for the ideal

configuration of these variables, then it is possible to manufacture features that are half the size of a more general "worst-case" scenario.

- Feature survivability during cleaning was tied to cross-sectional area (for VW+ features) and feature connectivity (for TB+ features). While cantilevered connectivity must be used for very small TB+ diameters, the flexible TB+ specimens can still survive when fixed at both ends, though it requires a significantly larger diameter than the stiff VW+ material.
- Finally, the self-supporting angle in the absence of support material was driven by the orientation of the surface with respect to the roller, with y-dominated specimens offering better self-supporting angles. The recommended self-supporting angle is 85 degrees from horizontal, though it is possible to use a minimum of 80 degrees if all angled faces are oriented in the y-direction.

Identifying these key variables and the associated trends and quantitative design thresholds is crucial to ensuring that designs are manufacturable, whether designed manually or by an automated method, such as TO. While this work included investigation of important manufacturing constraints, all of the constraints were investigated through the lens of a single material printed at a time. There are still additional constraints that stem from the PolyJet process's capacity to deposit multiple materials in a single structure. Future work will focus on investigating these multi-material constraints. This will include investigation the effects of changing feature size on digital material properties (i.e., "when do the as-manufactured properties of intermediate 'grey materials' match the as-designed properties?").

4. PROCESS/STRUCTURE RELATIONSHIPS IN COMPOSITE PARTS MANUFACTURED VIA MULTI-MATERIAL JETTING

Coauthors: Dr. Christopher Williams

4.1. Abstract

The PolyJet material jetting process is one of the few additive manufacturing systems capable of creating monolithic, multi-material structures with a wide range of material properties potentially ranging from polypropylene-like to rubber-like. However, this multi-material capability introduces new design considerations that stand apart from considerations inherent in single-material processes. This paper investigates some of these key considerations necessary to understand the as-manufactured properties of PolyJet composite materials and how they relate to both the process itself and the structure of the printed part. Specifically, this includes an investigation of 1) observed changes in the elastic properties of PolyJet composites as the concentration of the base materials changes and 2) the effect of feature width on the material properties of PolyJet composites. By establishing process-structure-behavior relationships for these considerations, designers can better ensure that properties of their manufactured multi-material parts will meet the original design specifications.

4.2. Multiple Materials in Additive Manufacturing

Multi-material parts play a crucial role in engineering product design, ranging from consumer electronics to high-performance military parts. However, the majority of commercially available additive manufacturing (AM) processes are only capable of manufacturing parts consisting of a single material at a time. While researchers are looking to expand multi-material AM capabilities to other AM process types (such as polymer extrusion [68], stereolithography [69], laser sintering [70], and shape deposition manufacturing [34]), Optomec's LENS system and Stratasys' PolyJet technology are two of the only commercially available process types capable of creating monolithic, multi-material parts. The Optomec LENS system is a powder-based process capable of creating graded, multi-material metal structures. This capability has been demonstrated in literature through the creation of functionally graded implants using Co-Cr-Mo and Ti6Al4V [71]. The PolyJet process on the other hand, is a material jetting system capable of depositing up to three different polymeric

model materials in a single structure, with material properties ranging from polypropylene-like to rubber-like. It is this PolyJet process and its unique multi-material capabilities that are of interest to the study presented in this paper.

4.2.1. Prior Investigations of PolyJet Multi-Material Characterization and Design

While there is some existing research in the area of PolyJet material characterization (see for example work in [5,59–61]), little of it focuses on what is arguably the PolyJet process's most unique characteristic, namely its ability to create multi-material structures. The multi-material investigations that do exist focus on either i) the material properties of multi-material structures or, more commonly, ii) the aesthetic nature of multi-material parts.

On the area of multi-material property characterization, Moore and Williams conducted an investigation of the fatigue characteristics of the multi-material PolyJet parts [58]. They found that fatigue life is highly variable depending on how failure occurs within these specimens. Specifically, they found that having a sharp interface between TB+ and VW+ phases in a multi-material specimen could have a drastic impact on the fatigue life of the part. When loaded, specimens would often fail at the interface between the material types (92% of their specimens failed at the shear interface while only 8% failed at the weaker TB+ material). Failure at this interface location caused high variation when predicting of the specimen's number of cycles before failure.

While the multi-material capabilities of the PolyJet process offer mechanical advantages in product design, they likewise offer aesthetic and design opportunities of interest to the research community. For example, Vidimce and co-authors proposed a pipeline to more efficiently represent and manufacture multi-material products with the PolyJet process [72]. Their process, dubbed OpenFab, avoided the computational issues associated with representing geometry and materials in the PolyJet process and allowed for material composition to be specified for individual voxels at the resolution of the printer. Chen and co-authors designed a similar process (Spec2Fab) to assign PolyJet materials on a voxel-by-voxel basis [73]. They utilized a combined reducer tree and tuner network approach to determine the optimal material composition of a structure based directly on a description of the desired aesthetic behavior. Hasan and co-authors propose a third method for representing and fabricating heterogeneous structures with the PolyJet process [74]. In their work, they used an optimization-based approach to achieve desired

subsurface scattering properties based on input performance specifications. While the three studies discussed here demonstrate their performance through aesthetic specifications, the way in which they facilitate the design and fabrication of complex, multi-material structures could be easily transferred to more mechanically-minded products.

Apart from these experimental research investigations, there are also researchers approaching multi-material characterization and design from a computational standpoint. While perhaps not as immediately transferrable to the PolyJet process, these studies nevertheless offer insight that may assist in better understanding how the detailed design of multi-material composites may affect performance across jetting AM processes. For example, Hiller and Lipson investigated the theoretical performance or voxel-based digital materials through the use of finite element analysis [75]. One area of particular interest in their study was the quantification of elastic modulus properties for composite structures of varying composition. Through their modeling, they identified an exponential change in elastic modulus as the percent composition of their digital materials was adjusted. In addition, they were able to demonstrate that the elastic modulus of their composite structures was highly dependent on the microstructural distribution/arrangement of their base material phases. The main limitation of their study is that they did not have the opportunity to compare the predicted performance of their digital materials against true manufactured structures. Without manufacturing the structures, it is difficult to assess the impact that the manufacturing process might have on the material performance. The discussion and experimentation that follow in this paper are informed by the desire to investigate the process-structure-behavior relationships that arise from manufacturing such digital materials.

4.2.2. Context

The work within this paper is motivated by a desire to answer two key questions within the process-structure-behavior realm of multi-material PolyJet composites. The first of these questions is: *how do the elastic properties of the PolyJet's out-of-the-box digital composites change with respect to the percentage of the VW+ and TB+ phases within them?* Currently, the OEM does not provide this key relationship information, instead just providing a general range that all of the predefined digital materials will fall within. The second research question to be answered is *how (and why) do the material properties of the PolyJet's out-of-the-box digital composites change with respect to feature width?* Because of the way in which the PolyJet

process uses dithering to design and create its digital composites, there is a concern that smaller features may exhibit different elastic properties than large features due to incomplete representation of the intended dithering pattern. This is a crucial gap because, if a relationship is demonstrated, then it will identify a link between product structure and material behavior that users must consider when designing parts using the PolyJet's digital materials.

To answer the proposed research questions, the PolyJet process will first be discussed in more detail in Section 4.3, along with theory that will assist in quantifying the effects of phase composition and distribution on PolyJet composites. Dynamic mechanical analysis (DMA) is then introduced as a method for experimentally measuring changes in elastic material properties (Section 4.4). Results of experimentation and analysis are presented in Section 4.5. This section is separated into three subsections to clearly answer the gaps identified within the research questions: Section 4.5.1 contains results of experimentation on fixed-width specimens to identify the relationship between phase composition and elastic properties, Section 4.5.2 contains experimental results that relate material properties to feature width for several different composite blends, and Section 4.5.3 contains edge density calculations that serve to identify distribution changes which may trigger any property shifts seen in Section 4.5.2. Closure and recommendations for future work are presented in Section 4.6.

4.3. Multi-Material Composite Manufacturing via PolyJet 3D Printing

4.3.1. PolyJet Overview

The PolyJet process is the only commercially available system able to recreate fine geometric design features while simultaneously offering multi-material capabilities. Material jetting PolyJet printing is an AM material jetting process, wherein droplets of liquid photopolymer are deposited directly onto an elevator via a series of inkjet print heads [10]. As the material is deposited, two ultraviolet (UV) lamps cure the photopolymer in multiple passes. Each subsequent layer is jetted on top of the previous one. As droplets are ejected onto the build platform, a roller smoothes the droplets to create a consistent layer thickness. After printing, a sacrificial, hydrophobic support material must be manually removed using the recommended water jet cleaning station. Figure 4.1 shows a representation of the process and the print head assembly.

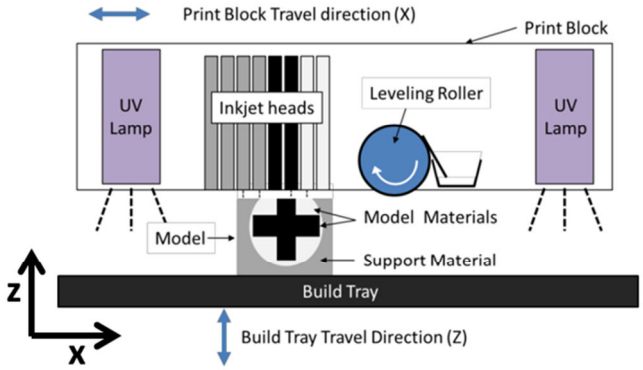

Figure 4.1. Representation of Direct 3D PolyJet Printing Process

The PolyJet process is able to create small features with a layer thickness of 16-32 microns and an in-plane resolution of 42 microns. In addition, the PolyJet process offers one significant, unique advantage among additive manufacturing process: the PolyJet process is capable of depositing two different materials on a pixel-by-pixel basis. This allows for creation of monolithic structures from multiple materials in a single build. One material combination of engineering relevance is VeroWhite+ (VW+), a rigid, white plastic-like material, and TangoBlack+ (TB+), an elastomeric, flexible black material. By patterning these two base materials on a voxel-by-voxel basis, it is possible to create material composites that possess elastic modulus properties ranging along the continuum between the two extremes. However, the system manufacturer currently only allows for out-of-the-box creation of nine specific material composites that they have designated.

4.3.2. Composite Manufacture via Dithering

As with a traditional two-dimensional color inkjet printer, PolyJet utilizes a process of dithering to create its series of intermediate materials (dubbed "digital materials"). Dithering can be considered a type of optical illusion, where the liquid photopolymer droplets are placed on a drop-by-drop basis in a specific pattern at a small scale. When the pattern is observed by the naked eye, the eye interprets the two-color pattern into an intermediate blend somewhere between the two extremes. Figure 4.2 demonstrates this concept using black and white pixels to mimic a greyscale image.

Figure 4.2. Example of Dithering to Represent Greyscale Images with Only Black and White Pixels

While some research has been done into demonstrating how the concept of dithering can be used for adjusting aesthetics in PolyJet printing [72], this concept is also what drives the material properties of the PolyJet process's intermediate digital materials. In the creation of the digital materials, the two extreme material properties are placed in a pattern which allows them to replicate macroscopic properties somewhere between the two.

The research presented in [75] suggests that there are three significant factors that have the potential to alter the material properties of composite materials such as the PolyJet's intermediate digital polymers. These factors include i) the percent composition of each phase, ii) the base material properties of each phase, and iii) the microstructural spatial distribution of the phases within the composite. These factors are crucial in the investigation of potential differences in the as-manufactured properties of PolyJet parts. Assuming that the base properties of the VW+ and TB+ materials remain constant, then any changes in the PolyJet's digital composites would be due to either i) a change in the percent composition of each material phase in the composite or ii) a change in the spatial distribution of the phases within the composite.

While the composition of VW+ and TB+ is known to change between the preset PolyJet composites, less is known regarding potential changes in distribution. For example there is concern that the intended dithering pattern is not properly replicated when observed in thin-walled or small-featured geometries. In essence, the printer may not have significant space to accurately recreate the ideal digital material pattern. This in turn may result in a change of spatial distribution and thus the material properties may not match the intended as-designed properties (an example of the concept is demonstrated in Figure 4.3, where a significantly

smaller feature size will have a drastically different pattern and thus different composite behavior).

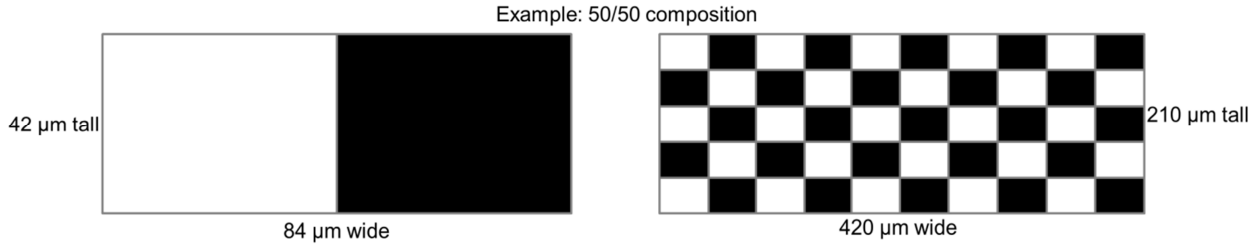

Figure 4.3. Example of Patterning Changes that Arise between Small Features (on the Left) and Large Features (on the Right)

4.3.3. Quantifying PolyJet Composite Composition and Distribution Information

To understand the effects that composition and distribution may have on the performance of PolyJet materials, the authors turn to the area of existing composite theory. As a general rule of thumb, a composite's overall modulus of elasticity design envelope can be described by the rule of mixtures. This concept relies on the properties of the base materials as well as the percent composition of each phase to predict the performance of an intermediate composite [76]. There are two bounds that can be predicted by this rule. The upper bound is representative of an iso-strain ("Voight") material arrangement (Equation 4.1), while the lower bound denotes an iso-stress ("Reuss") material arrangement (Equation 4.2). The two bounds enclose the potential performance envelope for any given composite consisting of two distinct material phases, such as the VW+ and TB+ composites of interest to this study. In these equations, E_{VW+} and E_{TB+} represent the elastic modulus values of the pure VW+ and TB+ materials while f_{VW+} and f_{TB+} are the volume fractions of the VW+ and TB+ materials in any given mixture.

$$E_{upper} = f_{VW+}E_{VW+} + f_{TB+}E_{TB+} \tag{4.1}$$

$$E_{lower} = (f_{VW+}/E_{VW+} + f_{TB+}/E_{TB+})^{-1} \tag{4.2}$$

While the rule of mixtures can identify the potential material design space based on the percent composition and distribution of phases within a composite, another method is needed to

quantify changes in the distribution pattern itself. To quantify the complex distribution information contain the PolyJet process's slices, the authors turn to existing work in the field of landscape ecology. Researchers in the realm of landscape ecology utilize numerous metrics to quantify natural distribution patterns, such as the distribution of forests covering a given geographic space. One such metric is called edge density (ED). ED is a simple metric that indicates the fragmentation of phases within landscape pattern data. ED is calculated as the ratio of total edge length between different material phases ($EL_{interphase}$) to the maximum possible edge length in the area of interest (EL_{max}, where the area of interest is defined by length x and width y) [77]. Equation 4.3 expresses this ratio mathematically. The result is a percent value between 0% and 100% where a large value suggests increased shape complexity and a more highly fragmented landscape configuration.

$$ED(\%) = 100 * \frac{EL_{interphase}}{EL_{max}} = 100 * \frac{EL_{interphase}}{x(y-1)+(x-1)y} \tag{4.3}$$

This distribution metric can be used to analyze the theoretical distribution of the different material phases in a TB+ and VW+ composite. By using this metric to analyze the distribution of phases in PolyJet composite bitmaps, it is possible to quantify differences in pattern that arise from changes in feature size (such as that seen Figure 4.3). The literature suggests that ED is an appropriate metric for this type of investigation, as research has shown it to be relatively insensitive to changes in the extents of the measured landscape [77] (which is a key consideration when comparing the distribution among specimens with different widths).

4.4. Methods

Three separate experimental and analytical tests are conducted in order to quantify the effects that phase composition and distribution have on the material properties of printed PolyJet composites. First, to quantify the relationship between material properties and composition, the elastic properties of both pure VW+ and pure TB+ will be experimentally measured. In addition to the pure materials, eight of the PolyJet's out-of-the-box digital material composites will also be measured (Section 4.5.1). This will not only allow for a general trend to be established for the PolyJet process's out-of-the-box composite options, but it will also allow for identification of where the properties of these composites fall within the theoretical space predicted by the rule of

mixtures. With this initial benchmarking performed, the elastic properties of these same digital materials will then be measured for decreasing feature widths (Section 4.5.2). By measuring these properties with respect to width, it will be possible to identify any property shifts that may occur due to incomplete dithering pattern recreation (a concern that was raised in Section 4.3.2). Finally, the slice information being sent to the PolyJet printer will be analyzed using edge density calculations to identify any changes in distribution within the dithering patterns (Section 4.5.3). In this way, changes identified in the phase distribution of slices can be related to any experimental shifts observed in testing.

For this purposes of this study, the elastic properties of the PolyJet digital materials will be measured using Dynamic Mechanical Analysis (DMA). While a detailed explanation of DMA theory is outside of the scope of this work, in general terms, DMA is an experimental materials testing method where an oscillatory force is applied to a material sample while temperature is varied. From analysis of this testing, it is possible to determine the storage modulus, loss modulus, and glass transition range of the material sample, among other properties. The storage modulus is representative of the elastic properties of the tested material and the loss modulus quantifies its damping properties. For more information on the theory behind DMA, the authors direct readers to [78]. DMA is an advantageous testing method for PolyJet materials due to 1) the small specimens needed for testing (thus conserving the PolyJet's relatively expensive materials) and 2) the method's sensitivity to material property shifts that should allow it to identify even small as-manufactured property changes. Testing is performed for all specimens using a TA Instruments Q800 Dynamic Mechanical Analysis system (Figure 4.4). Key testing parameters for all experimentation, such as oscillation frequency and temperature sweep values, are collected in Table 4.1.

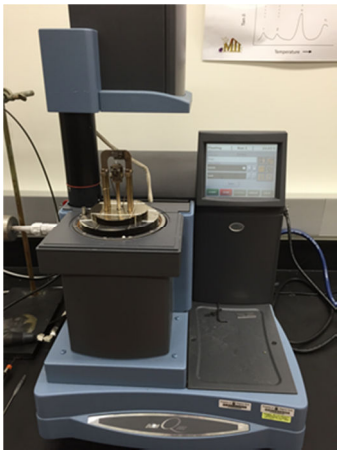

Figure 4.4. TA Instruments Q800 DMA System

Table 4.1. Key Parameter Values for DMA Testing

Preload Force	0.0100 N	*Soak Time*	5 min
Amplitude	15.0000 µm	*Ramp Rate*	3 ^{0}C/min
Frequency	10 Hz	*Final Temperature*	27 ^{0}C
Start Temperature	18 ^{0}C		

4.5. Results

4.5.1. Benchmarking of Fixed-Width Composite Materials

To answer the question "*how do the elastic properties of the PolyJet's out-of-the-box digital composites change with respect to the percentage of the VW+ and TB+ phases within them?"* the two pure PolyJet materials (TB+ and VW+) were tested using DMA, along with eight of the out-of-the-box intermediate digital composites. Tested samples are 6 mm wide, 1 mm deep, and 30 mm tall. The composites all contained different percent compositions of VW+ within them, with compositions at 18%, 25%, 36%, 82%, 90%, 95%, and 99% VW+. These percent composition values were derived through analysis of the bitmap slices being sent from the printer software to the printer itself; the bitmaps use different colors to designate different voxels of materials being deposited. The storage modulus and loss modulus value of each material is extracted from the test data at room temperature (21 degrees Celsius) and plotted in Figure 4.5 and Figure 4.6, respectively. By plotting this data, it is possible to form a preliminary working

curve that identifies a general trend between material percent composition and storage/loss modulus.

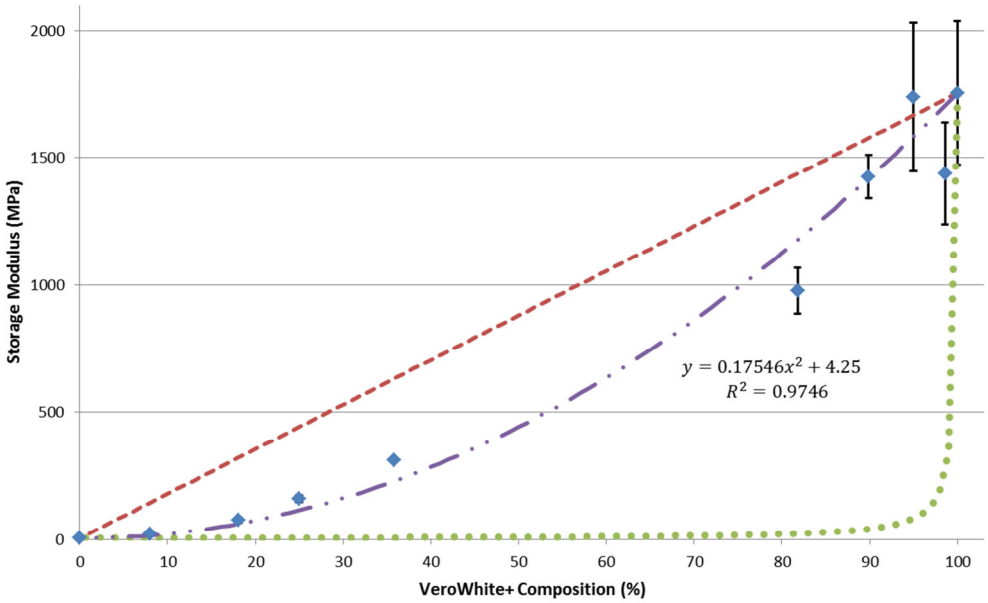

Figure 4.5. Polynomial Relationship between Material Composition and Storage Modulus at Room Temperature

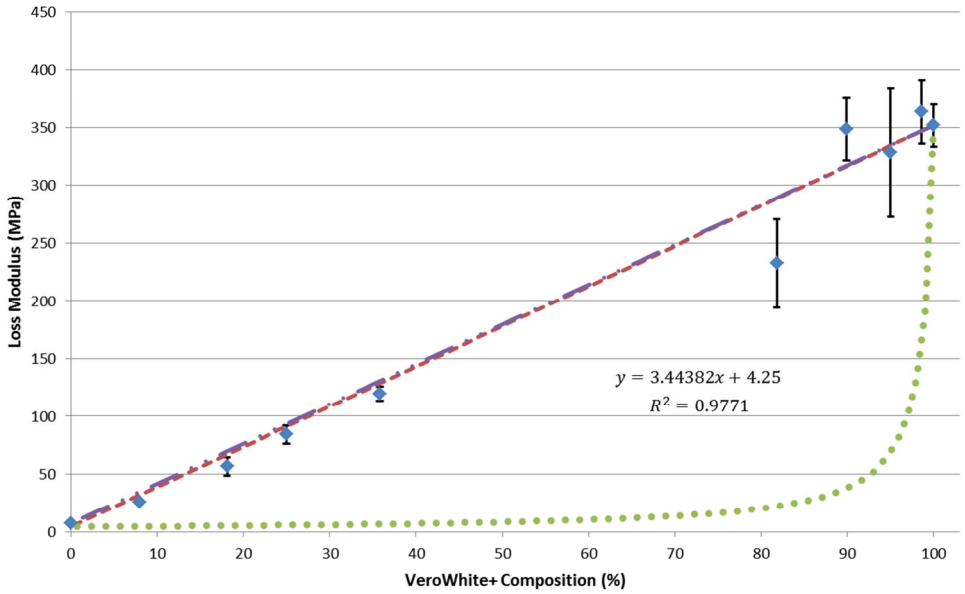

Figure 4.6. Linear Relationship between Material Composition and Loss Modulus at Room Temperature

Analyzing the storage modulus at room temperature demonstrates a clear polynomial relationship where the modulus value increases proportional to the amount of VW+ base material present in the composite material; this relationship is denoted by the central best fit line in Figure 4.5. The five data points on the left side of the curve represent digital materials that are mostly flexible, while the five points on the right are stiff materials. The out-of-the-box digital materials commercially available in the PolyJet process fall either below the 36% VW+ point or above the 82% VW+ point, hence the gap in data towards the center of the plot. Meanwhile, the loss modulus data demonstrates a linear relationship between loss modulus and VW+ composition (Figure 4.6). As both of these graphs show, predominantly VW+ composites also produce significantly more variation than predominately TB+ composites. This variation may be due in part to experimental variation in the actual deposited composition of the primarily VW+ composites. As Figure 4.5 demonstrates, the slope of the best-fit line for storage modulus increases with increasing VW+ composition. Because of this, any variation in the actual experimental composition of the specimen will cause a larger variation in the storage modulus values. In addition, it is possible that some of this variation is due to minor variations in spatial distribution of the base materials in the composite specimens. As the analytical work in [75] demonstrated, variations in how particles are randomly distributed will cause more variation in the elastic modulus of stiffer composites than flexible composites. As such, some of the variation in Figure 4.5 may be caused by an experimental distribution of VW+ and TB+ particles that is not completely consistent from specimen to specimen.

In addition to the line of best fit, Figure 4.5 also shows the upper and lower bounds predicted by the rule of mixtures. As discussed in Section 4.3.3, these bounds provide general estimates of the envelope in which a VW+/TB+ composite may fall. The PolyJet process offers a unique advantage over other most traditional composites in that its digital materials can, in theory, be custom-designed on a precise, pixel-by-pixel basis. Because of this, the authors hypothesize that it would be possible to design a custom composite pattern that could impart storage modulus properties anywhere within this envelope, with changes in percent composition causing a horizontal shift of any given baseline point and distribution changes causing a vertical shift of the point. For example, the VW+ and TB+ material phases could be distributed in a more

continuous, fiber-like pattern, which may impart composite properties closer to either the upper or lower bounds (depending on orientation).

4.5.2. Storage Modulus as Related to Feature Size

With the general trend of percent composition of VW+ established for a fixed feature width, this section seeks to answer *how do the established material properties of the PolyJet's out-of-the-box digital composites change with respect to feature width?* DMA is once again used to measure the elastic properties of four of the PolyJet's default digital materials: 95% VW+, 82% VW+, 36% VW+ and 18% VW+. Three additional specimen widths (4mm, 2mm, and 1mm) are tested to be compared to the 6mm wide specimens already examined in Section 4.5.1. Example test specimens are shown in Figure 4.7. By testing a variety of digital material compositions in this fashion, a relationship can also be drawn between digital material phase composition (i.e., how much TB+ and VW+ is present in the composite) and the change in material properties with respect to feature size. The DMA testing parameters remain identical to those presented earlier in Table 4.1.

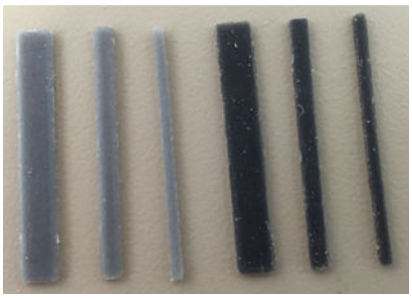

Figure 4.7. Example Test Specimens for Dithered Digital Materials

Each candidate width was repeated three times for a final total of 12 tested specimens per material blend. Figure 4.8, Figure 4.9, Figure 4.10, and Figure 4.11 present the average, room-temperature storage modulus as a factor of specimen width for the 95%, 82%, 36%, and 18% VW+ digital materials, respectively. Figure 4.12, Figure 4.13, Figure 4.14, and Figure 4.15 contain the loss modulus data for these same specimens. Along with each plot is a table that summarizes the p-values resulting from a series of t-tests. Each t-test compares the room-temperature storage modulus of the 4mm, 2mm, or 1mm wide specimen against that of the 6mm

wide specimen from Section 4.5.1 to determine if there is a statistically significant ($p < 0.05$, denoted by an asterisk) change in the storage modulus values as feature size decreases.

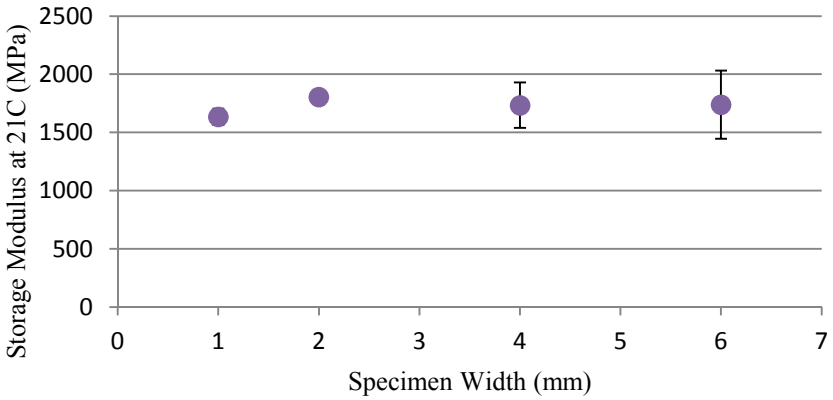

Comparison	*P-Value*
4 mm vs. 6 mm	0.491
2 mm vs. 6 mm	0.360
1 mm vs. 6 mm	0.289

Figure 4.8. Room Temperature Storage Modulus of 95% VW+ Specimens as a Function of Width, with Accompanying T-Test P-Values

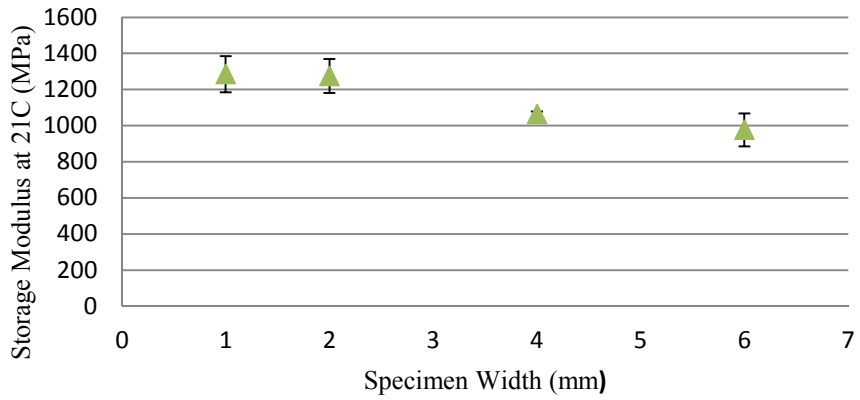

Comparison	*P-Value*
4 mm vs. 6 mm	0.091
2 mm vs. 6 mm	0.008*
1 mm vs. 6 mm	0.008*

Figure 4.9. Room-Temperature Storage Modulus of 82% VW+ Specimens as a Function of Width, with Accompanying T-Test P-Values

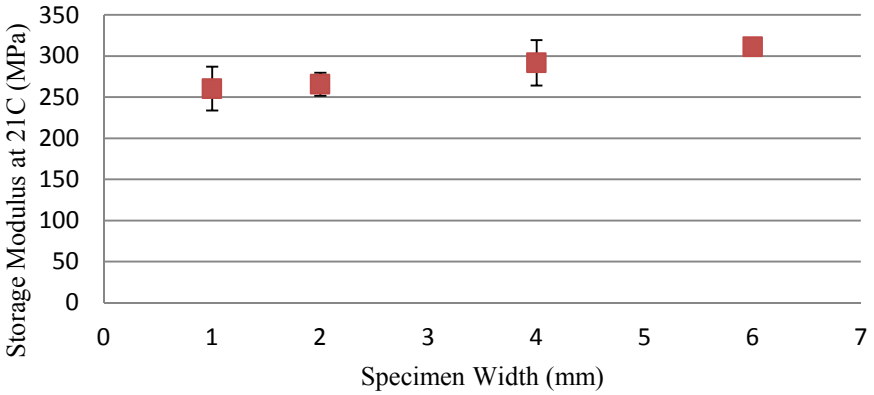

Comparison	*P-Value*
4 mm vs. 6 mm	0.145
2 mm vs. 6 mm	0.002*
1 mm vs. 6 mm	0.015*

Figure 4.10. Room-Temperature Storage Modulus of 36% VW+ Specimens as a Function of Width, with Accompanying T-Test P-Values

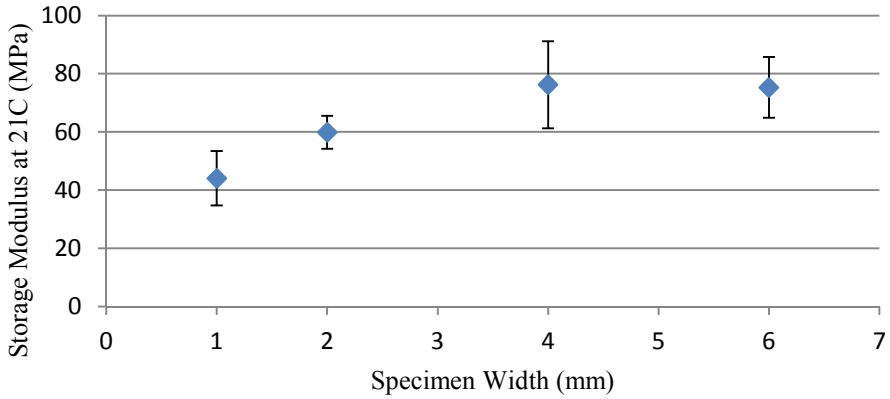

Comparison	*P-Value*
4 mm vs. 6 mm	0.466
2 mm vs. 6 mm	0.044*
1 mm vs. 6 mm	0.009*

Figure 4.11. Room-Temperature Storage Modulus of 18% VW+ Specimens as a Function of Width, with Accompanying T-Test P-Values

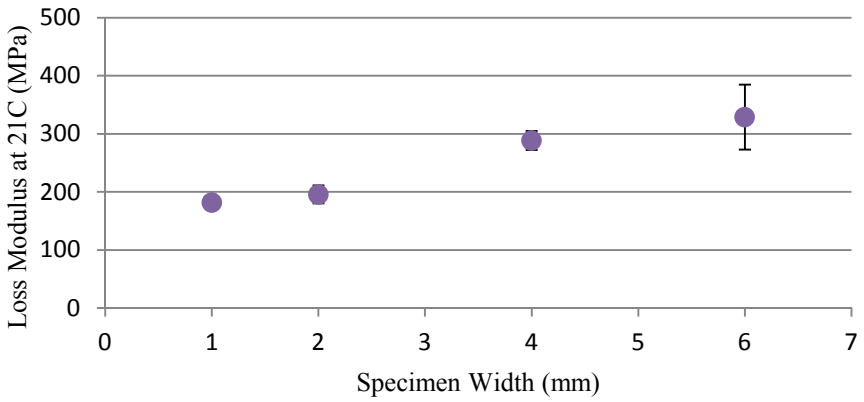

Comparison	*P-Value*
4 mm vs. 6 mm	0.150
2 mm vs. 6 mm	0.008*
1 mm vs. 6 mm	0.005*

Figure 4.12. Room-Temperature Loss Modulus of 95% VW+ Specimens as a Function of Width, with Accompanying T-Test P-Values

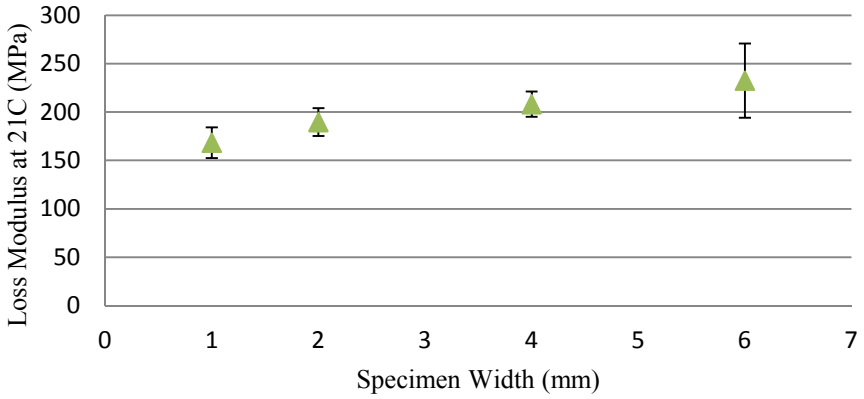

Comparison	*P-Value*
4 mm vs. 6 mm	0.178
2 mm vs. 6 mm	0.072*
1 mm vs. 6 mm	0.028*

Figure 4.13. Room-Temperature Loss Modulus of 82% VW+ Specimens as a Function of Width, with Accompanying T-Test P-Values

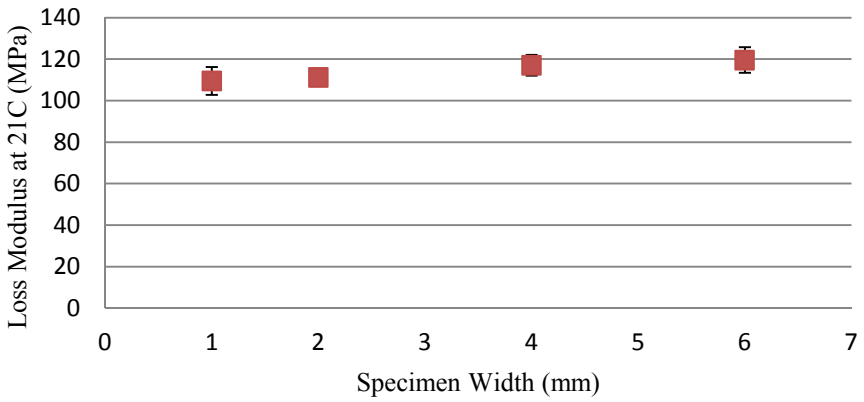

Comparison	*P-Value*
4 mm vs. 6 mm	0.307
2 mm vs. 6 mm	0.042*
1 mm vs. 6 mm	0.064*

Figure 4.14. Room-Temperature Loss Modulus of 36% VW+ Specimens as a Function of Width, with Accompanying T-Test P-Values

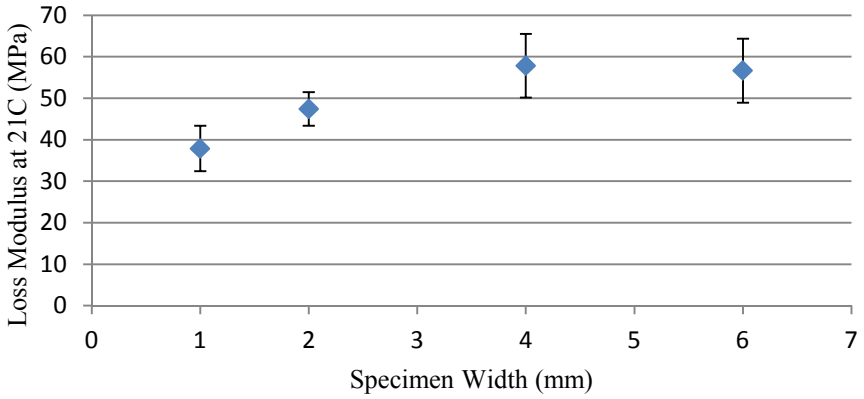

Comparison	*P-Value*
4 mm vs. 6 mm	0.431
2 mm vs. 6 mm	0.070*
1 mm vs. 6 mm	0.013*

Figure 4.15. Room-Temperature Loss Modulus of 18% VW+ Specimens as a Function of Width, with Accompanying T-Test P-Values

The data gathered from DMA testing shows different behavior for each of these specimens. The 95% VW+ experimentation exhibits no statistically significant difference in storage modulus between the 1mm wide specimen and the 6mm wide specimen (likely due to the large standard deviation in the initial 6mm wide specimen). However, the other three digital material types do exhibit significant storage modulus changes with respect to feature width, beginning at the 2mm width specimens. In general, the 18%, 36%, and 82% VW+ composites exhibit a pattern where the material properties shift towards that of the most heavily concentrated material as feature width decreases (i.e., predominately VW+ specimens become stiffer, predominately TB+

specimens become more flexible). In contrast, the loss modulus data shows that all of the composition types experience a downward shift as the specimen size decreases from 6mm wide to 1mm wide (with a significant difference again occurring at the 2mm specimen width). These experimental shifts in both storage modulus and loss modulus suggest that there is indeed a difference that exists between the as-designed and as-manufactured properties of thin walled, digital material structures.

An additional experiment was performed in order to determine if the modulus shifts seen in Figure 4.9-Figure 4.15 are also dependent on part orientation during printing. For this orientation experiment, the 36% specimens were reprinted rotated 90 degrees about the printer's x-axis (so that they were standing on their thin, long sides). DMA testing was performed on these re-oriented specimens using the same testing parameters from Table 4.1. The resultant storage modulus data is presented in Figure 4.16, while the loss modulus data is in Figure 4.17.

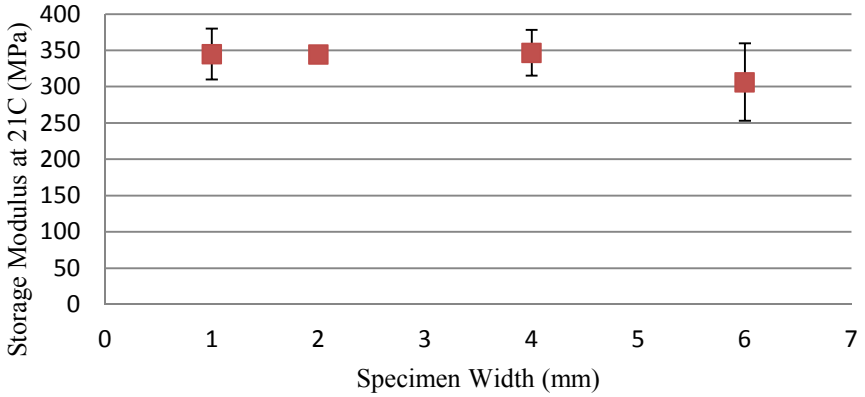

Comparison	*P-Value*
4 mm vs. 6 mm	0.162
2 mm vs. 6 mm	0.142
1 mm vs. 6 mm	0.222

Figure 4.16. Room-Temperature Storage Modulus of XZ-Oriented, 36% VW+ Specimens as a Function of Width, with Accompanying T-Test P-Values

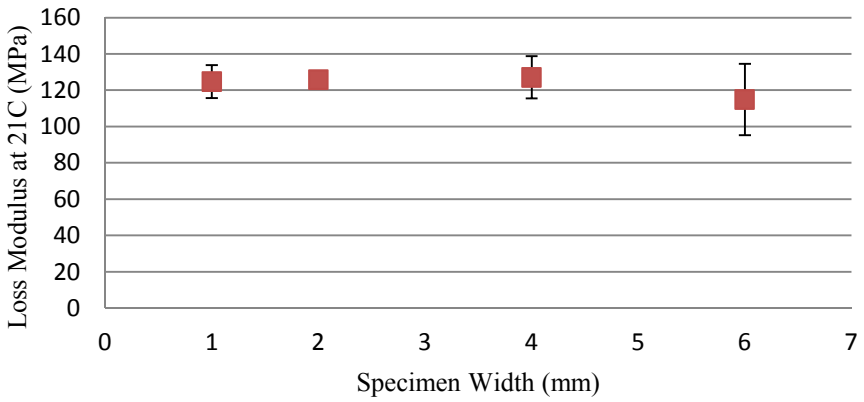

Comparison	*P-Value*
4 mm vs. 6 mm	0.204
2 mm vs. 6 mm	0.194
1 mm vs. 6 mm	0.283

Figure 4.17. Room-Temperature Loss Modulus of XZ-Oriented, 36% VW+ Specimens as a Function of Width, with Accompanying T-Test P-Values

As this data shows, there is no statistically significant difference between the XZ-oriented, 36% VW+ specimens of different widths. Unlike the modulus data for the 36% VW+ specimens in Figure 4.10 and Figure 4.14 (which decreases slightly as width decreases), the storage and loss moduli for the XZ-oriented specimens remain relatively constant with width. This suggests that orientation of a small feature will impact the magnitude of change in the as-manufactured properties. However, in order to confirm this, testing of additional digital material compositions oriented in the XZ plane is needed. Because of this, the analysis in the remainder of this paper will focus solely on the original XY-oriented specimens.

4.5.3. Edge Density Calculations

With a likely relationship between feature width and composite storage modulus identified through the DMA experimentation in Section 4.5.2, the authors now seek to understand why this relationship exists. Because of the concern over incomplete recreation of dithering patterns in small features (as discussed in Section 4.3.2) the authors seek to identify if distribution changes are occurring as the PolyJet system applies dithering patterns to thinner features. As such, the concept of edge density (from Section 4.3.3) is applied to the bitmap information being generated for each of these specimens. By calculating the edge density values of each of these slices, it is possible to determine if a change in distribution is occurring. If these calculations confirm a change in distribution, then it is likely the shift in material properties can be attributed to it.

In order to quantify the content of each specimen's slices, the distribution bitmap is extracted from the PolyJet system's software. One slice is extracted for the 6mm, 4mm, 2mm, and 1mm wide specimens for each composite from Section 4.5.2. An initial analysis of the percent composition of each of these slices shows that the percentage of VW+ in each specimen remains relatively constant (<1% change) regardless of specimen width. As such, attention is turned to the distribution of the TB+ and VW+ phases within the slices. Each slice is first divided along its length into 19 even segments (an arbitrary number chosen to allow for even division of the specimen's total pixel length). The ED is then calculated for each of the 19 segments, as well as the mean ED and standard deviation for all segments. These calculations were performed for all four digital materials of interest at 6mm, 4mm, 2mm, and 1mm widths. The results are collected in Figure 4.18-Figure 4.21.

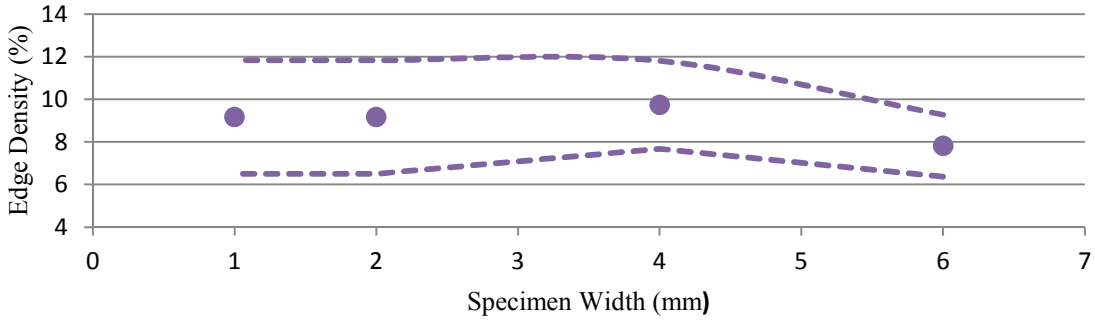

Figure 4.18. Mean Edge Density for 95% VW+ Different Specimens with Upper and Lower 2-Standard Deviation Bounds

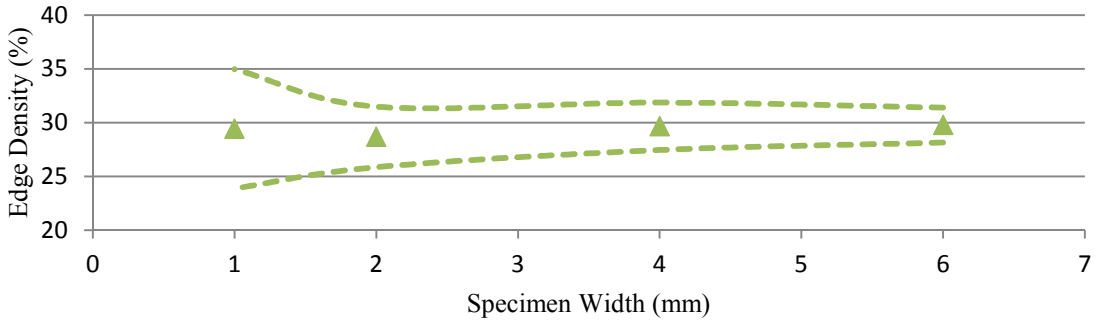

Figure 4.19. Mean Edge Density for 82% VW+ Different Specimens with Upper and Lower 2-Standard Deviation Bounds

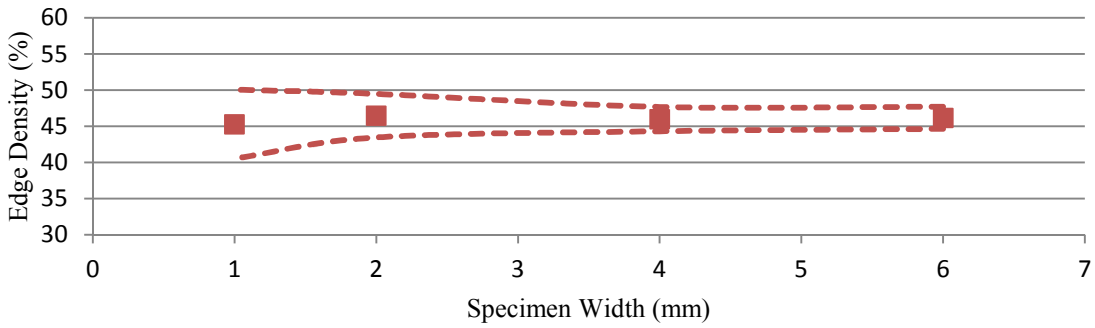

Figure 4.20. Mean Edge Density for 36% VW+ Different Specimens with Upper and Lower 2-Standard Deviation Bounds

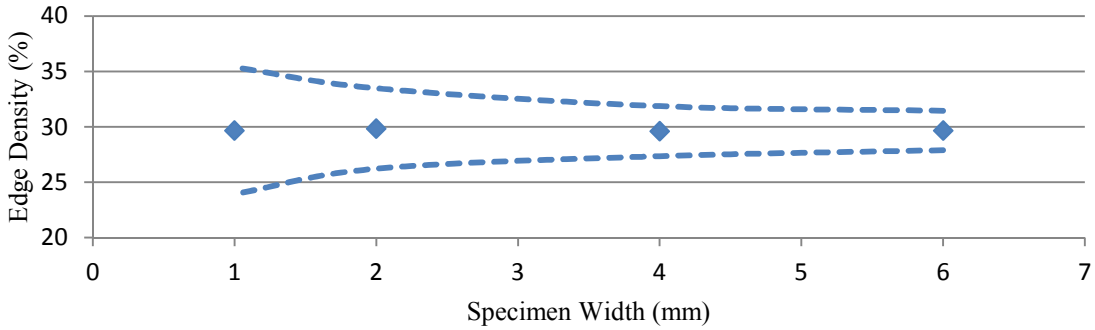

Figure 4.21. Mean Edge Density for 18% VW+ Different Specimens with Upper and Lower 2-Standard Deviation Bounds

Observation of the ED values for each digital material and feature width shows that the mean ED value remains relatively constant regardless of the specimen's width (hence applying ED simply to the entire specimen, rather than segments, would provide no revealing information). However, with the bitmaps divided into even segments along the length, there is a clear increase in the standard deviation of ED between segments as specimen width decreases. This increase in the standard deviation suggests that there is more variety in distribution patterns along the length of the thinner specimens, which will signify a change in distribution at certain points between specimens. As an example, consider the ED values presented in Table 4.2. These values are representative of the ED value in each of 19 segments along the length of a 6mm, 4mm, 2mm, and 1mm wide test specimen with 36% VW+ composition. As the values in this table

demonstrate, the ED variation increases as width changes from 4mm to 2mm to 1mm, which is caused by increasingly large distribution changes at certain segments in the specimen (such as in sections 3, 7, and 15).

Table 4.2. ED Values for Each Segment Along 36% VW+ Specimen

		36% VW+								
		Width						Width		
		6mm	*4mm*	*2mm*	*1mm*			*6mm*	*4mm*	*2mm*	*1mm*
Segment	*1*	47.19	45.52	46.77	47.39	Segment	*11*	45.91	46.99	47.14	44.91
	2	45.02	45.29	45.92	46.61		*12*	46.38	45.79	46.53	46.61
	3	46.13	46.38	47.87	41.64		*13*	46.86	47.05	45.86	45.56
	4	45.99	45.70	43.97	45.82		*14*	47.35	44.40	48.17	46.34
	5	46.58	45.85	43.85	44.39		*15*	47.29	45.43	43.67	42.30
	6	45.61	46.64	45.68	45.04		*16*	45.67	45.93	49.57	48.43
	7	45.73	46.32	47.08	39.69		*17*	46.68	45.79	47.26	43.86
	8	45.85	46.05	47.02	46.34		*18*	46.26	47.08	47.26	48.04
	9	45.04	44.14	46.22	42.95		*19*	44.79	47.20	47.31	46.07
	10	46.80	46.23	45.62	48.69						

The authors hypothesize that, if we consider the design envelope generated earlier with the rule of mixtures (Figure 4.5), this variation in distribution along the length of the thin specimens may be causing the baseline measurement to move vertically within the design envelope. This vertical shift is then likely responsible for the experimental property changes observed in Section 4.5.2, with distribution variation in predominately VW+ specimens causing an upward shift in storage modulus and distribution variation in predominately TB+ specimens causing a downward shift in storage modulus.

4.5.4. Implications for Material Jetting

The connections identified in Section 4.5.3 suggest that it is not sufficient to design digital materials based on percent composition alone. In its current state, the material jetting process causes a direct connection between the storage/loss moduli of digital composite materials and the

width of features made of these composites. In order to create more robust material properties that are independent of feature size, there are two avenues for change. The first is an increase in the XY resolution of the material jetting process, achieved through the use of smaller ejection nozzles. By implementing smaller nozzles, the dithering patterns could be more precisely recreated in small features, which would maintain constant material properties in feature widths smaller than the 2mm identified in this study. Alternatively, software improvements could be introduced that adjust the multi-material dithering pattern in direct response to the size of a designed feature. Pixel-by-pixel tailoring of the deposition/dithering pattern could create material properties that exactly match those desired by the designer (though this would necessitate further investigation into the micromechanical behavior of disparate multi-material droplets).

4.6. Conclusions and Recommendations for Future Work

In this paper, the authors sought to identify how the as-manufactured material properties of the PolyJet process's digital composite materials are affected by changes in both composition as well as feature size. DMA experimentation demonstrated a distinct relationship between the storage modulus of out-of-the-box PolyJet composite materials and the concentration of VW+ material in them. Using this same DMA experimentation on digital material features of decreasing width showed a shift towards the properties of the dominant material phase as specimen thickness decreases (e.g., predominately VW+ specimens would become stiffer, predominately TB+ specimens would become more elastomeric). Evaluation of the print slices suggests that the distribution of material phases within thinner specimens may be responsible for this shift in material properties. Edge density analysis showed increased variation of distribution patterns along the length of thin specimens; the authors hypothesized that this distribution variation in turn causes a vertical shift within the concentration-modulus design space (Figure 4.5) which, in turn, causes the experimental shift in properties seen during testing with decreasing feature width.

Future work will focus on further addressing the design elements that cause the experimental results seen in this study. As an example, efforts will be made to determine a material patterning method that can effectively fill in the space between 36% VW+ and 82% VW+ specimens along the polynomial benchmarking curve. In addition, specimens will be manufactured to

experimentally confirm the PolyJet material's adherence to the upper and lower rule of mixtures curves. Finally, the concept of functionally graded materials and how they might be designed and manufactured with the PolyJet process will be studied.

4.7. Acknowledgements

The authors would like to acknowledge Dr. Bruce Orler and Dr. David Dillard for their sharing their expertise in materials as well as their assistance with establishing appropriate experimentation methods. The authors also acknowledge MII as well as TA instruments for their support of the MII Materials Discovery Center.

5. A PROCEDURE FOR CREATING ACTUATED JOINTS VIA EMBEDDING SHAPE MEMORY ALLOYS IN POLYJET 3D PRINTING

Coauthors: Dr. Amelia Elliott, Dr. Christopher Williams

5.1. Abstract

Additive manufacturing's layer-by-layer fabrication approach allows the user to access the entire volume of the part throughout the build process. This allows for the embedding of functional components and actuators to enable the fabrication of complex systems in a single process. A process for the embedding of shape memory alloy actuating wire within direct PolyJet 3D printed parts is presented in this article. A series of "Design for Embedding" considerations are presented for achieving successful and repeatable embedding results. These considerations include guide channel design, design of shape converters for irregularly shaped elements, and design of wire fixation points. The embedding process is demonstrated with two case studies: a simple compliant joint specimen with a straight shape memory alloy wire and an antagonistic joint design with spring-shaped shape memory alloys. The process is characterized through an exploration of the potential for surface defects in the final specimens, as well as basic quantitative and qualitative evidence regarding performance of the final embedded actuators.

5.2. Embedding Components via Additive Manufacturing

Additive Manufacturing (AM) is a class of manufacturing processes whereby artifacts are built up in a layer-by-layer fashion. This is in direct contrast to traditional subtractive manufacturing where material is removed from stock raw material until the desired final shape is formed. The result is that AM processes can create complex parts that are impossible to create in any other way, while simultaneously reducing material waste. There are many AM processes; each is differentiated by the manner in which they deposit material and/or energy to create each layer.

A fundamental advantage of the layer-by-layer fabrication approach found in AM technologies is the ability to access the entire volume of the workpiece throughout the build process [79]. This lies in contrast to traditional manufacturing techniques, where one only has access to the external surfaces of the part. As such, AM affords the opportunity to embed components such as circuits, sensors and other functional components (e.g. motors, threaded

rods, etc.) into a part as it is being fabricated. This allows for the direct fabrication of functional assemblies and mechanisms within the AM machine without the need for a secondary assembly step. This embedding capability provides an opportunity for the realization of such applications as actuated robotic limbs, smart structures with embedded sensors, and energy harvesting devices with embedded piezoelectric materials.

For the work presented here, the authors are motivated by the possibility of creating actuated systems by embedding shape memory alloys into printed parts. Shape memory alloys (SMAs) are a type of active material capable of recovering their shape when exposed to a temperature increase. Because of their potential as simple, silent actuators that can perform reliably for millions of cycles, SMAs have been actively pursued in past research towards the design of morphing aircraft. One of the most notable, large scale examples of using SMA actuators in an aerospace context was the Smart Wing program, a collaboration between the AFRL, DARPA, and Northrop Grumman [80]. For a summary of the many studies that have been performed regarding morphing wings and SMA actuators, the authors suggest work by Sofla and co-authors [81]. Aside from research into morphing wings, researchers are also investigating the use of SMAs in the design of origami-like structures that are capable of folding and changing shape upon actuation of the SMAs. For example, Peraza-Hernandez and co-authors [82,83] have recently explored this concept through the theoretical modeling of SMA-based self-folding sheets. However, their work has been focused on the modeling of these types of origami structures, not yet in their actual fabrication.

In this paper, the authors look to expand the potential of AM technology by further exploring a method for the direct fabrication of systems with actuated joints without post-process assembly. Specifically, the authors propose a procedure for fabricating actuated joints in a single AM build session. The resulting procedure enables a designer to create actuated mechanisms via the Stratasys PolyJet 3D printing (3DP) process. As this 3DP technology is able to accurately deposit multiple materials in a single layer, mechanisms featuring rigid members and flexural joints can be created in a single build.

In general, embedding parts in an AM build process involves (a) designing a part with a specifically designed void to accept the foreign component, (b) pausing the print mid-build, (c) inserting the foreign object into the designed void, and (d) resuming the print over the inserted component (Figure 5.1).

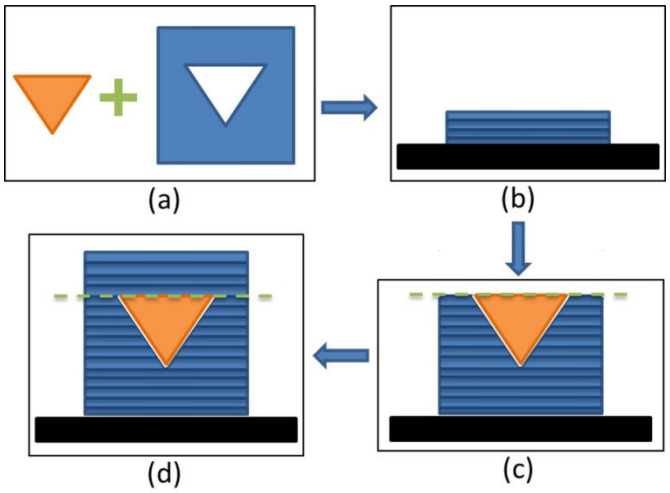

Figure 5.1. General Embedding Process of a) Selecting the Object for Embedding and Designing the Cavity to Accept the Object, b) Beginning the Build, c) Pausing the Build at the Top of the Cavity and Inserting the Object, and d) Resuming the Build to Print on Top of the Object

5.2.1. Existing AM Embedding Techniques

Prior efforts in embedding components into parts via AM are primarily centered in three technologies: Shape Deposition Manufacturing (SDM), Stereolithography (SL), and Ultrasonic Consolidation (UC).

Shape Deposition Manufacturing (SDM). Shape Deposition Manufacturing involves first depositing a layer of material followed by CNC (Computer Numerically Controlled) machining each layer to final dimensions. In this way, it is as almost a hybrid of AM with traditional subtractive machining. Layers of either metal or polymer are deposited via arc, thermal, or plasma spraying, laser or MIG welding, microcasting, or extrusion.

Li and coauthors used SDM in conjunction with laser sintering to embed optical fibers and fiber brag sensors for measuring the internal stresses in laser-assisted SDM. First, a stainless steel substrate was created with a cavity for the fiber. After inserting the fiber, a stainless steel powder is deposited onto the fibers and melted by a laser to form the layers. Finally, SDM was employed to attain the desired dimensions of each layer [84,85]. Similar fiber-embedding using laser-assisted SDM has been accomplished by Golnas [86] "to monitor in real-time thermo-mechanical responses of tools, equipment, and structural equipment".

Through a sequence of creating molds, bulk-depositing epoxy and other polymers, machining, and embedding components, researchers have used SDM to manufacture biomimetic robots with sensors, flexible joints, and pneumatic actuators embedded into the structure. "Sprawlita," an insect-like robot with flexible joints made exclusively of embedded components, was created using this process [87–90].

Hatanaka and coauthors [91,92] developed a similar process that combines photolithography with SDM to embed flexible components, such as fibers, fabrics, and electrical wires, for creating polymer mechanisms with flexible joints. This was achieved by first creating the polymer structure and cavity by SDM and then anchoring the fibers with a photopolymer that is selectively cured via masking a UV light source. Bulk material was then deposited around the secured ends of the fiber to create the remainder of the structure, and SDM was employed to create the desired surface finish.

Stereolithography. The stereolithography (SL) process uses a vat of photopolymer that is cured with an ultraviolet laser in a layer-wise fashion. Embedding components in SL is accomplished by designing a void for the object to be inserted, pausing the build, inserting the component via press-fit, and resuming the build [93]. Initially, this SL embedding process was used to embed sensors [94]. Since then, Geving [95,96] embedded larger components, such as a screwdriver that was embedded in a SL build. Subsequent work involved developing standards and process plans for embedding complex components to create functional assemblies and mechanisms.

The resulting approach involved the use of functional inserts and shape converters [97–99]. A functional insert is a solid member that is not made from AM, such as a motor, gear, bearing, wiring, etc. A shape converter is a solid member made from AM that is designed to fill the space between a printable cavity and the contours of a complex shape. Shape converters are used for objects which, if embedded, would cause laser-shadowing, undesired vacancies, or undesired submerging of components in the polymer resin. Kataria and Rosen's shape converter concept is shown in Figure 5.2. De Laurentis and Kong [93] demonstrated the value of using shape converters by creating a small, remote- controlled vehicle made of entirely SL-embedded components.

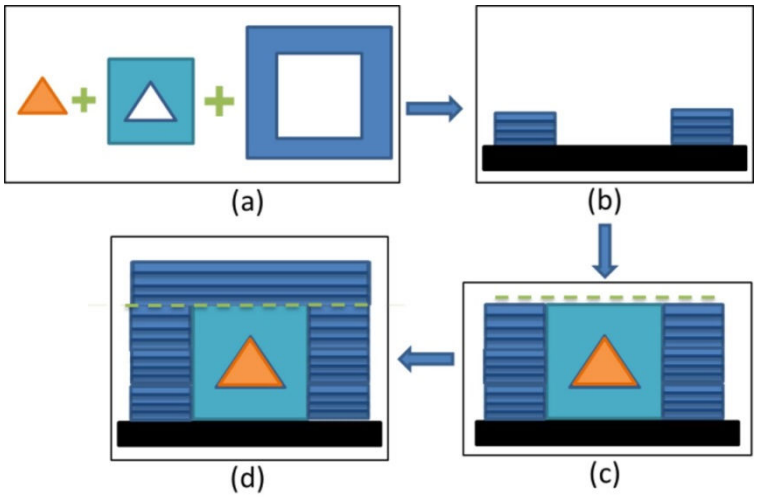

Figure 5.2. Shape Converter use in Embedding Following the Process of a) Selecting the Object for Embedding and Designing the Cavity and Shape converter to Accept the Object, b) Beginning the Build, c) Pausing the Build at the Top of the Cavity and Inserting the Object Inside the Converter, and d) Resuming the Build to Print on Top of the Object

Finally, another process for embedding in SL was developed to create embedded electrical systems by combining direct writing of circuits and stereolithography. This hybrid process worked by first pausing the SL build, using a direct write device to extrude a conductive paste onto the layer in the pattern of the desired circuit, and then resuming the build to embed the printed circuit [100–102].

Ultrasonic Consolidation. Ultrasonic consolidation creates nearly fully dense metal parts by ultrasonically welding foil sheets of material together and then CNC machining the layer to final dimensions [103]. Much like SDM, the embedding process involves CNC machining a pocket for the insert, embedding the insert, and then resuming the UC additive manufacturing process over the insert. Electronics and sensors have been embedded in UC builds to shield them from space and other harsh environments [103]. Composite structures were created that contained shape memory alloy fibers, optical fibers, and reinforcing fibers [104–106]. Janaki Ram and coauthors [107] investigated the compatibility of varying combinations of differing metals, such as aluminum- copper alloys, nickel based alloys, and stainless steel in UC and found that “most of the materials investigated could be successfully bonded to Al 3003 and vice versa.”. Finally, DW technology has been integrated by Robinson and coauthors into UC to create an aluminum panel with embedded circuitry [108].

Most recently, Willis and coauthors [109] used the PolyJet direct inkjet printing process to embed LED and IR components within printed parts. By combining these embedded components with 3D printed lenses and light pipes, the authors were able to create a series of interactive devices that leverage and control a variety of optical properties. The final devices fell within the categories of sensors, displays, and illumination. This work is the only other existing research pertinent to PolyJet embedding, which is the goal of the authors here.

5.2.2. Context

While our review has cited previous work regarding embedding of foreign components in AM parts, no research has been presented that (i) demonstrates embedding with the PolyJet 3D printing process for the actuation of a multi-material assembly and (ii) proposes a unified set of design rules and considerations to ensure consistent, quality embedding. Our research will begin to address these gaps through the embedding of foreign SMA elements within AM parts created via the PolyJet process.

The PolyJet process is described in the following section. The authors' PolyJet embedding procedure is then described, along with the introduction of three key elements in the "Design for Embedding" rule set. After presentation of the "Design for Embedding" considerations, preliminary experimentation is discussed which offers quantitative details into the implementation of these rules. Two case studies are presented as a means of displaying the process capabilities and the effectiveness of the embedding rules. These case studies are used to present quantitative and qualitative evidence of the embedded actuators' performance, as well as look at the potential for surface defects. Finally, closure is offered, along with potential for further process and design improvement.

5.3. PolyJet Direct Inkjet Printing

PolyJet is a material jetting, direct 3D printing technique that utilizes drop-on-demand inkjet printing to selectively deposit droplets of photopolymer directly onto a build platform [10,110]. An illustration of the print head assembly block of a PolyJet printer is presented in Figure 5.3.

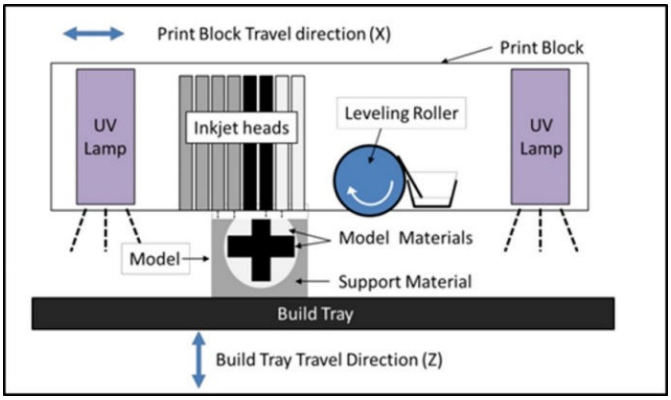

Figure 5.3. Objet PolyJet Print Head Assembly Block

Once a layer of droplets is deposited via inkjet print heads (64 µm in standard mode; 32 µm in high-resolution mode) and a roller evens out the layer surface, two UV lights (one leading and one trailing) pass over the printed layer multiple times to cure the photopolymer. As several inkjet print heads with separate material sources can be installed into the printing block, multiple materials can be deposited in a single layer, thus enabling the creation of graded materials. One of the materials printed is a dedicated hydrophobic gel that is used as a support material for the fabrication of complex geometries. This sacrificial material is removed using a compressed water jet in a post-processing step. Other materials include a flexible, elastomeric material (Tangoblack+) and a stiff, hard polymer (VeroWhite+).

The PolyJet process creates new layers by direct material addition [111], which is well suited for component embedding. The lack of a recoating step, wherein raw material is added in bulk in powder or resin form, eliminates the majority of concerns related to disturbing the previously printed layer typically found in embedding processes.

However, there are two inherent limitations in using the PolyJet process as a means of embedding components. First, as there is not yet a means in the PolyJet software to manually configure the deposition of support material, one must manually remove the deposited support material from the designed void in which a component will be embedded. Secondly, as the print head assembly block passes over the printed part at a clearance of only 100 µm, embedded components cannot protrude from the previously deposited layer, or damage to the printing nozzles could occur.

With the PolyJet process' ability to deposit multiple material phases on-demand, it becomes possible to create multiple-material compliant mechanisms which rely on the flexibility of the

machine's TangoBlack+ material to achieve deflection. In the simplest sense, the flexible material can be used as a "living hinge" when placed between pieces of stiff material. By developing a method for embedding actuating elements within mechanisms of this type, we can begin to automate their performance, in essence creating self-actuating, flexible members that might be used in a variety of applications.

5.4. Embedding Procedure

The authors' proposed process for embedding foreign actuating components within PolyJet printed parts follows the same basic steps as the general four-step process detailed in Figure 5.1: (i) designing a cavity for the component, (ii) pausing the build at the topmost layer of the cavity, (iii) inserting the component and (iv) resuming the build. More specifically, the embedding process for PolyJet printing takes the following form, as seen in Figure 5.4:

1. Design guide channels or cavities to accommodate the SMA wire (or spring-shaped SMA).
2. Design the fixation points to secure the ends of the SMA.
3. If necessary, design a shape converter to ensure a level printing surface on top of the embedded object.
4. Pause build and remove support material from channels.
5. Secure the SMA to the designed fixation points, using UV-curable adhesive, if needed.
6. Place shape converter on top of embedded component, ensuring that its surface is flush with the printed part.
7. Resume the build.

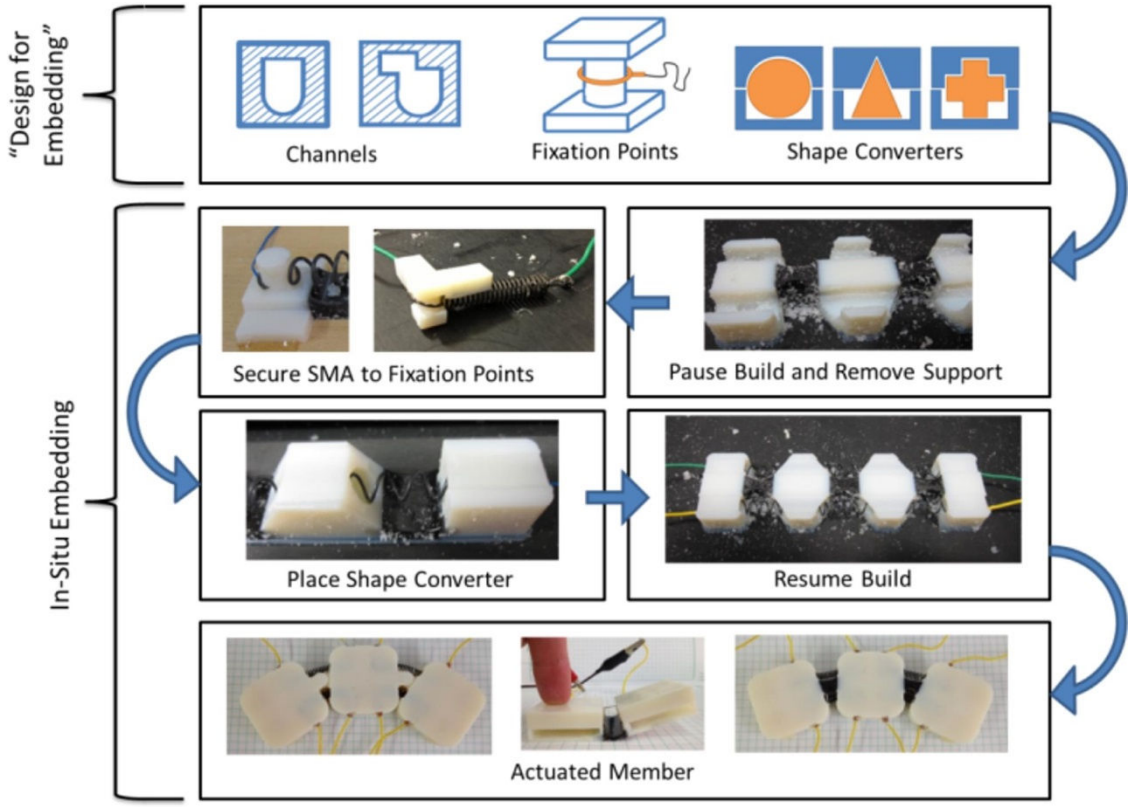

Figure 5.4. Overall Embedding Process for SMAs, Including "Design for Embedding" and In-Situ Steps

5.4.1. "Design for Embedding" Considerations

The first three steps in the general embedding process could be considered under the umbrella of "Design for Embedding." This entails all of the design work that must be performed with the guide channels, fixation methods, and shape converters before a build is begun. These three integral components will be the focus of discussion in the next three subsections, where they will be explained in detail. Note that, throughout the discussion and images in the following sections, axis labels are provided as X, Y and Z. Following ASTM F2921, the positive Z direction represents the vertical build direction (perpendicular to layer deposition), while X and Y represent the axes of the material deposition plane [112].

Channel Design for Complex Embedding Patterns. As discussed in the review of prior work in AM embedding, it is necessary to first design a cavity into the part. The foreign component will eventually be placed within this cavity. In the case of fiber embedding, these cavities take the form of "guide channels." These guide channels are designed to cut through the interior of

the printed part. This, in turn, designates the path that the fiber will take through the part once embedded. In the simplest implementation of the PolyJet embedding process, the guide channel design simply consists of an extruded U-shaped profile cut through the part. The fiber can then be placed directly into this channel and secured at its ends. This simple channel profile was used in preliminary work exploring the concept of embedding monofilament fibers in the PolyJet process [2].

While this simple channel design works well for straight-line embedding patterns, it is not sufficient for fiber embedding in more complex, curved patterns. The issue that arises when attempting to embed a fiber into a curved channel is out-of-plane bending during fiber placement. Unless the fiber is kept perfectly taut and level during placement in the channel, it will "pop out" of the channel. This can cause significant issues when resuming the build, since the low pass clearance of the print heads will catch on the fiber, pull it free of the part, and potentially damage the machine.

As such, the design of the embedding channel forms the first of three "Design for Embedding" considerations for embedding SMAs in a PolyJet part. To better secure the fiber and prevent out-of-plane bending when placed in curved channels, the authors have implemented a channel redesign that features a printed, compliant channel overhang, as seen in Figure 5.5. When the fiber is depressed onto the printed overhang during the embedding step, the overhang deflects enough so that the fiber can pass around and underneath it and settle into the U-shaped portion of the channel. The natural out-of-plane bending that occurs during embedding is not forceful enough to deflect the flap upwards, thus keeping the fiber secured in the channel space for the duration of the embedding placement. The result is an embedding process that is fast, repeatable, and can be easily performed by only a single operator.

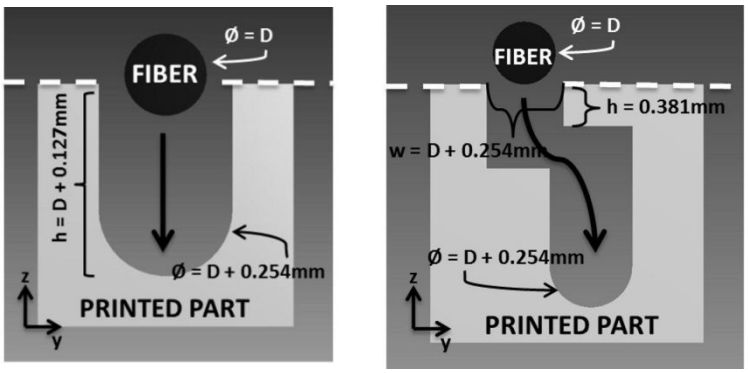

(a) (b)

Figure 5.5. Cross-Sectional Diagram of (a) Simple and (b) Alternative Channel Design for Complex Embedding

This alternative channel profile is a necessity when considering the embedding of shape memory alloys. Because their limited stroke distance is a percentage of their overall length, it is desirable to embed as long a length of wire as is feasible. To accomplish this, the channel will likely need to curve back and forth several times within the part. Unfortunately, each curve provides an opportunity for the wire to become accidentally removed from the channel during placement. The alternative channel design prevents this from occurring.

In general, with the two guide channel designs, the channel should be designed approximately 0.25mm larger than the embedded fiber (justification for this clearance is provided in the "Preliminary Experimentation" section). For the simple channel design, this includes the distance from the top of the fiber to the embedding plane. However, due to the unique nature of the alternative channel design, the depth of the fiber from the embedding plane is highly variable, depending on the needs of the designer. In Figure 5.5b, the channel depth was selected as 1.143 mm. This channel depth is much larger than the 375 micron SMA wire that was eventually embedded in the channel. However, because of the flap that covers the top of the channel, the depth of the channel will not cause build errors (though there is still little incentive to design an egregiously deep channel). The only potential point for build errors in the alternate channel design lies at the top entry point of the channel. The entry point must be as wide as the fiber being embedded (and also include the 0.25 mm clearance) in order for the fiber to fit into the channel. For small scale fibers such as the 375 micron SMA wires being investigated in this paper, the entry point remains small enough that material will not fall into it (confirmation of this

is shown in tolerancing experiments in the "Preliminary Experimentation" section). For entry points that must be larger than this, the designer will need to press the fiber into the channel without removing the support material first. In doing so, the fiber will displace enough support material to lie in the channel, but, due to the slightly gelatinous nature of the support material, it will reform behind the fiber. In doing so, the support material should reform closely enough to provide an even surface for new material deposition at the entry point to the channel.

Obviously, the detailed design of the guide channels will depend on the exact type of actuating element being embedded (e.g. passive or active) as well as the dimensions of the element. The two designs in Figure 5.5 can serve as a general rule of thumb for the initial design stages, with the U-shaped channel serving as an appropriate design for passive actuators (e.g. monofilament fiber) and the alternate channel design for active actuators (e.g. SMA wires). As already alluded to, testing of the tolerances associated with the U-channel design will be discussed and demonstrated in the "Preliminary Experimentation" section later in this paper.

Method for Fixing Embedded Shape Memory Alloys. While the guide channels serve to specify the desired path for the embedded SMA fiber or spring, the resultant printed part will not actuate unless the ends of the SMA are directly connected or fixed to the printed piece. To address this need, we design "fixation points" into the initial digital representation of the printed piece, which forms the second of the three "Design for Embedding" considerations. These fixation points can take a variety of forms depending on the shape and behavior of the actuator being embedded; the only constant is that there must be a fixation point at each end of the embedded actuator. However, for this process, there are two main methods of fixation: adhesive and mechanical.

The simplest form of fixation for an embedded actuator is simply the manual deposition of an epoxy adhesive. By designing in a small cavity at each end of the guide channel, the designer can deposit adhesive onto the end of the actuator which fixes it to the printed part. The ideal adhesive for this fixation method is one which cures quickly with the addition of UV light, thus removing the time traditionally needed waiting for an adhesive to dry. This simple adhesive fixation method has proven successful for the embedding of monofilament fibers [2]. However, this method of simple adhesive fixation proves to be inappropriate for the in-situ embedding of SMAs within a part. When heated, a SMA fiber's length will contract; however, as its volume remains constant, the diameter of the fiber must expand. Likewise, when cooled, the SMA will

return to its original length, with the diameter decreasing back to its original size. Repeated actuations in this fashion can cause the wire to free itself from a simple adhesive fixation point.

To provide a secure fixation point for the straight SMA wire, crimp terminals are attached to each end of the wire. Crimps have shown to attach securely to SMAs, despite the tendency of SMAs to change diameter during activation. However, it is still necessary to determine an appropriate method of fixing the crimps to the actual printed part. In order to remove any reliance on adhesive, a cylindrical post shape is designed into the part, to be used as an attachment point for the circular crimp terminals. In essence, as the part is printed, the post is printed as well. When the print is paused, the top of the post should be even with the embedding plane. This allows for the crimp terminal to then be placed over the post. When the print is resumed, the post becomes embedded within the part, securing the crimped terminal around the post, thus securing the SMA wire in place. This concept is shown in Figure 5.6. The printed post mechanical fixation method is easily implemented with either the straight SMA (with an added crimp) or the spring-shaped SMA (which already has circular shapes pre-formed at each end).

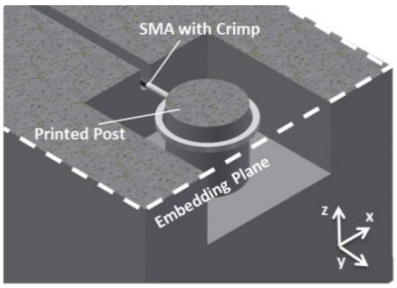

(a)

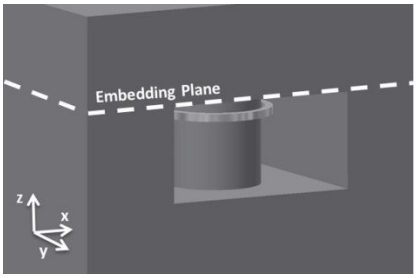

(b)

Figure 5.6. CAD Representations of Printed Post Fixation Method a) at the Embedding Plane Cross-Section and b) at the End of the Build

As with the guide channels, the detailed design of the fixation points will be dependent on the specific geometry of the printed part and the dimensions of the actuator being embedded. However, generally speaking, an adhesive fixation will suffice for a low-loading, passive actuating element, such as the monofilament fiber discussed earlier. In contrast, the printed post method of fixation will serve as a viable starting point for the design of parts with active actuators, such as SMA wires.

Shape Converter Design for the Embedding of Irregular Surfaces. If the embedded fiber is of a sufficiently small scale, it is relatively simple to press the fiber into the support material present in the originally-designed guide channels without concern for how subsequent material will rest on the embedded element. This is because the support material will help to prevent compounding build errors, despite the shape of the embedded component's surface. However, as the embedded piece grows in size or has an irregular surface, design steps must be taken to ensure that material will be deposited evenly over the embedded object when printing resumes.
To accommodate the embedding of irregular objects within the PolyJet process, it is possible to adopt the shape converter concept from Kataria and Rosen [98]. The inclusion of a shape converter is the final "Design for Embedding" consideration necessary for PolyJet embedding. Applying this concept allows one to embed irregularly shaped objects in AM processes (a general example of which has already been shown in Figure 5.4, for multiple embedded shapes). The shape converter consideration also helps to prevent surface defects that would result from having a foreign body present in the printed part.

As an example, we can consider the embedding of a spring-shaped SMA wire within a printed part. If the spring were placed in a basic U-shaped channel, any subsequently deposited material would fall between the coils in the spring and cause build errors. In addition, the curved, cylinder-like surface of the spring would not create an even surface for further deposition. To accommodate this, a shape converter is printed alongside the main part. When placed on top of the spring, the converter changes the cylindrical shape into a rectangular prism, which can easily have fresh material deposited on its flat surface. This concept is presented for a simple circular profile (such as in a spring-shaped SMA) in Figure 5.7 (note that clearances are exaggerated).

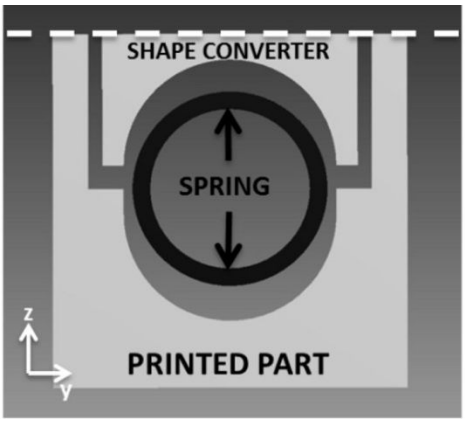

Figure 5.7. Diagram of Shape Converter Concept for Embedded SMA Spring

It is important to note that the shape converter concept can be easily and usefully combined with the previously discussed printed-post mechanical fixation method. As the case studies in this paper will show, printing the post as an attachment to the shape converter helps to simplify the in-situ embedding process. Also, by merging the fixation point with the shape converter, multiple fixation/converter designs can be printed and tested without needing to redesign the base printed part for each iteration.

5.4.2. Support Material Removal

One of the key aspects of the embedding process for PolyJet AM is the need to remove support material from the cavities in the printed part in order to properly place any desired embedded components. It is important to note that, during the removal of support, the printed part is not removed from the build tray. As the next layer after the embedding step must perfectly align with the previous layers, it would prove near impossible to remove the part for cleaning and then attempt to replace it for further layer deposition. Instead, the gel-like support material is removed using a series of fine tipped tools, potentially including but not limited to precision knives or dental picks. The appropriate support removal tool is dependent on the geometry of the cavities. While inconvenient, the manual removal of support material from the designed cavities does not often prove to be problematic, even with fine features, as long as sufficient care is used.

5.5. Preliminary Experimentation

To gain a general understanding over the appropriate clearances for simple fiber embedding with a nominal U-shaped channel, a series of preliminary experiments were conducted in which fibers were embedded into channels with varying clearance of 0 – 0.035 in. As can be observed in Figure 5.8, channels with large clearances resulted in a poor surface finish due to layer build errors propagating throughout the build process. Examination of the resulting surface finish above each channel confirmed that a channel width equal to the diameter of the fiber (i.e., a zero clearance) is ideal for embedding. At zero clearance, the channel is filled by the fiber, and thus provides a proper surface for material deposition. However, it should be noted that minor variations in printing the size of the fiber is decreased may cause the fiber to not fit properly in a zero-clearance channel. For this reason, the slight 0.01 in. channel size increase is added for the case studies. This minor increase will ensure that the smaller fiber will be able to fit in the channel despite any minor variations, but is still small enough so that no build errors will occur.

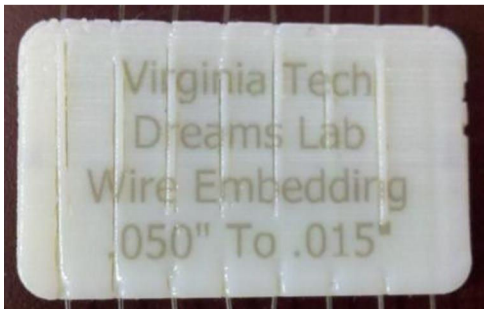

Figure 5.8. Surface Finish Test Part where the Clearance between the Fiber and the Designed Channel is Varied between 0.035 Inch (Left) to 0 Inches (Right)

While this initial wire embedding shows that the optimal simple channel embedding occurs at zero clearance, shape converters cannot usually be designed at dimensions nominal to the cavity size (initial trials demonstrated that the converters will not always fit if designed as such, due to minor variations in printing). To determine the appropriate clearance for shape converters, another simple specimen is constructed to test various clearances. The objective is to determine a clearance that allows the converter to fit easily within the cavity, but to not be so loose as to cause compounding build errors from newly jetted material falling between the clearance gaps. Initial experimentation focusing solely on the gap in clearance is shown in

Figure 5.9. The clearances range from the nominal 0.00 – 0.07 in. on all sides of the converter. Looking at this specimen, there are no build errors present in the 0.00 in. and 0.01 in. tolerance shape converters; however, small defects begin to appear at the 0.02 in. tolerance, with the errors becoming increasingly dramatic as the tolerance grows. In this particular case, the nominally designed converter and cavity were able to be mated, but, as already mentioned, this is not always the case. Because of this, a tolerance of 0.01 in. (or potentially slightly less) is recommended as the base tolerance for embedding design.

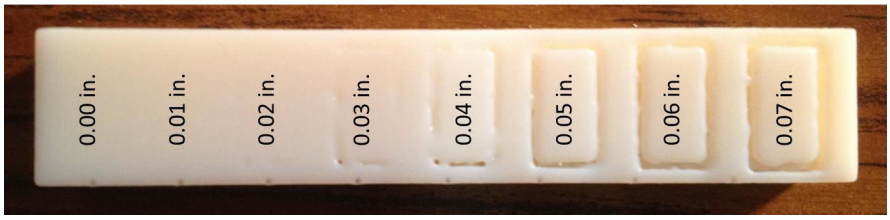

Figure 5.9. Surface Finish Test Part Accounting for the Effect of Shape Converter Clearance Gap

While this test offers a general feel for how build errors may propagate as tolerances grow, there are other design-specific factors which may affect how obvious the build errors are. Also of notable importance are the length of the shape converter's perimeter (a long perimeter with a large gap provides more area for jetted material to fall through) and the thickness of material above the embedding plane (the thicker the material is above the embedding plane, then the more likely the newly deposited liquid droplets will disperse and even out the surface as the layers grow and eliminate any clear defects).

5.6. Case Studies

Two case study examples are presented here in order to provide a testbed for evaluating the performance of the PolyJet embedding procedure. In addition, they demonstrate the applicability of the three "Design for Embedding" considerations for different actuating element shapes and different printed structures. The first case study is the embedding of a standard, straight SMA wire, which demonstrates the importance of channel design in embedding. The other case study is of a mechanism with two joints connecting three rigid square sections, very similar in approach to the antagonistic design concept presented by Sofla and coauthors [113]. The

mechanism is designed to utilize the spring shaped SMAs (which are more geometrically complex than straight SMA wire), due to their higher deflection when compared to a similar length of straight SMA wire. Two derivatives of this case study are presented: one with a flexible, compliant joint connecting the square sections, and one with a printed pin joint connecting them.

5.6.1. Straight SMA Wire Specimen

To successfully and repeatedly embed a straight SMA wire into a printed part, all three of the discussed "Design for Embedding" techniques must be implemented. The alternative channel design from Figure 5.5 is used to create a serpentine pattern within the piece, allowing for significantly more wire to be embedded, which in turn increases the total contraction of the SMA. In addition, a combined printed-post/shape converter is used to simultaneously secure the crimped SMA and ensure a level printing surface when printing resumes (Seen in Figure 5.10). The converter is given a clearance of 0.2 mm (0.00787 inches) on all sides. This clearance places it squarely in the region where no build errors should be observed, based on the preliminary test specimen shown earlier in Figure 5.9. The depth of the U-shaped portion of the channel was set at 1.5 mm; this depth allows for the SMA and crimp to intersect the printed post perpendicularly at approximately the midpoint of the post's length.

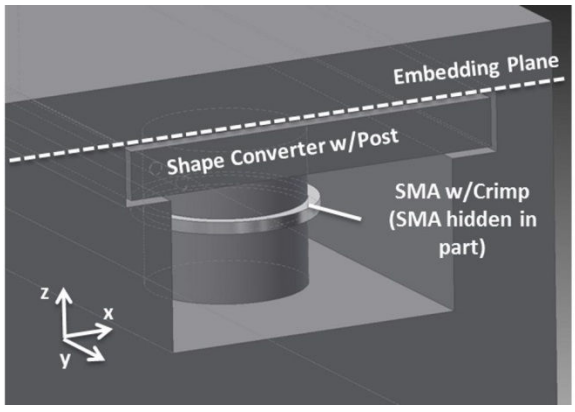

Figure 5.10. CAD Representation of Shape Converter/Fixation Point Hybrid for Straight SMA Fiber Case Study

The resultant specimen uses a living-hinge joint with a single SMA wire crossing over the joint towards the top of the piece. The joint is made of TangoBlack+, the most flexible material

offered with PolyJet 3D printing. The SMA wire is 375 μm in diameter, with an approximate contraction of 4% when resistively heated with 2.75A of current. The resulting specimen is shown at the paused embedding step of the build in Figure 5.11a, where the serpentine channel can be seen on the surface of the part, along with hybrid shape converters/fixation points printed next to the part. The SMA specimen is shown heated and actuated in Figure 5.11b. The resultant angular displacement of the joint is approximately 17.8 degrees from horizontal.

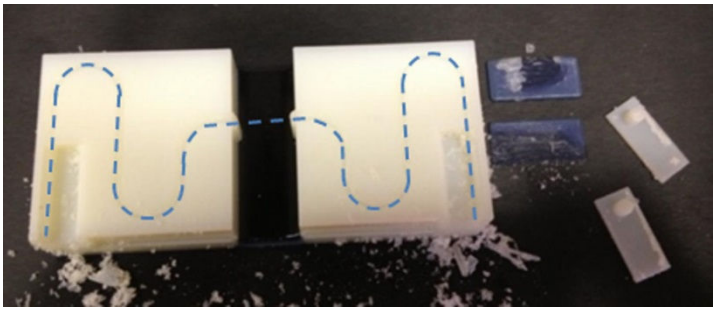

(a)

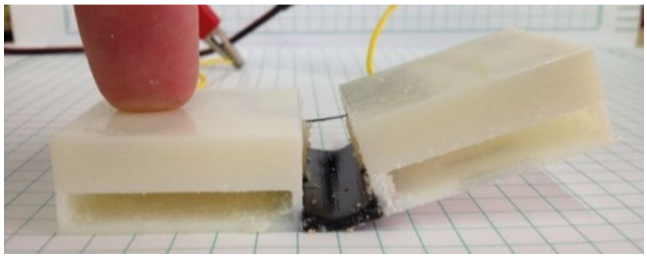

(b)

Figure 5.11. a) Straight SMA Specimen Paused Mid-Print at Embedding Step (with Wire Path Denoted with a Dashed Line) and b) Actuation of Straight SMA Specimen

5.6.2. Antagonistic, SMA Spring Specimens

Taking advantage of the multiple material capabilities provided by the PolyJet process, a compliant joint was first used in this second case study design. The joint took the form of an extruded hourglass shape, again printed out of flexible TangoBlack+. The square sections of the test piece were printed using the rigid VeroWhite+ material. For the actual embedding of the piece, it relies on the hybrid printed post/shape converter design presented earlier. Each rigid square section has four cavities. This allows each section to accommodate four posts, allowing for one SMA to be attached on either side of the joint and on either side of the square section. A

cross section of this overall design is shown in Figure 5.12, along with the shape converter used to secure each spring. As with the converters for the previous case study, the shape converters use a clearance of 0.2 mm (0.0078 inches) between each surface of the converter and each surface of the cavity. This extra hole is placed in the side of each square to allow for a lead wire to be easily connected to each end of the spring-shaped SMA.

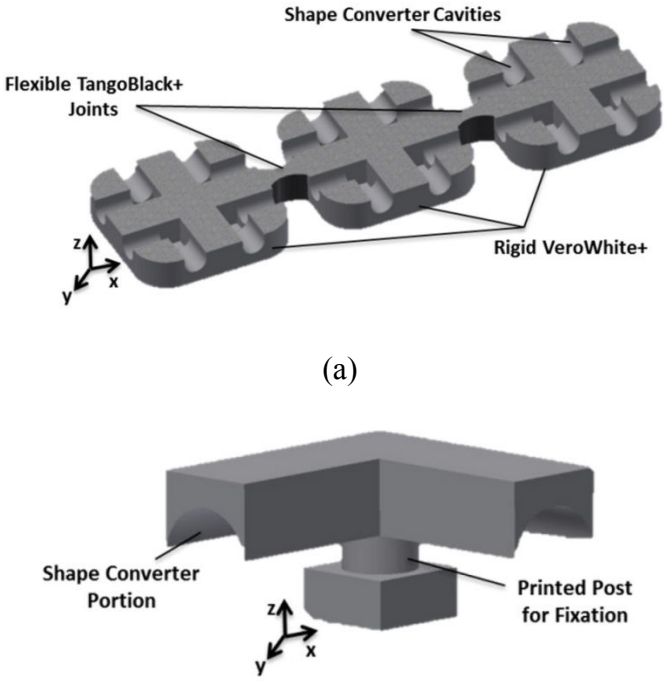

Figure 5.12. CAD Representations of the a) Embedding Plane Cross-Section of Compliant Joint Case Study Specimen and the b) Corresponding Shape Converter/Fixation Point Hybrid

Using the embedding procedure discussed herein, all four spring-shaped SMAs were successfully embedded within the specimen. The specimen, with the two lower springs resistively heated via the recommended 3.0A of current, is shown in Figure 5.13b. The antagonistic spring arrangement presented in this specimen makes it so that, as the bottom springs cool to their low-temperature, twinned martensite phase, the upper springs can be heated. This, in turn, provides the opposing stress necessary to return the lower springs to their detwinned martensite phase. An example of this specimen was stopped at the embedding plane to clearly demonstrate how the SMAs, lead wires, and shape converters are oriented with respect

to the base part (Figure 5.13a). The "L" shape of the shape converter allows for lead wires to be connected to the SMA while simultaneously diverting them away from the part so that they can be easily attached to a power source.

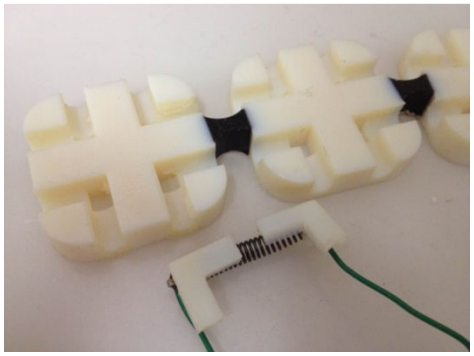

(a)

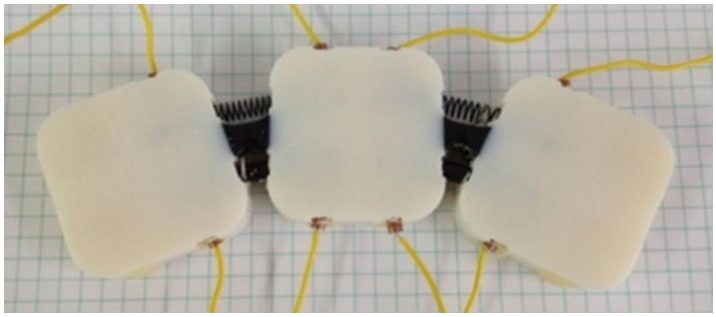

(b)

Figure 5.13. a) Print Stopped at the Embedding Plane with Shape Converter Example, and b) Fully-Embedded and Actuated Compliant Joint Specimen

Regarding the compliant joint specimen, the flexible nature of the material can potentially cause undesired compression. The desired mode of deformation is rotational; however, as seen in Figure 5.14, the compressive force of the SMA can instead cause simple translational deflection within the joint. This is evidenced by the out of plane bulging that occurs in the joint.

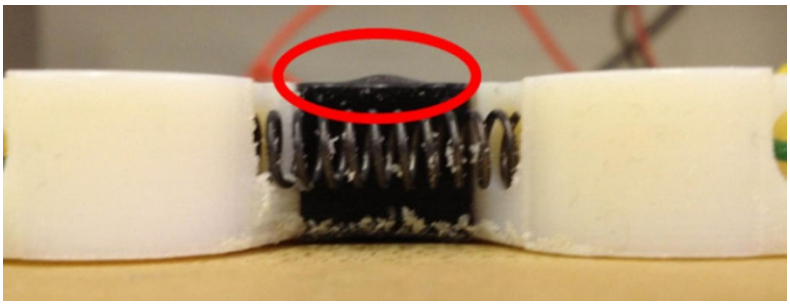

Figure 5.14. Out-of-Plane Bulging in Compliant Joint

To compare the multiple material compliant joint, the case study was also performed using a pin joint. The pin joint was designed to occupy a similar volume envelope as the flexible joint, allowing for it to be directly substituted without the need for additional redesign of the case study specimen. The layer-by-layer nature of AM gives it the unique ability to create multi-part assemblies (like the pin joint) in a single print. For example, with the pin joint shown in Figure 5.15, a clearance is designed between the pin and the through hole. The printer acknowledges the presence of this hole and automatically fills it will the sacrificial support material. Once the piece is done printing, the support material can be washed away with a high powered water jet, which frees the joint to move.

(a)

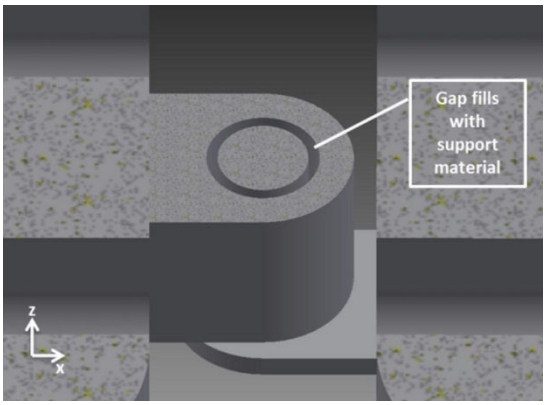

(b)

Figure 5.15. CAD Images of a) Pin Joint and b) Cross-Section View of Joint with Clearance Gap

As with the compliant joint specimen, the embedding procedure was successful. The resulting specimen is shown in Figure 5.16, with the lower springs resistively heated.

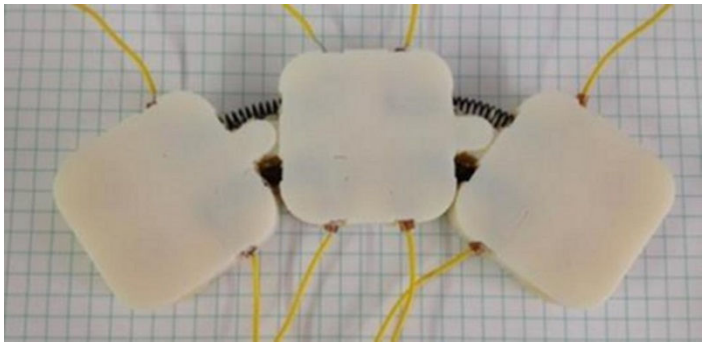

Figure 5.16. Fully-Embedded and Actuated Pin Joint Specimen

Careful observation of the pin joint specimen reveals small imperfections at the top surface of the specimen (Figure 5.17). This minor build defect can be related to those seen earlier in Figure 5.9. Even though the tolerance of the shape converters in this case study were smaller than the 0.01 in. recommended limit determined from the earlier test specimen, visible build defects still occurred. This can likely be attributed to the thickness of the material above the embedding plane. As mentioned earlier, as more material is deposited, the liquid droplets may serve to even out the build surface and remedy any build errors. However, in this case study, the thickness of material above the embedding plane was not as large as in the original test specimen. As such, there is potential for build defects to appear even at smaller clearances. This case study also shows that minor printing variations may make it so that, even with proper tolerancing, build defects may still not be entirely avoidable (in this case all converters and holes were the exact same size, but only a few exhibited surface defects). The compliant joint specimen, which used identically sized shape converters and cavities, displayed no surface defects.

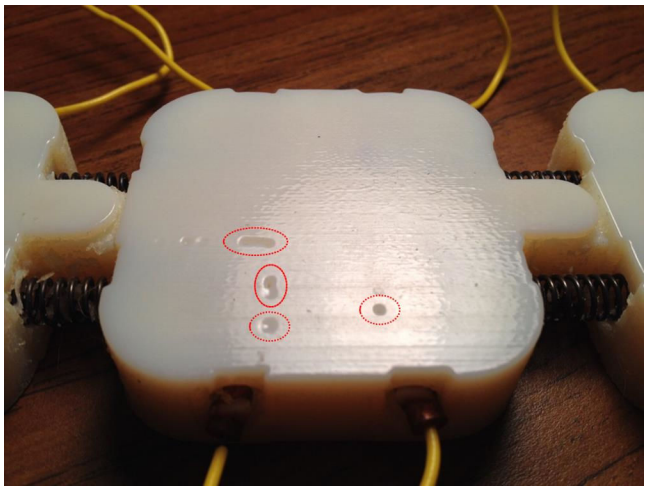

Figure 5.17. Surface Defects in Pin Joint Specimen

In order to gain a general understanding of the performance of each joint type with the embedded spring-shaped SMAs, measurements were taken to compare the approximate time needed for a single joint to reach maximum deflection with respect to the input current. The results are presented in Figure 5.18. Between each data point, the springs were allowed to cool to room temperature and were stressed to return the specimen to its default horizontal position.

The curves for each joint type demonstrate similar exponential trends, suggesting similar performance. In addition, the approximate, average, maximum deflection of the two joints is similar, with the pin joint at 26.82 degrees on average compared to the compliant joint at 27.34 degrees. It is worth noting that the performance of the compliant TangoBlack+ joint may degrade with use. Fatigue characteristics of TangoBlack+, which might be pertinent to evaluation the compliant joint's extended performance, can be found in [58].

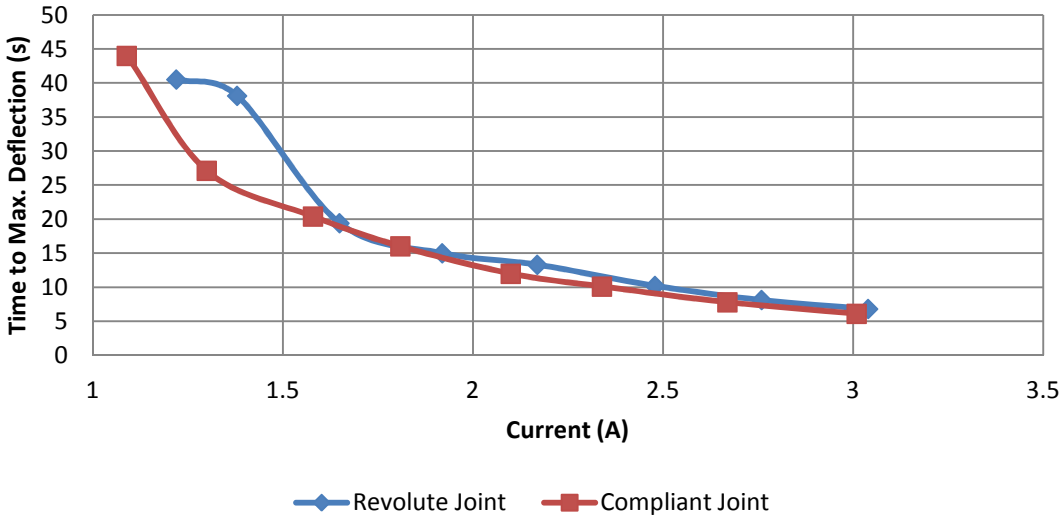

Figure 5.18. Maximum Deflection of Each Joint Specimen with Respect to Input Current

5.7. Generalizability of Findings

As these case studies demonstrate, the "Design for Embedding" considerations presented in this paper are key components for the successful design and creation of PolyJet parts with embedded SMA actuators. While the detailed design implementation may change from scenario to scenario, the importance of channel design, fixation points, and shape converters will prove essential to the embedding of any shape SMA actuator – or any foreign object – in a PolyJet process. Outside of PolyJet AM, these considerations will still find value. The importance and use of shape converters has already been demonstrated in stereolithography [98]; the concept could easily be extended to other AM processes including extrusion (provided that support material in the cavities can be manually removed) and powder bed fusion or binder jetting (provided that loose powder can be selectively removed from the cavities). Likewise, the ideas of guide channel design and fixation points can also be transferred to these other processes (with

the same stipulations on support material and loose powder). Obviously, when transferring the design for embedding considerations to other processes, the detailed dimensions for tolerancing would need to be adjusted to better account for the resolution of the new printer.

The presented design for embedding considerations can continue to play a role outside of SMA embedding as well. Referring to the simple "finger" case study in [2], the lessons learned in regards to channel design and fixation methods can be incorporated for the manually controlled monofilament fiber actuation. The design for embedding considerations may also be utilized in the embedded of non-actuating foreign elements in PolyJet parts as well (e.g., passive sensor packages, light sources, power sources, etc.). Finally, it is worth noting that the shape adapters need not necessarily be printed using the PolyJet process. Since the shape adapters are essentially specially designed foreign embedded components, they could theoretically be made of any material type, provided that they still offer a flat top surface for additional material deposition. By using a variety of materials as shape converters, one could essentially embed multi-functionality into parts (e.g., flexibility, heat sinks, insulation, etc.).

5.8. Conclusions and Recommendations for Future Work

In this paper, the authors have presented a procedure for embedding foreign actuating components into parts being fabricated via PolyJet 3D printing. This procedure, combined with the multi-material capabilities of PolyJet 3D printing, enables a designer to create actuated mechanisms without any post-processing or assembly. In addition, the authors have presented a series of "Design for Embedding" considerations to facilitate the embedding process, in hopes of ensuring consistent embedding quality regardless of the SMA form or the geometry of the printed part. This could simplify the realization of existing actuated systems and enable the design of completely new systems.

The case studies presented herein demonstrate the ability of the embedding process to enable the creation of functional, actuated printed pieces via PolyJet printing. All three final specimens show significant deflection when heated with the recommended current. In addition, the case studies show how "Design for Embedding" concepts can be adapted to ensure repeatable and quality embedding results with a range of actuating components. The printed shape converters in particular help to prevent the presence of most surface defects, while the alternative guide channel design allows for the embedding of complex wire patterns by just a single operator. The

concepts that drive the design tools from this study can be further generalized to allow for the embedding of other actuating components.

Future work will focus on further characterization of the interactions between the SMA actuators and the printed PolyJet parts. Specific attention will be paid to the effects of SMA heat on the material properties of the part. Because of the relatively low heat deflection temperature of the PolyJet photopolymer materials (approximately 50 degrees Celsius compared to the SMA's actuation temperature of 70 degrees Celsius), there is concern that prolonged actuation time could cause heat damage to the printed part. This in turn could decrease the actuated part's performance over time. In addition, the specimen for the actuated part will be redesigned to better account for the unique advantages offered by PolyJet printing. For example, the joints used in the presented case studies are based on existing designs, and are thus inherently influenced by traditional manufacturing techniques. However, the PolyJet process offers the opportunity to create entirely new "living hinge" designs based on topology optimization and multi-material compliant mechanism techniques. Future work will implement these techniques into the specimen joint design. Finally, we will investigate potential techniques for automating the process of wire embedding, such as the use of ultrasonic wire embedding.

6. CONCLUSIONS AND BROADER IMPACTS

6.1. Summary of Research

With the successful completion of this research study, the novel design tools of topology optimization and in-situ embedding have been successfully investigated within the manufacturing context of PolyJet AM. This includes an emphasis on understanding the main advantages and limitations that the PolyJet manufacturing process imposes on single and multi-material product design. This emphasis formed the overall motivating goal for this work.

The **Overall Motivating Goal** is to gain an understanding of how the manufacturing constraints of the PolyJet material jetting process affect the creation and mechanical properties of multi-material structures. Understanding these constraints is essential to furthering the use of innovative design tools, such as Topology Optimization (TO) methods, for the realization of optimized, multi-material, self-actuating compliant mechanisms.

This overall motivating goal was highly influenced by the work performed in conjunction with experts in the topology optimization community (Drs. James Guest and Andrew Gaynor) and presented in Chapter 2. Through the work in Chapter 2, the authors presented a study of the development of a start-to-finish process for the design and manufacture of optimized, multi-material compliant mechanisms as well as demonstrate an effective increase in experimental deflection. An appropriate compliant mechanism design and optimization approach was selected, taking care to consider the unique opportunities afforded by multi-material PolyJet printing. A robust topology optimization algorithm was developed by the topology optimization community to design manufacturable, multi-material topologies. Experimental results of the compliant force inverter problem show that the addition of a second non-zero candidate material with stiffness of approximately one-half the base phase increases the deflection (and efficiency) of the compliant inverter by as much as 84%. This deflection increases by nearly a factor of 30 when the second non-zero, TangoBlack+ phase is introduced. This demonstrated improvement, as well as geometric features observed in the final mechanism design, drove the research questions in the remainder of the dissertation.

6.2. Guiding Research Questions

The overall motivating goal of this dissertation was further supported by a series of primary, secondary, and supplemental research questions. Each of these questions was addressed through a journal publication, which form the basis of Chapters 3-5. The citations for the individual journal papers can also be found in Section 6.5.

6.2.1. Research Question 1

Design for Additive Manufacturing (DfAM) guidelines have the potential to assist designers in better preparing manufacturable products for creation with multi-material jetting. However, as Chapter 3 discussed, there is currently a lack of information regarding the manufacturing limitations of the PolyJet process and the constraints that these limitations place on design. As such, Chapter 3 sought to answer the first primary research question tied to these DfAM considerations.

Primary Research Question 1 (PRQ 1): How do the single-material manufacturing constraints of PolyJet AM, such as machine resolution and support material usage, affect the as-manufactured geometric features of final parts?

From this question, a corresponding hypothesis was created that predicted which key aspects of the PolyJet process might inform part manufacturability.

Primary Hypothesis 1: The machine resolution, support material attributes, and post-processing requirements will each impose a lower bound on the smallest geometry that can be manufactured by the PolyJet process. Each of these lower bounds will be driven by key process and geometric parameters that have a statistically significant impact on the constraint.

After establishing this primary hypothesis, two separate secondary research questions (and associated hypotheses) were created to drive investigation into the machine resolution, support material usage, and post processing.

Secondary Research Question 1.1 (SRQ 1.1): What geometric or process parameters influence the minimum manufacturable feature size in PolyJet AM? What is the quantifiable value of this geometric limitation on part design?

Secondary Research Question 1.2 (SRQ 1.2): What geometric or process parameters influence the geometric limitations imposed by i) the need to clean a part without damaging it, ii) the need to clean channels of support material, and iii) the need for faces to be self-supporting in the absence of support material? What are the quantifiable values of these geometric limitations on part design?

Secondary Hypothesis 1.1: The PolyJet printing process will limit the smallest feature that can be manufactured in an optimum topology, based on the orientation of the part, the chosen part surface finish, the printed material type, the direction of the part's features, and the general shape of the part's features.

Secondary Hypothesis 1.2: The PolyJet process's support material will limit the diameter, shape, and connectivity of cavities allowed within an optimized part, to ensure that they are possible to clean. It will simultaneously affect the minimum feature size that can be manufactured, driven by the feature's material type, length, diameter, and connectivity. In the absence of support material, the quality of self-supporting faces will be dictated by material type and face orientation.

To investigate these hypotheses, Chapter 3 presented a series of designed experiments to determine the key parameters that influence minimum feature size, support material removal from channels, feature survivability and self-supporting angles. Once the key parameters were identified, additional experiments were performed to quantify the trends and minimum recommended values for the manufacturing constraints under investigation.

- *From Section 3.4.4:* Support material removal was limited by the cross-sectional area of the manufactured channel; experimentation showed that a minimum cross-sectional area approximately equal to the diameter of the post-processing water jet spray (approximately 50

mm^2) would result in highest percentage of support material removed (and thus the most efficient cleaning).

- *From Section 3.5.4:* The minimum resolvable feature size was shown to rely on surface finish and feature shape, as well as the interactions between surface finish and orientation, surface finish and feature direction, and orientation and feature direction. If a designer can account for the ideal configuration of these variables, then it is possible to manufacture features that are half the size of a more general "worst-case" scenario (in this case, 0.897 mm for the worst case vs. 0.372 mm for the best case).
- *From Section 3.6.4:* Feature survivability during cleaning was tied to cross-sectional area for stiff features and to connectivity for flexible features. However, it was demonstrated that it is possible for flexible specimens to survive in a fixed arrangement, though it requires a significantly larger diameter than the stiff VW+ material (3 mm diameter for TB+ vs. 1.13 mm diameter for VW+).
- *From Section 3.7.4:* Finally, the self-supporting angle of printed parts was found to be driven by the orientation of the surface with respect to the print head's roller. Y-dominated specimens offered better self-supporting angles (at 80 degrees from horizontal) over X-dominated specimens (at approximately 85 degrees from horizontal).

Identifying these key variables and the associated trends helps to guide designers in the creation of manufacturable structures, whether designed manually or by an automated method, such as TO.

6.2.2. Research Question 2

While Research Question 1 sought to shed light on some of the more common AM manufacturability considerations, there are still a host of other manufacturability considerations that arise from the PolyJet process's unique multi-material capabilities. Primary Research Question 2 was intended to investigate these concerns, especially surrounding how the process's deposition methods affected the properties of printed multi-materials.

Primary Research Question 2 (PRQ 2): How do the PolyJet process's multi-material deposition methods affect the as-manufactured properties of final parts?

The earlier motivating example of the multi-material compliant mechanism from Chapter 2 led the author to believe that there were two key areas of interest in the creation of multi-material structures: the existing and theoretical composite design space as well as the incomplete recreation of intermediate digital materials. These concerns formed the basis for Primary Hypothesis 2.

Primary Hypothesis 2: The composite deposition method and bitmap representation of digital materials are key features of the PolyJet process which affect the as-manufactured properties of multi-material PolyJet parts. These aspects will inform the baseline material properties of the digital materials as well as cause material property shifts within small features.

This primary hypothesis was further discretized into secondary questions which sought to capture the nature behind digital material recreation, as well as the relationship of material properties to the size of printed features.

Secondary Research Question 2.1 (SRQ 2.1): How do the material properties of the PolyJet's digital materials change with respect to the percent composition of base materials? How do these properties affect the potential digital material design space?

Secondary Research Question 2.2 (SRQ 2.2): How does feature size affect the manufactured properties of printed digital materials? Why do the material properties of digital materials shift as feature size decreases?

Secondary Hypothesis 2.1: As the proportion of VW+ increases in the PolyJet's digital materials, the storage modulus of the structures will increase following a consistent relationship. Because of the great difference in material properties between the base materials (VW+ and TB+) the resultant composite design space will be significantly larger than what the commercial PolyJet system currently allows for.

Secondary Hypothesis 2.2: As the size of printed features decreases, the as-manufactured storage modulus will change for parts which utilize the PolyJet's digital materials. This is because the necessary deposition pattern of multi-material droplets cannot be fully replicated in a small feature space.

Chapter 4 allowed the author to investigate these research questions through a series of experiments design to identify connections between the design of monolithic, multi-material structures and their as-manufactured properties when printed with the PolyJet process. Specific elements of interest included i) benchmarking of existing PolyJet materials with respect to composition and ii) identifying material property shifts in digital materials of decreasing size.

DMA experimentation demonstrated a polynomial relationship between the storage modulus of existing PolyJet materials and the concentration of VW+ material in them (Figure 4.5). Comparing this line of best fit against the upper and lower bounds predicted by the rule of mixtures allowed the author to identify a theoretical digital material design domain for TB+/VW+ composites. Using this same DMA experimentation on digital material blends showed a shift towards the properties of the dominant material phase as specimen thickness decreases. This shift was shown to potentially be caused by variation in the as-designed material phase distribution in thinner specimens.

6.2.3. Supplemental Question 1 (Development)

In addition to identifying key manufacturing and design considerations for multi-material PolyJet compliant mechanisms, the author also sought to establish a method by which this mechanisms might be actuated (akin to the muscles in the bat wing scenario discussed in Chapter 1). To accomplish this, it was not only necessary to create a process for in-situ embedding with the PolyJet process, but also to determine key design considerations to ensure repeatable embedding for complex actuators. Supplemental Question 1 reflects these two needs.

Supplemental Question 1 (Development): How can foreign actuating components be embedded into parts manufactured with the PolyJet process? What design considerations drive the ability to successfully embed these components?

To successfully develop such an embedding process, the author hypothesized three potential design features to be incorporated when attempting to adapt the process for complex actuating elements.

Supplemental Approach 1: Key design features such as actuator fixation points, shape converters, and channel design must be considered in the detailed design stage of the design process to successfully adapt parts for manufacturing with the PolyJet in-situ embedding method.

As such, in Chapter 5, the author presented a procedure for embedding foreign actuating components into parts being fabricated via PolyJet 3D printing, without the need for any post-processing or assembly. In addition, the author presented a series of "Design for Embedding" considerations based on the three areas of Supplemental Hypothesis 1. These considerations facilitated the embedding process, in hopes of ensuring consistent embedding quality regardless of the actuator's form or the geometry of the printed part. The embedding process and the Design for Embedding concepts were subsequently demonstrated with three case studies. The case studies demonstrated how the proposed Design for Embedding concepts could be successfully adapted to different part and actuator geometries.

6.3. Research Synthesis

With the results of this dissertation research summarized throughout Section 6.2, synthesis reveals a common thread present throughout the entire study: the concept of Design for Additive Manufacturing. This thread allows the content of this dissertation to be further generalized to assess its potential effect on the future of material jetting processes and materials, as well as the field of AM in general.

6.3.1. Design for Additive Manufacturing

Though the research presented in this dissertation touches on a wide variety of topics within AM (e.g., topology optimization, in-situ embedding, and multiple materials), each chapter is driven at its core by the concept of Design for Additive Manufacturing (DfAM). Specifically, the DfAM studies that have been conducted herein center around developing both a conceptual

and quantitative understanding of the impact that multi-material jetting processes have on the manufacturability of designs. This DfAM thread is seen in each chapter as follows:

- Chapter 2: The study of AM/TO in Chapter 2 emphasizes the connection between automated multi-material TO design methods and their manufacturability with material jetting AM processes. TO is a widely researched area in the field of DfAM because of its ability to leverage the geometric complexity and design freedom allowed by AM (as evidenced by the work in this chapter).
- Chapter 3: The design of experiments (DOE) approach in Chapter 3 served to establish quantitative relationships between material jetting process parameters and manufacturable geometry. These relationships and the identified quantitative design limits help establish a framework for DfAM, which guides designers to incorporate specific geometric manufacturability limits into their designs. This framework also alerts designers to key process parameters that need to be considered when assessing the manufacturability of their designs.
- Chapter 4: As with Chapter 3, Chapter 4 identified key limitations that the material jetting process imparts on manufacturable designs. In this Chapter, the DfAM concept was addressed by offering an experimental connection between feature width and the material properties of digital materials. This connection alerts designers to the need to consider how small feature sizes in their designs will affect their as-designed material properties.
- Chaper 5: Finally, while Chapter 5 offers a process for in-situ embedding, it also identifies three conceptual DfAM concepts that drive successful embedding (i.e., shape converters, fixation points, and channel design). These DfAM concepts are what allow the embedding process to be expanded to actuators of varying complexity, as the cases studies in the chapter demonstrated.

6.3.2. Generalizability and Implications for Future Processes/Materials

While the experimentation and analysis presented throughout this paper are centered on existing material jetting processes, the relationships and knowledge that have been derived from these studies can be generalized in a way that suggests improvements for the future of material

jetting processes and materials. The implications that each chapter has on this future are discussed in turn.

- Chapter 2: The advantages of design and manufacture through the combination of multi-material AM and TO methods were shown in Chapter 2. The implications of the work in this chapter lean heavily to the realm of future design software. With the advantages offered by combined AM/TO methods, one potential route for future development is in more common incorporation of TO algorithms into existing CAD design software. While some software packages do currently incorporate TO for product design, this software tends to be highly specialized. By incorporating basic TO into more CAD packages, designers will begin to gain an intuitive understanding of optimal design and how it can be beneficial for AM parts

  In addition, the complex multi-material structures that result from the TO methods proposed in this chapter may serve to convince material jetting OEMs of the importance of fine control of material placement within their software. Existing software for multi-material processes allows material definition based only on shell assignment; however, finer assignment of material properties on a voxel-by-voxel basis would allow for easier recreation of the complex designs created by multi-material TO methods.
- Chapter 3: Chapter 3 emphasized a DfAM framework based on the relationship between various material jetting process parameters and the manufacturability of design features. The relationships identified in this study have implications for future material jetting processes. Adjustments to the material jetting process's support material would have the most immediate and significant impact on the manufacturability of designs. The development of soluble support material for material jetting would relax the design constraints associated with support material removal in small channels. In addition, it would remove the need for a high pressure water jet station to remove support material, which would allow the minimum survivable feature size to be equivalent to the minimum manufacturable feature size. Regarding the possible self-supporting angles in material jetting, experimentation suggests that, if a system either removes the need for a print head roller or redesigns the roller, the dependence of the self-supporting angle on orientation can be reduced or eliminated entirely.

  The understanding gained from this study can also be transferred to other AM processes outside of material jetting. For example, the experimental procedures can be used to

characterize similar manufacturing constraints in other process types (e.g., the self-supporting angle constraint also present in extrusion-based processes). Direct-metal AM systems in particular may benefit from the support material study conducted in Chapter 3. Though direct-metal systems use scaffolding in place of a separate support material type, the need to manually remove these scaffolds has the potential to introduce similar manufacturing limitations as were discovered for material jetting (e.g., cleanable geometry, survivable features).

Finally, the as researchers continue to identify and quantify design considerations such as those seen in this study, this may serve as a catalyst for software developers to incorporate AM manufacturability limitations into CAD design software. This could take the form of something as simple as a geometric check that would search a given design for feature diameters that may not survive the post-process cleaning.

- Chapter 4: The work presented in Chapter 4 emphasized the connection between part design and the properties of printed digital composites in multi-material jetting. Analysis suggests that the multi-material dithering method used to design these composite materials is responsible for the observed property changes as feature width decreases. There are two possible avenues of development that may lessen or completely eliminate this dependence. The first is an increase in XY resolution in future material jetting processes. By increasing the resolution through use of smaller ejection nozzles, the dithering patterns could be accurately recreated in smaller features, which would allow them to maintain their material properties. Alternatively, software improvements could be introduced that incorporate a more robust dithering method that is able to adjust material patterning to account for changes in feature size.
- Chapter 5: The embedding process and Design for Embedding considerations that were the focus of Chapter 5 were established in such a way as to make them generalizable to future material jetting processes. While the detailed dimensions of the considerations may need to be reestablished with changes in system resolution or layer thickness, the general concepts should remain transferrable. Likewise, certain aspects of the embedding process and design considerations should also be transferrable to process types outside of material jetting (although the unique characteristics of powder or liquid-based AM types will likely still necessitate alterations and concessions).

The creation of multifunctional, actuated elements, such as those seen in Chapter 5 may also influence the development of materials for future multi-material jetting processes. As the impact of multifunctional AM structures becomes more apparent, OEMS would benefit from investigating materials that better facilitate this multifunctionality (such as conductive materials for the direct jetting of circuitry).

6.4. Limitations and Future Work

Throughout the execution of this research study, several limitations were encountered. These limitations are discussed in the following subsections, along with potential avenues for expanding the work performed in each chapter.

6.4.1. Chapter 2: Multiple-Material Topology Optimization of Compliant Mechanisms Created via PolyJet 3D Printing

Though Chapter 2 was able to demonstrate the experimental deflection improvement offered by the introduction of additional material phases into a TO algorithm, there were still several limitations to be addressed in future expansions of this work. On the algorithmic side, the final designs exhibited both pixilation as well as an undesired flexible material border around the perimeter of the final design. Boundary smoothing should be implemented to remove any undesirable stress concentrations that may be present because of the pixelated nature of the final printed specimen. The TO algorithm should also be adjusted in future work to remove the TB+ outline around the part, since it appears to be a numerical artifact that does not seem to contribute to the performance of the part. Finally, a more thorough study of the printed polymer's modulus of elasticity and yield strength should be performed to allow for better incorporation of the material properties into the design algorithm. This, in turn will allow for better prediction of the mechanism's experimental performance.

The experimental deflection increase shown in Chapter 2 also served to inspire an additional research question, focused on the deflection improvement (as well as geometric and material complexity) that may be gained from the introduction of yet more material phases in the TO algorithm.

New Research Question 1: How does the introduction of additional intermediate material phases between VeroWhite+ and TangoBlack+ further improve the experimental performance of the manufactured compliant mechanisms? In addition, how does the introduction of additional material phases increase the material and geometric complexity of the final designed part?

6.4.2. Chapter 3: An Investigation of Key Design for Additive Manufacturing Constraints in Multi-Material 3D Printing

While the DfAM experimentation in Chapter 3 addressed a variety of single-material manufacturing constraints through the lens of numerous geometric and process constraints, there is still work to be performed in this domain. Namely, the experimentation focused on factors associated with the manufacturing process itself (e.g. orientation, surface finish) but did not account for the impact that variations in post-processing might have on printed products. This forms the basis for a potential new research question.

New Research Question 2: How do variables associated with post-process cleaning (e.g., distance from water spray, movement of water jet, post-cleaning sodium hydroxide bath) affect the removal of support material from channels and the survivability of fragile printed features?

In addition to these new post-processing considerations, the existing study is naturally limited by the factors that were not explored in experimentation (e.g., cross-sectional geometry in feature survivability) and the levels that were chosen for the test factors (e.g., testing circular and rectangular geometries, but not more complex geometries in minimum feature size experimentation). Expanding these factors and levels in future experimentation would be beneficial and would likely provide even more insight into the complex relationship between the PolyJet process and the parts that it is able to manufacture.

6.4.3. Chapter 4: Process/Structure Relationships in Composite Parts Manufactured via Multi-Material Jetting

Though Chapter 4 was able to identify experimental trends regarding digital material properties and the effect of decreasing feature size of digital materials, these studies are partially limited. One such limitation comes from specimen size that the chosen DMA system is able to

accommodate. Specifically, a system is needed that can test specimens wider than the 6mm specimens used here. This will allow for additional digital composite testing and allow the author to identify the width at which the material properties begin to plateau, which in turn indicates the recommended minimum feature size to ensure digital material properties that match the properties of "bulk" material.

In addition, future work will focus on addressing the design elements that influence the experimental results seen in this study. For example, dithering methods will be investigated to effectively fill in the space between 36% VW+ and 82% VW+ specimens along the polynomial benchmarking curve. Alternate dithering methods will also be applied to the existing material concentrations in the PolyJet process to observe how different patterns can be used to shift existing PolyJet concentration blends closer to either the upper or lower bounds predicted by the rule of mixtures. This informs the creation of an additional research question.

New Research Question 3: How do different dithering patterns affect the relationship between PolyJet digital materials' mechanical properties and their concentration of VW+?

6.4.4. Chapter 5: A Procedure for Creating Actuated Joints via Embedding Shape Memory Alloys in PolyJet 3D Printing

One of the main limitations of the embedding study presented in Chapter 5 is that the emphasis was placed solely on embedding with the PolyJet process. While generalizability was discussed, future work will include experimentally adapting the embedding process and "Design for Embedding" rules to alternative processes. This includes extrusion and powder-based processes (both of which will likely present unique challenges). This expansion leads to an additional research question.

New Research Question 4: How can the embedding procedure and "Design for Embedding" considerations be adjusted/generalized to allow for embedding with other process types (e.g., material extrusion, laser sintering?)

The existing work was also limited in the way that it characterized the performance of compliant mechanisms after prolonged exposure to heated actuating elements. Future work will

focus on addressing this gap through characterization of the interactions between the SMA actuators and the printed PolyJet parts. Specific attention will be paid to the effects of SMA heat on the material properties of the part and any damage that the actuator may be causing to the mechanism. This forms a final additional research question from this study.

New Research Question 5: What effect does long term use of heated actuating elements (such as SMAs) have on the performance characteristics of compliant PolyJet mechanisms?

6.5. Publications

As mentioned in Section 1.6, each chapter of this dissertation is comprised of a published or submitted journal paper. These journal papers, as well as their associated chapters and research questions are as follows:

1. ***Chapter 2 (Motivating Goal):*** Gaynor, A. T., Meisel, N. A., Williams, C. B., Guest, J. K. 2014. "Multiple-Material Topology Optimization of Compliant Mechanisms Created Via PolyJet Three-Dimensional Printing." *ASME Journal of Manufacturing Science and Engineering*, 136(6), 061015, doi: 10.1115/1.4028439
2. ***Chapter 3 (PRQ 1):*** Meisel, N. A., Williams, C.B. 2015. "An Investigation of Key Design for Additive Manufacturing Constraints in Multi-Material 3D Printing." *ASME Journal of Mechanical Design*, in revision.
3. ***Chapter 4 (PRQ 2):*** Meisel, N.A., Williams, C.B. 2015. "Process/Structure Relationships in Composite Parts Manufactured via Multi-Material Jetting." *Rapid Prototyping Journal*, in preparation.
4. ***Chapter 5 (Supplemental Question 1):*** Meisel, N. A., Elliott, A. M., Williams, C. B. 2014. "A Procedure for Creating Actuated Joints via Embedding Shape Memory Alloys in PolyJet 3D Printing." *Journal of Intelligent Material Systems and Structures*, advance online publication, doi: 10.1177/1045389X14544144

Two conference papers were also published to present preliminary findings prior to journal publication. These conference papers are:

1. Meisel, N. A., Gaynor, A., Williams, C. B., Guest, J. K. 2013. "Multiple Material Topology Optimization of Compliant Mechanisms Created Via PolyJet 3D Printing." *Proceedings of the 24th Annual International Solid Freeform Fabrication Symposium*, Austin, TX, August 12-14.
2. Meisel, N.A., Williams, C.B. 2014. "Design for Additive Manufacturing: An Investigation of Key Manufacturing Considerations in Multi-Material PolyJet 3D Printing." *Proceedings of the 25th Annual International Solid Freeform Fabrication Symposium*, Austin, TX, August 4-6.

Finally, several additional journal and conference papers were published by the author throughout the timeframe of this dissertation study. While not directly related to the research questions central to this dissertation, the work in the following papers nonetheless contributes to the broader fields of AM design, process, and education research:

1. Meisel, N.A., Williams, C.B. 2015. "Design and Assessment of a 3D Printing Vending Machine." *Rapid Prototyping Journal*, in press.
2. Snelling, D., Li, Q., Meisel, N.A., Williams, C.B., Batra, R., Druschitz, A. 2015. "Lightweight Metal Cellular Structures Fabricated via 3D Printing of Sand Cast Molds." *Advanced Engineering Materials*, advance online publication, doi: 10.1002/adem.201400524
3. Meisel, N.A., Williams, C.B. 2013. "Design and Assessment of an AM Vending Machine for Student Use." *Proceedings of the 24th Annual International Solid Freeform Fabrication Symposium*, Austin, TX, August 12-14.
4. Meisel, N. A., Williams, C. B., Druschitz, A. 2012. "Lightweight Metal Cellular Structures via Indirect 3D Printing and Casting." *Proceedings of the 23rd Annual International Solid Freeform Fabrication Symposium*, Austin, TX, August 6-8.

6.6. Scientific Contribution

The following scientific contributions have been made through the successful completion of this dissertation study:

1. Demonstrated means for combining the manufacturing realm of material jetting AM with the design realm of multi-material TO (Chapter 2)
2. Experimentally validated deflection improvement offered by the introduction of multiple material phases in compliant mechanism optimization (Chapter 2)
3. Understanding of key single-material manufacturing constraints in material jetting AM and their relationship to process parameters (Chapter 3)
4. Understanding of the relationship between out-of-the box digital composite materials with respect to phase composition and the potential design space associated with these materials (Chapter 4)
5. Understanding of how digital composite materials are created in multi-material jetting AM and how part width can affect the properties of these materials (Chapter 4)
6. Understanding of the process and design considerations necessary for the in-situ embedding of foreign actuating elements in PolyJet AM (Chapter 5)

6.7. Broader Impact

The presented work in the development of an understanding of the manufacturing characteristics for the reliable fabrication of optimized, multi-material, self-actuating structures supports the following broader impacts (i.e. outside of improving the scientific knowledge base of the research community):

1. The unification of material jetting AM and multi-material TO along with experimental validation of the performance increase offered by multi-material compliant designs provides new understanding of design improvement opportunities in a combined multi-material AM/TO space.
2. Identification and experimental investigation of key single and multi-material material jetting manufacturing constraints provides new understanding of the material jetting process and how it impacts design manufacturability and has the potential to influence next-generation material jetting processes.
3. The experimental methods for identifying key process constraints for the material jetting process can be translated to other AM process types, which allows for similar benchmarking of their design and manufacturing capabilities.

4. Development of an in-situ embedding process for use with printed multi-material products helps further the capabilities of designers to realize true biomimetic structures (e.g. morphing wings) and allows for the creation of multifunctional products via AM.

REFERENCES

[1] Norberg U. M., 1972, "Functional osteology and myology of the wing of the dog-faced bat Rousettus aegyptiacus," Zeitschrift fur Morphol. der Tiere, **73**, pp. 1–44.

[2] Stiltner L. J., Elliott A. M., and Williams C. B., 2011, "A Method for Creating Actuated Joints via Fiber Embedding in a Polyjet 3D Printing Process," 22nd Annual International Solid Freeform Fabrication Symposium.

[3] Hiller J. D., and Lipson H., 2009, "Design Automation for Multi-Material Printing," 20th Annual International Solid Freeform Fabrication Symposium, pp. 279–287.

[4] Li Y., and Chen Y., 2010, "Beam Structure Optimization for Additive Manufacturing Based on Principal Stress Lines," 21st Annual International Solid Freeform Fabrication Symposium, pp. 666–678.

[5] Kim G. D., and Oh Y. T., 2008, "A Benchmark Study on Rapid Prototyping Processes and Machines: Quantitative Comparisons of Mechanical Properties, Accuracy, Roughness, Speed, and Material Cost," Proc. Inst. Mech. Eng. Part B J. Eng. Manuf., **222**(2), pp. 201–215.

[6] Vayre B., Vignat F., and Villeneuve F., 2013, "Identification on Some Design Key Parameters for Additive Manufacturing: Application on Electron Beam Melting," Procedia CIRP, **7**, pp. 264–269.

[7] Howell L. L., 2001, Compliant Mechanisms, Wiley.

[8] Vogel S., 1995, "Better Bent Than Broken," Discover, (May), pp. 62–67.

[9] Aguirre M. E., and Frecker M., 2010, "Design and optimization of hybrid compliant narrow-gauge surgical forceps," ASME 2010 Conference on Smart Materials, Adaptive Structures and Intelligent Systems, American Society of Mechanical Engineers, Department of Mechanical and Nuclear Engineering, Pennslyvania State University, University Park, PA, United States, pp. 779–788.

[10] Stratasys, 2013, "Objet 350 Connex: Build Mid-Size Prototypes in Multiple Materials" [Online]. Available: http://stratasys.com/3d-printers/design-series/precision/objet-connex350.

[11] Sigmund O., 1997, "On the Design of Compliant Mechanisms Using Topology Optimization," Mech. Struct. Mach., **25**(4), pp. 493–524.

[12] Frecker M. I., Ananthasuresh G. K., Nishiwaki S., Kikuchi N., and Kota S., 1997, "Topological Synthesis of Compliant Mechanisms Using Multi-Criteria Optimization," J. Mech. Des. Trans. ASME, **119**(2), pp. 238–245.

[13] Brackett D., Ashcroft I., and Hague R., 2011, "Topology Optimization for Additive Manufacturing," 22nd Annual International Solid Freeform Fabrication Symposium, pp. 348–362.

[14] Brackett D., Ashcroft I., and Hague R., 2011, "A Dithering Based Method to Generate Variable Volume Lattice Cells for Additive Manufacturing," 22nd Annual International Solid Freeform Fabrication Symposium, pp. 671–679.

[15] Aremu A., Ashcroft I., Wildman R., Hague R., Tuck C., and Brackett D., 2011, "A Hybrid Algorithm for Topology Optimization of Additive Manufactured Structures," 22nd Annual International Solid Freeform Fabrication Symposium, pp. 279–289.

[16] Watts D. M., and Hague R., 2006, "Exploiting the Design Freedom of RM," 17th Annual International Solid Freeform Fabrication Symposium, pp. 656–667.

[17] Wang H. V., and Rosen D. W., 2001, "Computer-Aided Design Methods for the Additive Fabrication of Truss Structures," Georgia Institute of Technology.

[18] Wang H. V., and Rosen D. W., 2006, "An Automated Design Synthesis Method for Compliant Mechanisms with Application to Morphing Wings," ASME Mechanisms and Robotics Conference, pp. 1–9.

[19] Wang H. V., Chen Y., and Rosen D. W., 2005, "A Hybrid Geometric Modeling Method for Large Scale Conformal Cellular Structures," ASME Computers and Information in Engineering Conference, pp. 421–427.

[20] Graf G. C., 2009, "Development of Specialized Base Primatives for Meso-Scale Conforming Truss Structures," Georgia Institute of Technology.

[21] Graf G. C., Chu J., Engelbrecht S., and Rosen D. W., 2009, "Synthesis Methods for Lightweight Lattice Structures," ASME 2009 International Design Engineering Technical Conferences and Computers and Information in Engineering Conference, ASME, pp. 579–589.

[22] Chu J., Engelbrecht S., Graf G., and Rosen D. W., 2010, "A Comparison of Synthesis Methods for Cellular Structures with Application to Additive Manufacturing," Rapid Prototyp. J., **16**(4), pp. 459–472.

[23] Rosen D. W., 2007, "Computer-Aided Design for Additive Manufacturing of Cellular Structures," Comput. Aided. Des. Appl., **4**(5), pp. 585–594.

[24] Chu C., Graf G., and Rosen D. W., 2008, "Design for Additive Manufacturing of Cellular Structures," Comput. Aided. Des. Appl., **5**(5), pp. 686–696.

[25] Chen Y., and Wang S., 2008, "Computer-aided product design with performance-tailored mesostructures," Comput. Aided. Des. Appl., **5**(1-4), pp. 1–11.

[26] Li Y., Chen Y., and Zhou C., 2009, "Design of Flexible Skin for Target Displacements Based on Meso-Structures," Proceedings of the ASME 2009 International Design Engineering Technical Conferences, pp. 1–14.

[27] Maheshwaraa U., Bourell D., and Seepersad C. C., 2007, "Design and Freeform Fabrication of Deployable Structures with Lattice Skins," Rapid Prototyp. J., **13**(4), pp. 213–225.

[28] Hiller J. D., and Lipson H., 2009, "Multi material topological optimization of structures and mechanisms," 11th Annual Conference on Genetic and Evolutionary Computation, pp. 1521–1528.

[29] Bendsøe M. P., 1989, "Optimal shape design as a material distribution problem," Struct. Optim., **1**(4), pp. 193–202.

[30] Bendsøe M., and Sigmund O., 1999, "Material Interpolation Schemes in Topology Optimization," Arch. Appl. Mech., **69**, pp. 635–654.

[31] Yin L., and Ananthasuresh G. K., 2001, "Topology Optimization of Compliant Mechanisms with Multiple Materials Using a Peak Function Material Interpolation Scheme," Struct. Multidiscip. Optim., **23**, pp. 49–62.

[32] Saxena A., 2005, "Topology Design of Large Displacement Compliant Mechanisms with Multiple Materials and Multiple Output Ports," Struct. Multidiscip. Optim., **30**(6), pp. 477–490.

[33] Saxena A., 2002, "On Multiple-Material Optimal Compliant Topologies: Discrete Variable Parameterization Using Genetic Algorithm," ASME 2002 International Design Engineering Technical Conferences and Computers and Information in Engineering Conference, pp. 1–12.

[34] Bailey S. A., Cham J. G., Cutkosky M. R., and Full R. J., 1999, "Biomimetic Robotic Mechanisms via Shape Deposition Manufacturing," Robotics Research: The 9th International Symposium, pp. 403–410.

[35] Rajagopalan S., Goldman R., Shin K.-H., Kumar V., Cutkosky M., and Dutta D., 2001, "Representation of heterogeneous objects during design, processing and freeform-fabrication," Mater. Des., **22**(3), pp. 185–197.

[36] Bejgerowski W., Gerdes J. W., Gupta S. K., and Bruck H. A., 2011, "Design and Fabrication of Miniature Compliant Hinges for Multi-Material Compliant Mechanisms," Int. J. Adv. Manuf. Technol., **57**(5-8), pp. 437–452.

[37] Bejgerowski W., Gerdes J. W., Gupta S. K., Bruck H. A., and Wilkerson S., 2010, "Design and Fabrication of a Multi-Material Compliant Flapping Wing Drive Mechanism for Miniature Air Vehicles," ASME 2010 International Design Engineering Technical

Conferences and Computers and Information in Engineering Conference, ASME, pp. 69–80.

[38] Gouker R. M., Gupta S. K., Bruck H. A., and Holzschuh T., 2006, "Manufacturing of Multi-Material Compliant Mechanisms Using Multi-Material Molding," Int. J. Adv. Manuf. Technol., **30**, pp. 1049–1075.

[39] Rajkowski J. E., Gerratt A. P., Schaler E. W., and Bergbreiter S., 2009, "A multi-material milli-robot prototyping process," 2009 IEEE/RSJ International Conference on Intelligent Robots and Systems, IEEE Computer Society, Mechanical Engineering Department, Institute for Systems Research, University of Maryland, College Park, MD 20742, United States, pp. 2777–2782.

[40] Vogtmann D. E., Gupta S. K., and Bergbreiter S., 2011, "A Systematic Approach to Designing Multi-Material Miniature Compliant Mechanisms," ASME 2011 International Design Engineering Technical Conferences and Computers and Information in Engineering Conference, ASME, pp. 211–221.

[41] Gaynor A., Guest J., and Moen C., 2012, "Reinforced Concrete Force Visualization and Design Using Bilinear Truss-Continuum Topology Optimization," J. Struct. Eng., **139**(4), pp. 607–618.

[42] Guest J. K., and Smith Genut L. C., 2010, "Reducing Dimensionality in Topology Optimization Using Adaptive Design Variable Fields," Int. J. Numer. Methods Eng., **81**(8), pp. 1019–1045.

[43] Guest J. K., Prévost J. H., and Belytschko T., 2004, "Achieving Minimum Length Scale in Topology Optimization Using Nodal Design Variables and Projection Functions," Int. J. Numer. Methods Eng., **61**(2), pp. 238–254.

[44] Guest J. K., 2009, "Topology Optimization with Multiple Phase Projection," Comput. Methods Appl. Mech. Eng., **199**(1–4), pp. 123–135.

[45] Svanberg K., 1987, "The Method of Moving Asymptotes—a New Method for Structural Optimization," Int. J. Numer. Methods Eng., **24**(2), pp. 359–373.

[46] Guest J. K., Asadpoure A., and Ha S.-H., 2011, "Eliminating Beta-Continuation from Heaviside Projection and Density Filter Algorithms," Struct. Multidiscip. Optim., **44**(4), pp. 443–453.

[47] Buhl T., Pedersen C., and Sigmund O., 2000, "Stiffness Design of Geometrically Nonlinear Structures Using Topology Optimization," Struct. Multidiscip. Optim., **19**, pp. 93–104.

[48] Bruns T. E., and Tortorelli D. A., 2001, “Topology Optimization of Non-Linear Elastic Structures and Compliant Mechanisms,” Comput. Methods Appl. Mech. Eng., **190**(26–27), pp. 3443–3459.

[49] Hascoet J. Y., Ponche R., Kerbrat O., and Mognol P., 2012, “From Functional Specifications to Optimized CAD Model : Proposition of a New DFAM Methodology,” Innov. Dev. Virtual Phys. Prototyp., pp. 467–472.

[50] Ponche R., Kerbrat O., Mognol P., and Hascoet J. Y., 2013, “Consideration of the Manufacturing Trajectories in a Global Design for Additive Manufacturing Methodology,” ASME 2012 Biennial Conference on Engineering Systems Design and Analysis, pp. 1–9.

[51] Harzheim L., and Graf G., 2005, “A Review of Optimization of Cast Parts Using Topology Optimization: I - Topology Optimization without Manufacturing Constraints,” Struct. Multidiscip. Optim., **30**(6), pp. 491–497.

[52] Harzheim L., and Graf G., 2005, “A Review of Optimization of Cast Parts using Topology Optimization: II - Topology Optimization with Manufacturing Constraints,” Struct. Multidiscip. Optim., **31**(5), pp. 388–399.

[53] Maidin S. Bin, 2011, “Development of a Design Feature Database to Support Design for Additive Manufacturing,” Loughborough University.

[54] Seepersad C. C., Govett T., Kim K., Lundin M., and Pinero D., 2012, “A Designer’s Guide for Dimensioning and Tolerancing SLS parts,” 23rd Annual International Solid Freeform Fabrication Symposium, pp. 921–931.

[55] Schevenels M., Lazarov B. S., and Sigmund O., 2011, “Robust Topology Optimization Accounting for Spatially Varying Manufacturing Errors,” Comput. Methods Appl. Mech. Eng., **200**(49-52), pp. 3613–3627.

[56] Meisel N. A., Gaynor A., Williams C. B., and Guest J. K., 2013, “Multiple-Material Topology Optimization of Compliant Mechanisms Created via PolyJet 3D Printing,” 24th Annual International Solid Freeform Fabrication Symposium, pp. 980–997.

[57] Stratasys, 2015, “PolyJet Materials” [Online]. Available: http://www.stratasys.com/materials/polyjet. [Accessed: 13-Apr-2015].

[58] Moore J. P., and Williams C. B., 2008, “Fatigue Characterization of 3D Printed Elastomer Material,” Solid Freeform Fabrication Symposium, pp. 641–655.

[59] Pilipović A., Raos P., and Šercer M., 2007, “Experimental Analysis of Properties of Materials for Rapid Prototyping,” Int. J. Adv. Manuf. Technol., **40**(1-2), pp. 105–115.

[60] Vieira L. F., and Paggi R. A., 2012, "Thermal and Dynamic-Mechanical Behavior of Fullcure 3D Printing Resin Post-Cured by Different Methods," Innov. Dev. Virtual Phys. Prototyp., pp. 385–388.

[61] Gibson I., Goenka G., Narasimhan R., and Bhat N., 2010, "Design Rules for Additive Manufacture," Solid Freeform Fabrication Symposium, pp. 705–716.

[62] Udroiu R., and Mihail L., 2009, "Experimental Determination of Surface Roughness of Parts Obtained by Rapid Prototyping," 8th WSEAS International Conference on Circuits, Systems, Electronics, Control and Signal Processing, pp. 283–286.

[63] Udroiu R., and Nedelcu A., 2011, "Optimization of Additive Manufacturing Processes Focused on 3D Printing," Rapid Prototyp. Technol. -- Princ. Funct. Requir., pp. 1–28.

[64] Singh R., 2011, "Process Capability Study of Polyjet Printing for Plastic Components," J. Mech. Sci. Technol., **25**(4), pp. 1011–1015.

[65] Singh R., and Singh V., 2011, "Experimental Investigations for Rapid Moulding Solution of Plastics Using Polyjet Printing," Mater. Sci. Forum, **701**, pp. 15–20.

[66] Vayre B., Vignat F., and Villeneuve F., 2012, "Designing for Additive Manufacturing," Procedia CIRP, **3**, pp. 632–637.

[67] Moylan S., Slotwinski J., Cooke A., Jurrens K., and Donmez M. A., 2012, "Proposal for a Standardized Test Artifact for Additive Manufacturing Machines and Processes," Solid Freeform Fabrication Symposium, pp. 902–920.

[68] Craveiro F., Bártolo H., and Bártolo P., 2013, "Functionally Graded Structures Through Building Manufacturing," Adv. Mater. Res., **683**, pp. 775–778.

[69] Inamdar A., Magana M., Medina F., Grajeda Y., and Wicker R., 2006, "Development of an Automated Multiple Material Stereolithography Machine," Proc. 17th Annu. Solid Free. Fabr. Symp., pp. 624–635.

[70] Regenfuß P., Ebert R., and Exner H., 2007, "Laser Micro Sintering – a Versatile Instrument for the Generation of Microparts," Laser Tech. J., **4**(1), pp. 26–31.

[71] Bandyopadhyay A., Krishna B. V., Xue W., and Bose S., 2009, "Application of Laser Engineered Net Shaping (LENS) to Manufacture Porous and Functionally Graded Structures for Load Bearing Implants," J. Mater. Sci. Mater. Med., **20**.

[72] Vidimče K., and Wang S., 2013, "OpenFab: A programmable pipeline for multi-material fabrication," ACM Trans. Graph. (SIGGRAPH 2013), **32**(4), pp. 1–11.

[73] Chen D., Levin D. I. W., and Didyk P., 2013, "Spec2Fab: A Reducer-Tuner Model for Translating Specifications to 3D Prints," ACM Trans. Graph. (SIGGRAPH 2013), **32**(4), pp. 1–9.

[74] Hašan M., Fuchs M., Matusik W., Pfister H., and Rusinkiewicz S., 2010, "Physical reproduction of materials with specified subsurface scattering," ACM Trans. Graph., **29**(4), p. 61.

[75] Hiller J., and Lipson H., 2010, "Tunable Digital Material Properties for 3D Voxel Printers," Rapid Prototyp. J., **16**(4), pp. 241–247.

[76] Kim H. S., 2000, "On the Rule of Mixtures for the Hardness of Particle Reinforced Composites," Mater. Sci. Eng. A, **289**, pp. 30–33.

[77] Saura S., and Martinez-mlian J., 2001, "Sensitivity of Landscape Pattern Metrics to Map Spatial Extent," Photogramm. Eng. Remote Sensing, **67**(9), pp. 1027–1036.

[78] Menard K. P., 1999, Dynamic Mechanical Analysis: A Practical Introduction, CRC Press LLC, Boca Raton, FL.

[79] Kumar V., Rajagopalan S., Cutkosky M. R., and Dutta D., 1998, "Representation and Processing of Heterogeneous Objects for Solid Freeform Fabrication," Geometric Modeling Workshop, Tokyo, Japan, pp. 1–21.

[80] Kudva J. N., 2004, "Overview of the DARPA Smart Wing Project," J. Intell. Mater. Syst. Struct., **15**(4), pp. 261–267.

[81] Sofla A. Y. N., Meguid S. A., Tan K. T., and Yeo W. K., 2010, "Shape morphing of aircraft wing: Status and challenges," Mater. Des., **31**(3), pp. 1284–1292.

[82] Peraza-Hernandez E., Hartl D., Galvan E., and Malak R., 2013, "Design and Optimization of a Shape Memory Alloy-Based Self-Folding Sheet," J. Mech. Des., **135**(11), pp. 1–11.

[83] Peraza-Hernandez E. A., Hartl D. J., and Malak Jr. R. J., 2013, "Design and Numerical Analysis of an SMA Mesh-Based Self-Folding Sheet," Smart Mater. Struct., **22**(9), pp. 1–17.

[84] Li X., Golnas A., and Prinz F. B., 2000, "Shape Deposition Manufacturing of Smart Metallic Structures with Embedded Sensors," Proceedings of SPIE's 7th International Symposium on Smart Structures and Materials, pp. 160–171.

[85] Li X., and Prinz F. B., 2003, "Embedded Fiber Bragg Grating Sensors in Polymer Structures Fabricated by Layered Manufacturing," J. Manuf. Process., **5**(1), pp. 78–86.

[86] Golnas A., 1999, "Thin-Film Thermo-Mechanical Sensors Embedded in Metallic Structures," Stanford University.

[87] Bailey S. A., and Clark J. E., 2000, "Sprawlita," Stanford Univ. Biomimetics [Online]. Available: http://www-cdr.stanford.edu/biomimetics/.

[88] Bailey S. A., Cham J. G., Cutkosky M. R., and Full R. J., 2001, "Comparing the Locomotion Dynamics of the Cockroach and a Shape Deposition Manufactured Biomimetic Hexapod," Exp. Robot. VII, **271**, pp. 239–248.

[89] Cham J. G., Pruitt B. L., Cutkosky M. R., Binnard M., Weiss L., and Neplotnik G., 1999, "Layered Manufacturing with Embedded Components: Process Planning Considerations," Proceedings of the 1999 ASME Design Engineering Technical Conference, pp. 1–9.

[90] Cham J. G., Bailey S. A., Clark J. E., Full R. J., and Cutkosky M. R., 2002, "Fast and Robust: Hexapedal Robots via Shape Deposition Manufacturing," Int. J. Rob. Res., **21**(10-11), pp. 869–882.

[91] Hatanaka M., 2005, "Design and Fabrication of Multimaterial Flexible Mechanisms with Embedded Components," Stanford University.

[92] Hatanaka M., and Cutkosky M. R., 2003, "Process Planning for Embedding Flexible Materials in Multi-Material Prototypes," Proceedings of the 2003 ASME Design Engineering Technical Conferences and Computers and Information in Engineering Conference, Chicago, Illinois, pp. 1–9.

[93] De Laurentis K. J., Kong F. F., and Mavroidis C., 2002, "Procedure for Rapid Fabrication of Non-Assembly Mechanisms with Embedded Components," Proceedings of the 2002 ASME Design Engineering Technical Conferences and Computers and Information in Engineering Conference, Montreal, Canada, pp. 1–7.

[94] Nau W. H., 1991, "Embedding Sensors Using Stereolithography," Clemson University.

[95] Geving B., 1999, "Build Around a Screwdriver Shaft" [Online]. Available: http://rpmi.marc.gatech.edu/?bgeving/ experiments/screwdriver.html.

[96] Geving B., and Ebert-Uphoff I., 2000, "Enhancement of Stereo-Lithography Technology to Support Building Around Inserts," Proceedings of the 2000 ASME Mechanisms and Robotics Conference, Baltimore, MD.

[97] Kataria A., 2000, "Standardization and Process Planning for Building Around Inserts in Stereolithography Apparatus," Georgia Institute of Technology.

[98] Kataria A., and Rosen D. W., 2001, "Building around inserts: Methods for fabricating complex devices in stereolithography," Rapid Prototyp. J., **7**(5), pp. 253–261.

[99] Liao Y. S., Li H. C., and Chen M. T., 2007, "The Study of Rapid Prototyping Process with Embedded Functional Inserts," J. Mater. Process. Technol., **192-193**(1), pp. 68–74.

[100] Palmer J. A., 2005, "Realizing 3-D Interconnected Direct Write Electronics Within Smart Stereolithography Structures," ASME International Mechanical Engineering Congress and Exposition, Orlando, FL, pp. 287–293.

[101] Medina F., Lopes A. J., Inamdar A. V., Hennessey R., Palmer J. A., Chavez B. D., Davis D., Gallegos P., and Wicker R. B., 2005, "Hybrid Manufacturing: Integrating Direct-Write and Stereolithography," Proceedings of the 2005 Solid Freeform Fabrication Symposium, Austin, TX, pp. 39–49.

[102] Lopes A. J., Inamdar A. V., Medina F., Hennessey R. E., Palmer J. A., Chavez B. D., Davis D. W., Gallegos P. G., and Wicker R. B., 2005, "Rapid Electromechanical Device Manufacturing Using a Hybrid Direct Write Stereolithography System," TexMEMS VII International Conference on Micro Electro Mechanical Systems, El Paso, TX.

[103] Siggard E. J., Madhusoodanan A. S., Stucker B. E., and Eames B., 2006, "Structurally Embedded Electrical Systems Using Ultrasonic Consolidation (UC)," Proceedings of the 17th Solid Freeform Fabrication Symposium, Austin, TX, pp. 70–83.

[104] Kong C. Y., Soar R. C., and Dickens P. M., 2004, "Ultrasonic Consolidation for Embedding SMA Fibres Within Aluminium Matrices," Compos. Struct., **66**(1-4), pp. 421–427.

[105] Kong C. Y., and Soar R., 2005, "Method for Embedding Optical Fibers in an Aluminum Matrix by Ultrasonic Consolidation.," Appl. Opt., **44**(30), pp. 6325–6333.

[106] Yang Y., 2008, "Fabrication of Long-Fiber-Reinforced Metal Matrix Composites Using Ultrasonic Consolidation," Utah State University.

[107] Janaki Ram G. D., Robinson C., Yang Y., and Stucker B. E., 2007, "Use of Ultrasonic Consolidation for Fabrication of Multi-Material Structures," Rapid Prototyp. J., **13**(4), pp. 226–235.

[108] Robinson C. J., Stucker B., Lopes A. J., Wicker R., and Palmer J. A., 2006, "Integration of Direct-Write (DW) and Ultrasonic Consolidation (UC) Technologies to Create Advanced Structures with Embedded Electrical Circuitry," Proceedings of the Solid Freeform Fabrication Symposium, pp. 60–69.

[109] Willis K., Brockmeyer E., Hudson S. E., and Poupyrev I., 2012, "Printed optics: 3D Printing of Embedded Optical Elements for Interactive Devices," Proceedings of the 25th Annual Symposium on User Interface Software and Technology, pp. 589–598.

[110] ASTM Standard F2792-12a, 2012, "Standard Terminology for Additive Manufacturing Technologies."

[111] Williams C. B., Mistree F., and Rosen D. W., 2011, "A Functional Classification Framework for the Conceptual Design of Additive Manufacturing Technologies," J. Mech. Des., **133**(12).

[112] ASTM Standard F2921-11e3, 2011, "Standard Terminology for Additive Manufacturing -- Coordinate Systems and Test Methodologies."

[113] Sofla A. Y. N., Elzey D. M., and Wadley H. N. G., 2008, "Two-way Antagonistic Shape Actuation Based on the One-way Shape Memory Effect," J. Intell. Mater. Syst. Struct., **19**(9), pp. 1017–1027.